Studies on the Roles of Viral Envelope Surface Proteins In Cell Attachment and Entry

by

Lindsey Lamboo

A Thesis submitted to the Faculty of Graduate Studies of

The University of Manitoba

In partial fulfillment of the requirements of the degree of

MASTER OF SCIENCE

Department of Medical Microbiology and Infectious Diseases

University of Manitoba

Winnipeg, Manitoba, Canada

Abstract

The Ebola virus (EBOV) surface glycoprotein (GP) is a trimeric class I viral fusion protein, which plays a key role in viral attachment and entry. The major cell entry mechanism during EBOV infection involves the endosomal pathway, where GP specifically binds to domain C of NPC1 (a cholesterol transporter) in the endosome, and causes fusion between the viral envelope and the endosomal membrane to allow entry of the viral nucleocapsid. Previously published evidence suggests that proteolytic cleavage of EBOV GP by host cell proteases is required before receptor binding can take place, and that luminal acidic pH may also be required to trigger EBOV GP membrane fusion within the endosome. A variety of previous studies have analyzed the structure of class I fusion proteins in their pre- and post-fusion states by crystallography. An experimental cell-free system was developed here that allows further dynamic time-resolved studies of viral attachment and fusion, specifically, the molecular interactions and intermediate fusion structures that may occur between GP and NPC1, using cryo-electron microscopy. The system utilizes the interaction between expressed EBOV virus-like particles (VLPs) and synthetic liposomes displaying an engineered NPC1-C receptor domain, (that contains the specific GP binding site) on their surfaces.

Two forms of non-infectious virus-like particles (VLPs) were produced by expression of the EBOV matrix protein VP40 along with either the full-length GP surface protein or a mucin-like domain deleted version. The conditions necessary to adequately cleave GP in purified VLPs, and thus prime them for receptor binding were determined using commercial thermolysin *in lieu* of cathepsins. A soluble version of luminal domain C of NPC1 was constructed with a 6-his tag for the purpose of purification of the protein

by high performance liquid chromatography and for specific binding of purified NPC1-C to the surface of liposomes that were produced with lipids containing a nickel ion complex. This resulted in NPC1-C receptor-decorated liposomes that could be easily purified from unbound receptor by density gradient centrifugation.

The interaction and binding of NPC1-C decorated liposomes with purified VP40 GP VLPs was investigated by cryo-electron microscopy. Specific high-affinity binding of these liposomes to GP was demonstrated only after prior thermolysin cleavage of the version of GP that had the mucin-like domain deleted. It was also shown that there was no binding of full-length GP to NPC1-C, irrespective of prior thermolysin treatment. This provides evidence, consistent with previous structural studies of the partial and intact GP trimer, that access of NPC1 to the receptor-binding domain requires proteolytic removal not only of the mucin-like domain, but some small and as yet undefined portion of the GP1 domain as well.

The cell-free system described here will allow future experimental studies of attachment and fusion, and investigation of the roles of pH or other factors, in isolation from complicating cellular and viral factors that might also affect viral entry into cells. In addition, the high-throughput screening of candidate antiviral drugs that target the binding and/or fusion mechanisms of viruses will be possible.

Acknowledgements

First I'd like to thank my supervisors Dr. Tim Booth and Dr. Daniel Beniac for their profound guidance and support during my Masters degree. Thank you for always being available for discussions of experiments and results and for allowing my abilities in molecular biology and electron microscopy to flourish. Thanks also to my committee members Dr. Kevin Coombs and Dr. Sean McKenna for your guidance along the way. Thanks as well to the Public Health Agency of Canada for funding this research.

Thank you to Erika Landry, Shari Tyson, and Travis Murphy of the DNA Core Facility at the NML for performing primer production and sequencing of the clones used in these experiments. Thanks also to the Mass Spectrometry and Proteomics Core Facility at the NML for processing of my samples for in-gel digestion, training me on the protocol, and for running the samples on the mass spectrometer.

Thank you to Shannon Hiebert, Melissa Rabb, and Christine Golding of the Diagnostic Microscopy and Imaging Section for your invaluable support during this degree. I couldn't have done it without you! A huge thank you to Dr. Michael Carpenter for your unfailing support and guidance in the cloning, stable cell line production, and protein purification aspects of this experiment. Thank you for always having an open door when I needed advice and guidance during these experiments. I've learned more from you these past few years than I could have ever imagined and I can't thank you enough.

Thanks also to the Medical Microbiology department at the University of Manitoba. Specifically to Angela Nelson, I would have been lost without your guidance and support during this degree.

Finally, thank you to my family and friends for your unwavering love and encouragement during this endeavour, for providing distractions when I needed them, and for shaping me into who I am today.

Table of Contents

List of Tables

List of Figures

Abbreviations

°C – degrees Celsius

6HB – six helix bundle

ASMase – Acid Sphingomyelinase

BCA – bicinchoninic acid

CCD – charge coupled device

Cryo-EM – cryogenic electron microscopy

Cryo-ET – cryogenic electron tomography

DC – dendritic cell

DC-SIGN – dendritic cell-specific intercellular adhesion molecule-3-grabbing non-integrin

DMEM – Dulbecco's Modified Eagle's Medium

DNA – deoxyribonucleic acid

DYKDDDDK – Flag tag

E – envelope protein of Tick-borne encephalitis virus

EBOV – Ebola virus

EDTA – ethylenediaminetetraacetic acid

EM – electron microscopy

F – fusion protein of Paramyxovirus

FBS – fetal bovine serum

FRET – Fluoresence Resonance Energy Transfer

gB – glycoprotein B of herpes simplex virus

GFP – green fluorescent protein

GP, pre-sGP, sGP, ssGP – glycoprotein (Ebola), pre-secreted, secreted, small soluble

GPFull – full version of Ebola glycoprotein

GPΔmuc – mucin-deleted glycoprotein

GP1 – receptor binding subunit of GP

GP2 – fusion subunit of GP

HA – hemagglutinin of influenza

HEK 293TN – human embryonic kidney 293TN cells

His-tag – polyhistidine tag

HPLC – high performance liquid chromatography

HRP – horseradish peroxidase

IR – infrared

L – RNA dependent RNA polymerase of Ebola

LB – Luria Bertani broth

L-domain – Late budding domain

LMV – large multilamellar vesicle

L-SIGN – liver/lymph node-specific intracellular adhesion molecule-3-grabbing non-integrin

LUV – large unilamellar vesicle

mAb – monoclonal antibody

MLD – mucin like domain

mRNA – messenger RNA

MS – mass spectrometry

MT – methylamine tungstate

NBD - nitrobenzoxadiazole

NML – National Microbiology Laboratory

NPC1 – Neimann Pick type C1

NPC1-C – NPC1 luminal domain C

NPC1-C-Rx-SC – NPC1-C RetroX second cluster

ORF – open reading frame

PBS – phosphate buffered saline

PCR – polymerase chain reaction

PSG – penicillin streptomycin glutamine

PVDF – polyvinylidene fluoride

R18 – octadecyl rhodamine B

RNA – ribonucleic acid

RNP - ribonucleoprotein

rVSV – replication-competent vesicular stomatitis virus

rVSV-ZEBOV – rVSV with Zaire EBOV GP

SDS – sodium dodecyl sulfate

SDS-PAGE – SDS polyacrylamide gel electrophoresis

SUV –small unilamellar vesicle

TBS – tris buffered saline

TBS-T – TBS plus 0.1% Tween 20

TEM – transmission electron microscopy

TIM-1 – T-cell Ig and mucin domain 1

TNE buffer – buffer containing Tris, NaCl, and EDTA

UA – uranyl acetate

VLP – virus-like particle

VP 24, 30, 35, 40 – viral protein 24, 30, 35, 40

1. Introduction

1.1 Fusion and Fusion Proteins

Fusion between cellular plasma membranes and the viral envelope, initiated by one or more viral surface glycoproteins, is the process by which all enveloped viruses enter to begin their disease-causing cycles of replication (White et al., 2008). Recent research has identified three classes of viral membrane fusion proteins according to their structural attributes: Class I, Class II, and Class III (White et al., 2008). However, there is some overlap between these classes as there are at least four distinct mechanisms by which these fusion proteins can be triggered to induce fusion. The theorized common functional mechanism across all viral fusion proteins is the conversion from a fusion-competent state, to a membrane-embedded trimeric coiled-coil rod called a pre-hairpin, and finally to a compact rod-like trimer-of-hairpins. Multiple pre-hairpins cluster together to bring the membranes together in stages of close apposition, hemifusion, and finally formation of the fusion pore with the trimer-of-hairpins containing the six helix bundle (White et al., 2008). This trimer-of-hairpins (Figure 1) across all three classes of viral fusion proteins is formed regardless of the fusion subunit structure (White et al., 2008).

1.1.1 Class I Fusion Proteins

Examples of virus families exhibiting Class I fusion proteins include the *Orthomyxoviridae, Retroviridae, Paramyxoviridae, Coronaviridae, Filoviridae*, and *Arenaviridae* (White et al., 2008). Class I fusion proteins exist as trimers in both their pre- and post-fusion states (Figure 1), and are known to have a central N-terminal trimeric α-helical coiled coil coated by 3 C-terminal helices, forming a 6-helix-bundle

(6HB) structure (White et al., 2008). The size and position of the 6HB structure varies widely across all Class I proteins. These include, for example, the influenza hemagglutinin (HA), paramyxovirus fusion protein (F), α-retroviral envelope proteins (Env), and the Ebola virus glycoprotein (GP) protein. All Class I fusion proteins are considered to be Type I integral membrane proteins. These fusion proteins require proteolytic processing to generate the fusion competent form of the protein (White et al., 2008). These proteins are also known to be metastable and project as spikes on the surface of virions, while the fusion peptide is buried in the subunit interface of the trimeric native fusion protein (White et al., 2008). Activation of Class I fusion proteins to their fusogenic form can be triggered by low pH in the case of the influenza HA, by binding of receptor in the case of the F protein of paramyxoviruses, or by binding to the receptor followed by low pH in the case of HIV Env (White et al., 2008). In the case of Ebola GP, initial findings suggested that low pH and binding of the receptor were required for fusion to occur (Brecher et al., 2012; White et al., 2008). However, recent reports have been conflicting. Some studies have concluded that low pH is not necessary for fusion to occur, rather it is only necessary for the activity of endosomal proteases that prime GP to a fusogenic state; fusion still occurs at neutral pH (Markosyan et al., 2016). The current study investigates the Ebola GP and its interaction with its major receptor, the Niemann Pick-C1 protein (NPC1) without the addition of low pH.

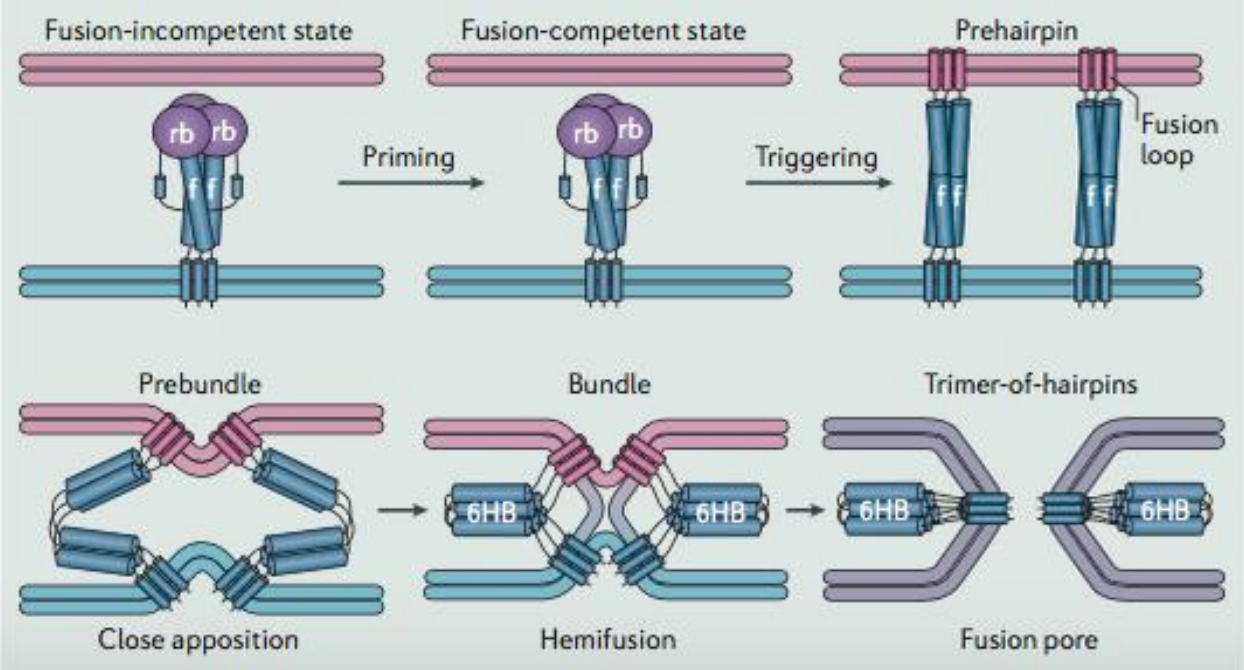

Figure 1. Pathway of viral membrane fusion. The Ebola GP is converted from a fusion-incompetent state to a fusion-competent state (metastable) by proteolytic priming that allows fusion to be triggered. Triggering of fusion exposes the fusion loop which can then hydrophobically bind to the target membrane. The pre-hairpin (a trimeric coiled-coil rod) is thought to be the bridge between membranes and is composed of three identical fusion subunits. Fold-back steps force the protein through prebundle, bundle, and trimer-of-hairpins configurations. The trimer-of-hairpins contains the 6HB. This forces the membranes through the following stages of contact: close apposition, hemifusion, and formation of the fusion pore. This pore will eventually grow large enough for the viral genome to pass through into the cell. Figure reproduced with permission from **(White and Schornberg, 2012)**.

1.1.2 Class II Fusion Proteins

Examples of virus families having Class II fusion proteins include the *Togaviridae, Flaviviridae,* and *Bunyaviridae* (White et al., 2008). Examples of viruses having Class II fusion proteins are the tick-borne encephalitis virus envelope (E) protein, and the Semliki Forest virus proteins E1/E2. Class II fusion proteins are primarily made up of β-sheet structures with internal fusion peptides that are formed as loops at the tips of these β-strands. Unlike Class I proteins, Class II proteins are associated with a chaperone protein that is cleaved during or shortly after assembly (White et al., 2008). After maturation, the ectodomains exist as anti-parallel dimers that lie along the surface of the virion, where each stem is at a threefold axis of symmetry with respect to the virion. After they have been triggered to the fusion conformation, these proteins realign as trimers that project from the membrane of the virus in threefold axes (White et al., 2008). Class II proteins are similar to Class I in that they are also Type I integral membrane proteins, and while some Class II proteins require low pH to be activated to their fusogenic state, it is not strictly required (Fields and Kielian, 2015). In the case of Togaviridae, release of E3 from E2 at neutral pH primes the virus for fusion during entry (Fields and Kielian, 2015). They also require proteolytic processing to generate the fusion competent form, but in the case of Class II proteins, this processing is of the accessory protein, not the fusion protein itself (White et al., 2008).

1.1.3 Class III Fusion Proteins

Examples of virus families that have Class III fusion proteins include the *Rhabdoviridae* and *Herpesviridae* (White et al., 2008). Their structure is a more recent discovery and they share some features with both Class I and Class II proteins. Like Class I, they exist

as trimers in their prefusion state and contain a central α-helical coiled coil. Like Class II, the fusion loops are located at the tips of extended β-strands (White et al., 2008). Like both Class I and II before it, Class III proteins are also Type I integral membrane proteins, but do not require proteolytic processing to generate a fusion competent form (White et al., 2008). The factors that affect stability of Class III proteins are poorly understood, but activation to the fusogenic form can be triggered by low pH or binding of a receptor (White et al., 2008).

1.2 Ebola virus

1.2.1 Ebola Virus History

The Ebola virus (EBOV) is an enveloped, non-segmented negative-sense stranded RNA virus that together with the Marburg virus makes up the *Filoviridae* family of filamentous viruses (Huang et al., 2002). The Ebola virus genus consists of five species; *Zaire, Sudan, Reston, Côte d'Ivoire,* and *Bundibugyo,* and is one of the main causes of viral haemorrhagic fever (Towner et al., 2008). The average case fatality rate is around 50%, while in past outbreaks, fatality rates have ranged from 25-90% (WHO, 2018). Ebola virus was first discovered to be a causative agent of viral haemorrhagic fever in 1976 when simultaneous outbreaks occurred in Sudan and the Democratic Republic of Congo (Wilson et al., 2001). The largest outbreak of Ebola virus occurred in West Africa in 2014, centered in Guinea, Liberia, and Sierra Leone (Davidson et al., 2015), which resulted in over 27,000 cases and over 11,000 deaths (Davidson et al., 2015).

1.2.2 Ebola Virus Proteins

The Ebola virus has seven viral structural proteins, encoded by the single species of negative-strand RNA genome. The filamentous virions have a diameter of approximately 75 – 80 nm and lengths of 975 nm and up to 22 μm or more, while virus-like-particles (VLPs) exhibit a diameter ranging from 50-91 nm (Beniac et al., 2012). Ebola virus matures by budding from the host cell, whereby virions acquire an envelope derived from the host cell membrane. Within the envelope is the nucleocapsid of 45 – 60 nm in diameter. The envelope is covered with surface spikes (Huang et al., 2002). The seven structural and regulatory proteins in no particular order are as follows; nucleoprotein (NP), virion protein (VP) 24, VP30, VP35, VP40, glycoprotein (GP), and the RNA-dependent RNA polymerase (L) (Huang et al., 2002). The two proteins that are the focus of this study are VP40 and GP.

The Ebola virus VP40 protein is a matrix protein and performs a similar function to those of other negative sense stranded RNA viruses (Noda et al., 2002). The VP40 protein is the most abundant protein in the Ebola virion and is located on the cytoplasmic side of the viral envelope. Matrix proteins maintain the structural integrity of virus particles (Noda et al., 2002), and play a key role in virus assembly and budding, a property associated with the late-budding domains (L-domains) at the N-terminus of the protein (Licata et al., 2004). These L-domains are thought to serve as docking sites that facilitate interactions with specific cellular proteins of the host that promote budding (Licata et al., 2004). Transfection of cells with a vector expressing VP40 result in the release of VLPs in the culture supernatant which have a similar morphology to wild-type

virions, but are hollow and do not contain a nucleocapsid (Noda et al., 2002).

Filamentous VP40 GP VLPs

The GP gene of Ebola virus can produce three different proteins through transcriptional editing: the full length $GP_{1,2}$ is 676 amino acid residues in length, the pre-secreted GP (pre-sGP) is 364 residues in length, and the small soluble GP (ssGP) is of 298 residues in length (de La Vega et al., 2015). Unedited GP mRNA leads to the formation of secreted (sGP), while the full length GP is produced as a result of slippage of the polymerase at the editing site within the GP gene: as a result, an eighth adenosine residue is added to the poly(A) tail of the mRNA, and the premature end GP transcription is overridden, allowing for the fusion of two separate open reading frames (ORFs), resulting in $GP_{1,2}$ (de La Vega et al., 2015). In my thesis investigation, I have focused on the full length GP of Ebola since it forms the spike, approximately 7 nm in size, on the surface of virions, which is spaced about every 5-10 nm along the virion. The GP spike is a class I viral fusion protein and a type I transmembrane protein. The GP1 domain contains the binding site, while the fusion function is contained within GP2 (Kuhn et al., 2006). Full length GP matures as a trimer and is post-translationally modified by N-glycosylation in the endoplasmic reticulum, followed by trafficking to the Golgi apparatus for refinement and addition of O-glycans (Kuhn et al., 2006). The polypeptide GP is then cleaved by furin-like proteases into the ecotdomain of GP1 (130 kDa) and the transmembrane domain of GP2 (20 kDa) (Kuhn et al., 2006; Wang et al., 2016); these subunits remain connected through disulfide bonds. The mature full length GP trimer is then incorporated into virions as spikes during budding (Kuhn et al., 2006). When GP is coexpressed along with VP40, GP spiked filamentous VLPs result, while

expression of GP alone results in pleomorphic enveloped particles that are inefficiently released because GP does not promote budding on its own (Noda et al., 2002).

1.2.3 Ebola Virus Infection and Treatment

Ebola virus is known to be transmitted by direct contact with blood and bodily fluids of infected patients while fruit bats have been suggested to be possible reservoirs for filoviruses (Wilson et al., 2001). Early symptoms of an Ebola virus infection include general flu-like symptoms including headache, fever, muscle aches, abdominal pain, vomiting and diarrhoea. These primary symptoms are followed by widespread endothelial haemorrhaging, necrosis of multiple organs, shock and death within 7 to 14 days of the appearance of the primary symptoms (Wilson et al., 2001). Fatal infections with Ebola virus typically show a very low acquired immune response, because viral replication occurs in mononuclear phagocytes that usually present antigens to the immune system (Wilson et al., 2001).

Currently, there are no approved vaccines or treatments available for an Ebola virus infection, but research is currently underway on therapies to reduce the severity and fatality of the infection that results (Davidson et al., 2015; Qiu et al., 2012). Currently the main treatment options are supportive care by means of intravenous-fluids as well as treatment of specific symptoms (WHO, 2018). During 2015, an experimental vaccine trial in Guinea proved highly protective against Ebola virus. This vaccine is based on an attenuated, replication-competent vesicular stomatitis virus (rVSV) in which the VSV GP has been replaced by the Ebola virus GP (rVSV-ZEBOV) (Regules et al., 2017). The vaccination initiates replication of viral particles similar to rVSV, but expressing the Ebola virus GP, resulting in an antibody mediated response against

Ebola (Regules et al., 2017). One other study found that a cocktail of three anti-GP monoclonal antibodies (mAbs), if the first dose was administered within 24 hours of infection, resulted in complete survival of Ebola virus challenged Cynomolgus Macaques (Qiu et al., 2012). Mapping of these mAbs indicated that 1H3, 2G4, and 4G7 all bound to a genetically modified version of GP that lacked the mucin like domain (MLD) of the Ebola GP, indicating that their binding sites are outside of the MLD (Qiu et al., 2011). Specifically, mAb 2G4 bound to the GP2 portion of GP, 4G7 bound to C-terminal epitopes of GP1, and 1H3 bound to sGP (Qiu et al., 2012). They found that survivors exhibited an Ebola-GP specific humoral response as well as a cell-mediated immune response (Qiu et al., 2012). Therefore, the GP is a key target for prevention and therapy of EBOV disease.

1.2.4 Ebola Virus Life Cycle

The first step in the life cycle of any virus is attachment to the host cell surface as shown in Figure 2. In the case of Ebola virus, the first cells to become infected are macrophages and dendritic cells (DC). Ebola virus can infect most cell types, except for lymphocytes or other non-adherent cells (White and Schornberg, 2012). All viruses utilize attachment factors and/or entry receptors when binding to host cells. However, an attachment factor only functions as a binding moiety, while an entry receptor is a molecule on the cell surface that actively promotes internalization of the virus or initiates the process of viral penetration (White and Schornberg, 2012). Ebola virus has been shown to interact with host cell attachment factors such as DC-specific ICAM3-grabbing non-integrin (DC-SIGN) and liver and lymph node SIGN (L-SIGN) (White and Schornberg, 2012). Recent evidence has also shown that T cell immunoglobulin and

mucin domain-containing 1 (TIM1) may serve as an Ebola virus receptor on epithelial cells, but details remain unclear (White and Schornberg, 2012).

Upon binding at the cell surface, Ebola virus then enters via a macropinocytosis-like method (Mulherkar et al., 2011; Nanbo et al., 2010; Saeed et al., 2010) and is then shuttled to the late endosome. The viral nucleocapsid then penetrates into the cytoplasm by fusion between the viral envelope and the late endosomal membrane via binding between GP and NPC1. Following entry, the Ebola virus genome is replicated within the ribonucleoprotein (RNP) complex or nucleocapsid (Yu et al., 2017). To date, the molecular mechanism of RNP and how the VP35 protein releases RNA from the nucleocapsid remains unknown. The genome is then converted to mRNA and is transcribed by the viral polymerase complex and viral proteins are translated. The GP mRNA is trafficked to the endoplasmic reticulum where it is translated, followed by modifications occuring in the Golgi (White and Schornberg, 2012). Finally at the plasma membrane, the RNP and associated viral proteins assemble with VP24, VP40 and GP and resulting virions bud from the cell surface (White and Schornberg, 2012). Figure 2 depicts an illustration of the Ebola life cycle (White and Schornberg, 2012).

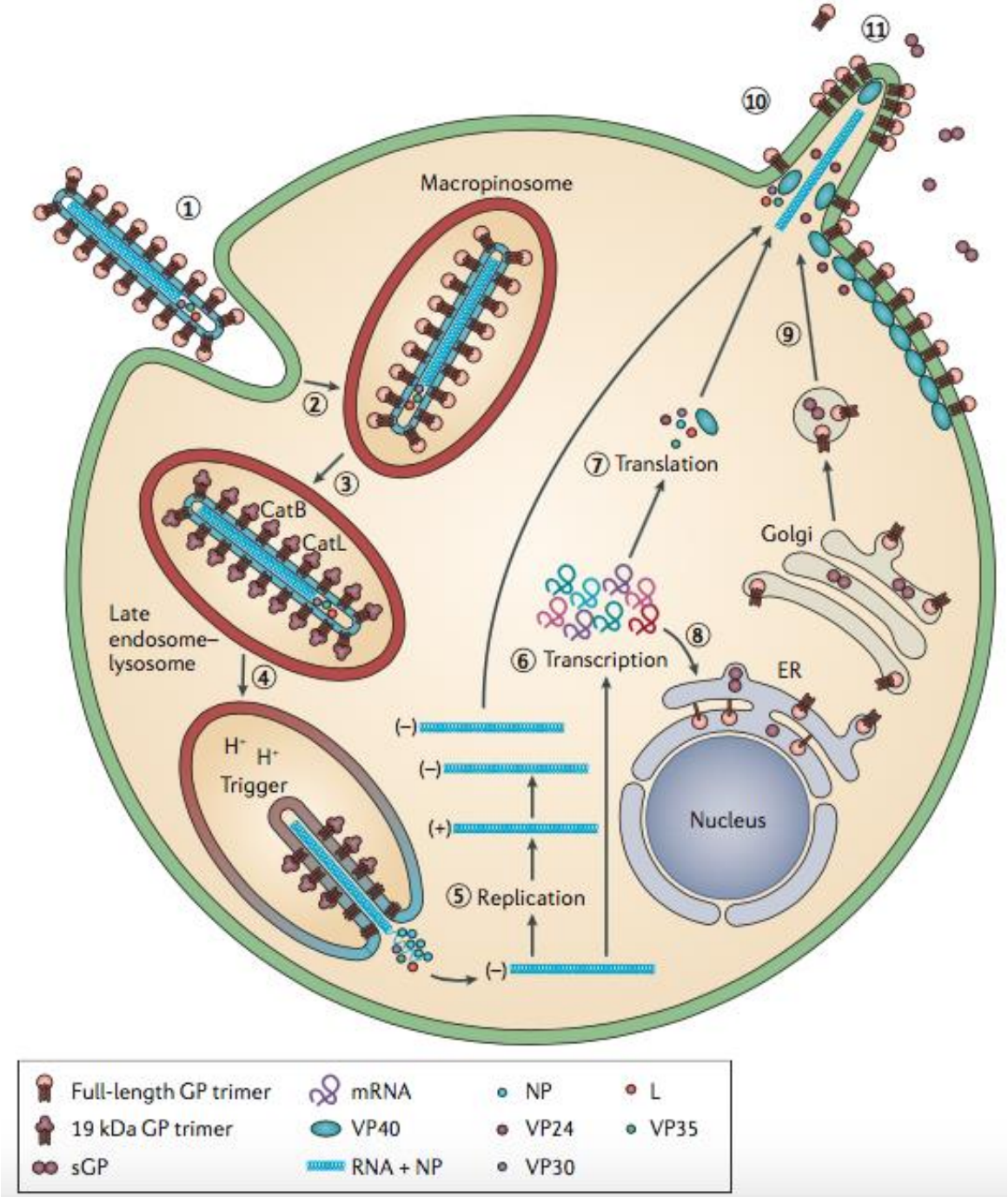

Figure 2. Ebola virus life cycle. The virus binds to cell surface receptors via GP (1) and is then internalized by macropinocytosis (2) followed by travel to the endosome and exposure to cathepsins (3). GP is digested to 19 kDa and triggers fusion to occur (4); the genome is replicated in the cytoplasm (5) and transcribed (6), and viral mRNA is translated (7). GP is synthesized in the endoplasmic reticulum (8) and modified in the Golgi to be delivered to secretory vesicles (9). At the plasma membrane, the RNP and VPs associate with membrane associated proteins and virions bud from the cell surface (10). Non-structural forms of GP are also secreted (11). Figure reproduced with permission from **(White and Schornberg, 2012)**.

The GP of Ebola virus plays a key role in the Ebola virus life cycle and infection process. As stated previously, as a Class I viral fusion protein, GP is responsible for both binding and fusion (Miller et al., 2012a). The Ebola GP protein differs from other Class I fusion proteins in that this simple furin cleavage to separate GP1 from GP2 is not sufficient to prime GP so that it is then able to achieve binding and fusion (White and Schornberg, 2012). It has previously been demonstrated that cleavage of GP by cathepins L and B results in removal of the MLD from the GP (Lee et al., 2008). However, it was later reported that full priming of GP, involves removal of ~60% of the amino acids from GP1 by proteases, including the N- and O-glycosylated MLD and N-glycosylated glycan cap (White and Schornberg, 2012). This discrepancy in whether or not cleavage of the glycan cap is needed is explored further in this thesis, but preliminary findings suggest that cleavage of the glycan cap is needed. The priming step actually appears to occur in several steps, starting with the transition of GP1 to a ~50kDa intermediate (Brecher et al., 2012), then cathepsin L cleavage of GP1 to 20kDa, followed by cleavage of this 20kDa species to 19kDa. The 20kDa and 19kDa forms of GP1 have varying biological and biochemical properties. Entry of pseudovirions exhibiting the 20kDa form is strongly inhibited by antogonists for cathepsin B, while the entry of pseudovirions expressing the 19kDa GP form are not (White and Schornberg, 2012). The 19kDa form is also more easily triggered to undergo a conformational change to expose the fusion loop and is also much more sensitive to proteolysis. One hypothesis that has been suggested in an attempt to explain why the GP must undergo such an intensive proteolytic priming event is that priming could expose the receptor binding domain of GP allowing it to interact with an endosomal receptor (Kaletsky et al.,

2007). It has also been shown that the receptor binding domain is covered by the MLD and glycan cap and may be removed at the same time to expose the receptor binding domain (Beniac and Booth, 2017).

After priming of GP, the GP fusion is triggered as described in the previous section. This exposes and repositions the fusion loop of GP, allowing it to bind to the hydrophobic target membrane (White and Schornberg, 2012). The bridge-like structure that forms as a link between the viral and target membranes is suspected to be a trimeric coiled-coil rod, or a prehairpin made up of three identical fusion subunits. Eventual fold-back steps push the fusion protein through the following steps: prebundle, bundle, and trimer-of-hairpins, as described previously and shown in Figure 1 from (White and Schornberg, 2012). These structural changes, suspected to occur in all Class I fusion proteins including influenza HA, force the viral and target membranes through various stages leading to formation of a fusion pore that eventually becomes large enough to allow the passage of the viral genome into the cell. Recent studies have shown that NPC1 is a crucial entry factor for Ebola virus as the primed GP binds to domain C of NPC1 (Carette et al., 2011).

1.3 Niemann-Pick C1

1.3.1 NPC1 Function in Mammalian Cells

Niemann-Pick type C disease is a rare autosomal recessive disorder that results in neurodegeneration and ultimately leads to death in early childhood (Davies and Ioannou, 2000). What appears to occur in affected patients is an accumulation of low-density lipoprotein-derived unesterified cholesterol in the lysosomes. As a result, cholesterol then accumulates in the trans-Golgi network where its relocation to and from the plasma membrane is delayed (Davies and Ioannou, 2000). The NPC1 and NPC2 proteins are needed for transportation, utilization and processing of this cholesterol that has been delivered to lysosomes (Deffieu and Pfeffer, 2011). The structure of the glycoprotein NPC1 is comprised of 13 transmembrane domains, three large luminal domains (A, C, and I), and a cytoplasmic tail, nomenclature as shown in Figure 3 (Davies and Ioannou, 2000). The process of exporting cholesterol from lysosomes into the cytosol occurs when the N-terminal domain of NPC1 binds cholesterol that it has received from NPC2, followed by export of the cholesterol to the cytosol by NPC1 (Deffieu and Pfeffer, 2011). Niemann-Pick type C disease results when a mutation occurs in NPC1 and/or NPC2 (Deffieu and Pfeffer, 2011).

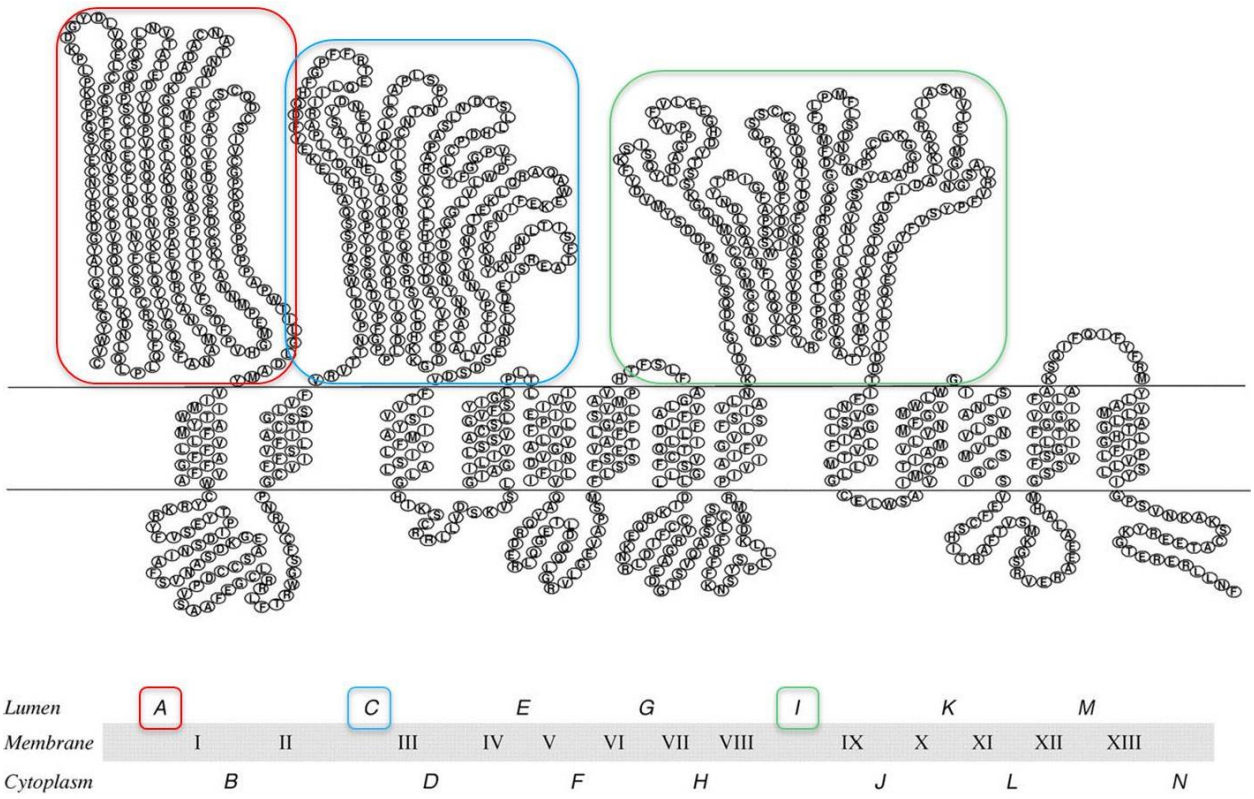

Figure 3. Model of NPC1 topology. This topological model was made using experimental data in **(Davies and Ioannou, 2000)**. Transmembrane domains are indicated by roman numerals, luminal domains A, C, and I are shown boxed in red, blue, and green respectively. The domain of interest for my project was domain C, outlined in blue. Open-access figure reproduced from **(Davies and Ioannou, 2000)**

1.3.2 NPC1 Interaction with GP

Although the main role of NPC1 in mammalian cells is for cholesterol trafficking in the late endosomes, recent studies have found that NPC1 also plays a major role as an essential host factor in Ebola virus infection (Carette et al., 2011; Cote et al., 2011; Miller et al., 2012a). A genome wide haploid genetic screen was conducted on human cells to determine host factors required for Ebola virus entry (Carette et al., 2011). The genetic screen found 67 mutations disrupting the homotypic fusion and vacuole protein-sorting complex, which has a role in fusion of endosomes to lysosomes (Carette et al., 2011). The screen also found 39 mutations that disrupted NPC1. Taken together, cells defective with either of these mutations were resistant to Ebola virus infection indicating the roles both endosomes and NPC1 play in Ebola virus infection (Carette et al., 2011). Another study took this experiment one step further and showed that reptilian cells that are normally resistant to Ebola infection, became susceptible to infection upon expression of human NPC1 in the cells (Miller et al., 2012a). Purified NPC1 was found to bind only the cleaved form of GP generated by cathepsin L and B proteolysis (Miller et al., 2012a). As described above, NPC1 contains three luminal domains, A, C, and I, where all three domains are required for cholesterol transport. However, it has since been shown that only domain C is required for filovirus entry, not the full-length protein. These experiments were carried out using a pseudotyped rVSV-GP-EBOV construct, followed by cleavage with thermolysin in lieu of cathepins, to produce the cleaved form of GP (Miller et al., 2012a). Incubation of domain C of NPC1 (NPC1-C) with both the uncleaved and cleaved forms of this GP construct only resulted in successful interaction between NPC1-C and the cleaved form of the glycoprotein (Miller et al., 2012a).

Up until 2012, all of the literature indicated that, as long as the GP was in its cleaved form, NPC1 should bind. However, in an endeavour to determine the crystal structure of the primed Ebola GP bound to NPC1-C (Wang et al., 2016), took the cleavage of GP one step further. They began with a form of GP that had been genetically modified to remove the transmembrane domain and MLD, prior to treatment with thermolysin (Wang et al., 2016). They found that NPC1-C only bound after additional treatment with thermolysin. Therefore, it is unclear if thermolysin cleavage of GP is sufficient to allow binding with NPC1, or if deletion of the two domains, in addition to thermolysin, was responsible for revealing the binding site. This seems to indicate that something more than simple proteolytic cleavage by cathepsins must be at play to allow GP to bind with NPC1-C.

1.4 Liposomes

1.4.1 Introduction to Liposomes

Liposomes are lipid vesicles with one or more bilayer, similar to the plasma membrane of a cell, that are formed when a variety of lipids are mixed in a desired ratio. Liposomes were first discovered by Alec D Bangham when he, along with a colleague, began testing a new electron microscope at the Babraham Institute in Cambridge (Bangham and Horne, 1964). When adding negative stain to dried phospholipids, they found a resemblance to the cell membrane, providing the first evidence that cell membranes were a bilayer lipid structure (Bangham and Horne, 1964). Within the next year, Bangham along with Standish and Weismann, had established liposomes as a closed bilayer structure, able to release its contents upon treatment with detergent (Bangham et al., 1965). Weismann went on to coin the term liposome after “lysosome”,

an organelle exhibiting this same characteristic when exposed to detergent (Bangham et al., 1965). Liposomes are formed by rehydration of dried thin lipid films. Upon addition of water, stacks of liquid crystalline bilayers become fluid and swell (Avanti Polar Lipids, 2017). The freshly hydrated sheets of lipids become detached from the vessel surface during agitation and self-close to form large multilamellar vesicles (LMV). Hydration of the lipid film is usually achieved in 1 hour with vigorous shaking. Overnight hydration of the particles prior to agitation can result in more uniform and homogeneous particles (Avanti Polar Lipids, 2017). The particles can then be reduced in size by some form of energy input such as sonication or extrusion (Avanti Polar Lipids, 2017).

Liposomes have become a very useful tool in various scientific areas including mathematics, biochemistry, and biology (Bozzuto and Molinari, 2015). As of late, liposomes have become an exceptionally useful tool as drug delivery systems, with the ability to target drugs to the specific tissue or cells their effect is desired (Akbarzadeh et al., 2013). This closed structure that the lipid vesicles form when the dried down suspension becomes rehydrated, enable these liposomes to carry aqueous or lipid drugs, avoiding toxicity in non-target tissues (Akbarzadeh et al., 2013). Liposomes are in use as carriers in the cosmetic and pharmaceutical industries, food, and farming industries. Extensive studies on the use of liposome encapsulation to trap and shield unstable compounds such as antimicrobials are also being carried out. Packaging antimicrobials inside the liposome protect them from degradation until they are delivered at target areas for therapy (Akbarzadeh et al., 2013). A few advantages of liposomes include: low toxicity, flexibility, solubility in biological systems, biodegradability, and non-immunogenicity. However, there are a few disadvantages of liposomes that should be

considered: they are relatively unstable, have a short half-life, leakage and fusion of liposomes can occur, and production can be costly (Akbarzadeh et al., 2013). Aside from being used in drug delivery, liposomes have also been used in studies of receptor binding and fusion, for example to study attachment and fusion of enveloped viruses such as influenza or VLPs (Citovsky and Loyter, 1985; Nussbaum et al., 1992; Tuthill et al., 2006). In the case of the influenza virus where the HA protein is responsible for binding and fusion with the host cell, studies have shown that influenza virus particles are able to fuse with liposomes composed of negatively charged or neutral phospholipids (Nussbaum et al., 1992). In this study, I utilized liposomes as a cell free model to develop a liposome-VLP model system for attachment and fusion. A similar experiment was conducted to study the early steps of how the non-enveloped poliovirus enters at the cell membrane (Hogle, 2002; Bubeck et al., 2005). They too utilized cryo-electron microscopy (cryo-EM) in an attempt to elucidate key structural features in the entry process. The model system used in this thesis studies the attachment and potential fusion of Ebola VLPs with receptor-decorated liposomes, also using cryo-EM.

1.4.2 Considerations When Selecting Lipids

One issue to consider when selecting lipids is the phase transition temperature of the components. This is the temperature required to induce a change in the lipid physical state from the more ordered solid/gel phase in which the hydrocarbon chains are fully extended and packed closely, to the more disordered crystalline or liquid phase in which the hydrocarbon fatty acid chains are oriented in a more random way and fluid (Burgess et al., 1996). Several factors affect the phase transition temperature of a lipid, including the hydrocarbon chain length, the degree of unsaturation, the polarity or

charge, and species of the headgroup. As the hydrocarbon length increases, van der Waals forces between molecules become stronger, requiring more energy to disrupt the ordered packing of the fatty acids; thus, phase transition temperatures increase. Introduction of a kink in the fatty acid chain in the form of a double bond results in an ordered arrangement at lower temperatures (Burgess et al., 1996).

Another issue to consider is the stability of the lipids. Generally speaking, the unsaturation leads to easier oxidation and therefore a shorter shelf life. Lipids from biological sources tend to be polyunsaturated, and therefore less stable. However, due to this polyunsaturation, the phase transition temperature is lower, resulting in a greater ease of use during processing (Burgess et al., 1996).

The next characteristic for consideration is the charge carried by the lipid. Many biological membranes carry a net negative charge on their surface, that is generally produced by the presence of anionic phospholipids in the membrane. The following lipids exhibit a net negative charge at pH 7.0: phosphatidic acid, phosphatidylserine, phosphatidylinositol, and cardiolipin. By contrast, phosphotidylcholine, sphingomyelin, and phosphatidylethanolamine are neutral at pH 7.0 (Nelson and Cox, 2008a). Phosphatidic acid as the sole member of its head group has a net negative charge. Phosphatidic acid has a large role in biosynthesis of triacylglycerols and other phospholipids serving as the backbone of these compounds. It is one of the simplest of all phospholipids but only occurs in small amounts in biological membranes (Nelson and Cox, 2008a). Phosphatidylserine is composed of phosphatidic acid and the amino acid serine, resulting in a net negative charge. Phosphatidylserine comprises about 10% of the total phospholipids in the cell membrane and is found exclusively in the inner leaflet

(Nelson and Cox, 2008a). Phosphatidylinositol is a unique phospholipid in that the headgroup is inositol. Inositol has the unique ability to become phosphorylated at its 3', 4', and 5' carbons resulting in a net negative charge. Phosphatidylinositol comprises about 5% of the lipids in the cellular membrane and are found exclusively in the inner leaflet (Nelson and Cox, 2008a). Phosphotidylcholine has an overall neutral charge due to the combination of a positive charge on the choline and a negative charge on the phosphate of the phosphatidic acid backbone. Phosphotidylcholine is one of the most abundant phospholipids (phospholipid) in the cellular membrane where it is found to account for over 50% of the total phospholipid composition and is found primarily in the outer leaflet of the bilayer (Nelson and Cox, 2008a). Sphinogmyelin is similar to phosphotidylcholine, but unlike phosphotidylcholine, it contains a sphingosine as its unsaturated 18-carbon fatty acid. Next to phosphotidylcholine, sphingomyelin is the most abundant lipid found in the outer leaflet (Nelson and Cox, 2008a). Phosphatidylethanolamine is almost as abundant as phosphotidylcholine and sphingomyelin in lipid membranes; however, it prefers to occupy the inner leaflet of the bilayer. Since phosphatidylethanolamine exhibits a smaller headgroup taking on a more conical shape, it exerts lateral pressure on the membrane allow it to assist the membranes curvature and stabilize the membrane proteins (Nelson and Cox, 2008a). In my investigation, I used phosphatidylcholine as a constant in the liposomes due to their high prevalence in biological membranes, with the addition of either phosphatidylethanolamine in the control liposomes for stability or the NTA Nickel salt of lipids in the experimental liposomes to produced liposomes with a Ni ion on the surface.

1.4.3 Extrusion vs Sonication

Following rehydration, liposome particles can be reduced to the required liposome size by an input of mechanical energy in the form of sonication or extrusion. Sonication is outlined briefly below. However, my method of choice for the project was the extrusion technique to produce liposomes of 100 nm in diameter, since it is rapid and reproducible.

Sonication is a way of disrupting the LMVs by using ultrasound energy or waves. This method typically produces small, unilamellar vesicles (SUV) with diameters that range from 15-50 nm (Avanti Polar Lipids, 2017). The most common instrument for producing liposomes through sonication is a bath sonicator. The test tube containing the LMVs is placed in the bath sonicator for 5-10 minutes at a temperature above the phase transition temperature of the lipids in the mixture (Avanti Polar Lipids, 2017). The lipid suspension will begin to clarify and yield a transparent, yet slightly hazy solution of SUVs. The haze that appears with this method is a result of light scattering induced by residual large particles that have remained in the suspension. Centrifugation of the SUVs can be completed to yield a clear, more uniform suspension of SUVs. The average size and distribution of SUVs obtained in this method is influenced by the composition, concentration, temperature, sonication power and time, volume, and the tuning of the sonicator. For this reason, there is great batch-to-batch variability using the sonication method (Avanti Polar Lipids, 2017). As such, I did not use this method in my investigation.

Extrusion is a process by which the lipid suspension is forced through a polycarbonate filter with a defined pore size to produce liposomes approximately the

size of the pores (Avanti Polar Lipids, 2017). Prior to extrusion, LMV suspensions are disrupted by 3-5 freeze/thaw cycles; this helps to reduce clogging of the filter and also improves the size homogeneity of the resulting liposomes (Avanti Polar Lipids, 2017). As stated previously in the sonication method, extrusion of the lipid suspension should also be conducted at a temperature above the phase transition temperature to ensure the sample remains liquid at all times. Extrusion through pores of 100 nm typically results in large unilamellar vesicles (LUVs) of about 120-140 nm in diameter. However unlike sonication, the size distribution obtained from batch-to-batch is much more uniform and reproducible (Avanti Polar Lipids, 2017).

1.4.4 Nanoparticle Tracking Analysis and Nanosight NS500

In this project, the Nanosight system was used as a secondary analytical technique to confirm both liposome size and that the NPC1 receptor was bound to liposomes. The Nanosight particle characterization system uses a laser light source to illuminate nanoscale particles. The light scattering is then measured in a time resolved manner to track the particles movement and gives the size, number, and concentration of particles present in the solution (Malloy, 2011). The solution of particles is either drawn through tubing from a jar of the liquid by suction or pushed through with a syringe. Appearing on a black background, the particles being tracked appear as individual points of scattered light under Brownian motion. The Nanoparticle Tracking Analysis software tracks and sizes the particles simultaneously using a camera. As sample is running through the system, smaller particles appear as fast moving dots, while larger particles appear as slower moving dots (Malloy, 2011). The Nanoparticle Tracking Analysis software provides many advantages as a sizing system, since it

provides live views of the sample via the camera and computer monitor, can size particles down to 10 nm, and is especially applicable for the analysis of samples containing multiple sizes of particles within a single sample (Malloy, 2011).

Both the Nanosight system and other Dynamic Light Scattering (DLS) systems, measure light dispersed from particles through Brownian motion. However, DLS measures changes in scattering intensity from a bulk sample, while the Nanoparticle Tracking Analysis software measures the particles being investigated individually, thus allowing this system to overcome intensity-biased results normally obtained through DLS (Malloy, 2011).

1.5 Transmission Electron Microscopy

In the early 1930s, the first electron microscope (EM) was developed by Ernst Ruska and was described as the pinnacle of his graduate research (Dykstra and Reuss, 2003). This first electron microscope with a magnification of a mere 14.4x had an electron source, and two magnifying lenses, but no condenser and actually had less resolution than regular light microscopes of that time (Ruska, 1986). In 1939, Ruska in collaboration with the German electronics company, Siemens, built the first commercially available transmission electron microscope (TEM) (Dykstra and Reuss, 2003). By 1946, the team had created a microscope with a resolving power of 1.0 nm, a vast improvement of the 10 nm capability developed in 1939 (Dykstra and Reuss, 2003). In the 1950s and 60s, further improvements were made to lenses, mechanical controls and vacuum systems, while power supplies were refined (Dykstra and Reuss, 2003). Early microscopes were actually produced with sliding objective lenses and glass viewing screens almost horizontal to the microscopist; eventually, the standard

TEM was developed with a vertical column (Dykstra and Reuss, 2003). The 1970s and 80s saw more minor system refinements and the development of instruments capable of less than 0.2 nm resolving power (Dykstra and Reuss, 2003). EM has been used for many years and it is still used as a main means of identifying viruses based on their morphology or structure (Goldsmith and Miller, 2009).

In electron microscopy, there are many ways in which a sample can be prepared, depending mainly on the type of research that is being conducted and what question is being investigated. There are different ways to prepare grids for TEM, as well as different grids that are used for specific types of specimens. Certain combinations of grids, support films, and stains can produce artifacts in the sample that can lead to misinterpretation of the sample. Nevertheless, electron microscopy has become an important facet in medical research and diagnostics. For example, many viruses were discovered to be the cause of illnesses by using EM, such as rotavirus, norovirus, and hepatitis B to name a few. With the ability to give the researcher a broad view of what is exactly in the sample, and not needing organism specific reagents like many molecular techniques, electron microscopy has become one of the prime analyses for investigating pathology and identifying infectious diseases (Goldsmith and Miller, 2009). An advantage with EM is that samples do not have to be live or intact: EM can identify pathogens that have been preserved in samples for decades, although fresh specimens are always preferred as freezing can damage many enveloped viruses.

1.5.1 Negative Staining

Sample preparation of aqueous suspensions for TEM involves applying a small volume to a support film coated grid, ~3 mm in diameter. In negative staining, ideal grids

to use are between 200 and 400 mesh copper grids with a carbon coated polyvinyl formal (Formvar) support film. The Formvar is necessary for support of the specimen, but it must not be so thick as to degrade the resolution of the image (Curry et al., 2006); 1% Formvar is a commonly used concentration. A thin film of carbon is usually applied to provide a conducting surface that stabilizes the sample and reduces damage that is caused by illumination under an electron beam (Curry et al., 2006). The basic purpose of negative staining is to improve contrast of biological specimens. By applying a heavy metal salt to negative stain the sample, such as uranyl acetate (UA) or methylamine tungstate (MT), the negative stain dries into a layer surrounding the specimen with a more electron dense material that scatters electrons more intensely than the material of interest. There are many different metal salts that can be used, but I chose MT due to its high solubility at neutral pH and relatively low contrast for visualizing membranes (Kolodziej et al., 1997), while UA exhibits a low pH that can affect morphology. Heavy metal salts scatter the electrons and improve contrast of biological material; the specimen appears light on a dark background (Kuo., 2007).

1.5.2 Cryo-Electron Microscopy

In cryo-electron microscopy (cryo-EM), samples are preserved in their near-native state by plunge freezing a TEM grid into liquid ethane (Iancu *et al.*, 2006); if the sample was frozen quickly enough, vitrification of the water in the specimen occurs instead of crystallization (Baker et al., 1999; Dubochet et al., 1988). Vitrified ice is an amorphous solid, and biological structures are preserved. The use of cryo-EM to observe specimens such as viruses reduces artifacts such as distortion due to dehydration of the sample that may result when using methods such as negative staining (Adrian et al.,

1984; Dubochet et al., 1988). For cryo-EM, special holey supports are used such as Quantifoil® (Quantifoil Micro Tools GmbH, Jena, Germany). These grids differ from regular EM grids in that they are specially manufactured with a carbon support film that contains regularly spaced holes (of usually 2 µm) for the sample and vitreous ice to lie in. The different grades with varying hole size and spacing can be used for optimum results with specific specimen particle sizes.

One technique that can be applied to cryo-EM data is single particle imaging and three-dimensional (3D) reconstruction. This process starts with preparing vitrified samples as described above and maintaining the samples at liquid nitrogen temperature in a specific cryo-holder for EM (Tao and Zhang, 2000). Next, the cryo-holder with grid in place is transferred into the microscope. An area of the grid is found that has relatively thin vitreous ice and evenly spaced viruses. Pictures are then taken with a charge-coupled device (CCD) camera or direct electron detector (Tao and Zhang, 2000). After this, single particle images are subfiled, for example using the EMAN (Ludtke et al., 1999) software program. Then similar images are aligned, classified, and averaged (Tao and Zhang, 2000). The computer can also calculate a 3D reconstruction of the virus by using the averaged images of particles taken in different orientations. Next, the first reconstruction is used to refine the parameters of the particles and create another 3D reconstruction (Tao and Zhang, 2000). This cycle of making reconstructions and using them to refine the next one is continued until the correlation between successive reconstructions is minimized (Tao and Zhang, 2000). This type of imaging will be explored later in regards to NPC1-C decorated liposomes binding to Ebola VLPs.

Another technique that can be done with cryo-EM is cryo-electron tomography (cryo-ET). In cryo-ET, the specimen holder is tilted and images are recorded at a range of different angles. A picture of the virions in the sample is taken at increasing degrees of tilt angles to try to obtain pictures of as much of the virus as possible (Bartesaghi et al., 2008). A tilt series is taken if possible ranging from +/- 70° simply due to physical limitations of the specimen in the cryo-holder and microscope column and the increasing thickness of the specimen at the increasing tilt angles (Subramaniam et al., 2007). After the images are taken, they can be analyzed with a computer software program to generate a 3D reconstruction of the virus (Subramaniam et al., 2007).

1.6 Rationale, Hypotheses, and Objectives

1.6.1 Study Rationale

In recent years, many studies have focused on how enveloped viruses, such as Ebola virus, enter host cells. A major goal of these studies is the development of therapeutics that would target this event (White and Schornberg, 2012). The GP of Ebola virus plays a big role in cell entry, and the discovery of the role of NPC1 as a receptor in this process has recently come to light (White and Schornberg, 2012). One study reported that low pH was required for fusion of the Ebola virus envelope with target membranes, but the likely reason that low pH is required is for optimal protease activity of cathepsins L and B that must cleave GP prior to fusion (White et al., 2008). One interpretation of this statement is that perhaps low pH is not strictly required for fusion to occur, but simply required to prime GP to a fusion-competent state. If this is the case, could fusion of the Ebola virus envelope with target membranes occur at neutral pH?

1.6.2 Hypotheses

A cell free system can be developed that models attachment and fusion between viral and cellular membranes. The use of VLPs and receptor-decorated liposomes will allow the study of the dynamics of the attachment and fusion process and allow for the investigation of factors such as pH that may trigger fusion. Development of this system will allow future experiments to investigate how viruses attach to host cells and how viral envelopes fuse with cellular membranes to start an infection. Such studies may identify new targets for potential antiviral therapeutic strategies. In addition, the use of this system along with the technique of cryo-EM, allows the visualization of time-resolved intermediate structures that may form during the attachment and fusion processes of a viral infection. Therefore the use of this approach has the potential to greatly increase our understanding of how the process of attachment and membrane fusion occurs across all Class I viral fusion proteins.

1.6.3 Objectives

The main objective of this project was to investigate the dynamics of virus-host receptor attachment and fusion. I produced VLPs and liposomes containing the viral receptor on their surface for use in experiments to model virus attachment and entry. I expressed and purified NPC1-C and chemically linked this to the liposome. The roles of pH, cathepsins, GP, and NPC1 in triggering attachment and fusion between the VLP membrane and the liposome membrane were investigated. The objective was to capture images of structures at various stages of attachment and fusion using cryo-EM.

2. Materials and Methods

2.1 Gene Design

Using the GenBank Accession # HV753274 for the full length GP of Ebola virus, a version of the EBOV GP gene lacking the mucin-like domain (GPΔmuc) was generated by deleting the MLD portion of the sequence from the full sequence as was previously done by Lee et al., 2008. Amino acid residues 312-462, corresponding to the MLD, were removed prior to submission of the sequence to Genscript U.S.A. Inc. (Piscataway, New Jersey, U.S.A.). The EBOV full length GP cDNA (GenBank Accession # HV753274), and the MLD-deleted form of GP were individually synthesized by Genscript U.S.A. Inc., with the inclusion of restriction endonuclease sites for subcloning into expression vectors (Table 1).

Table 1: Restriction Endonucleases Used for Gene Insertion

Gene	Restriction Endonuclease
GP	BamHI, NdeI
GPΔmuc	BamHI, NdeI
VP40	EcoRI, XhoI
NPC1	EcoRI/ApoI, ApoI
NPC1 stable	XbaI, BamHI

The gene encoding EBOV VP40 (GenBank Accession # EU224440.2) was synthesized as cDNA including restriction endonuclease sites by Genscript Inc. The VP40 gene was then subcloned by Genscript into the pCAGGs expression vector,

generously donated by Darwyn Kobasa of the National Microbiology Laboratory (NML) (Table 1) (Kobasa et al., 1997; Niwa et al., 1991).

For the purposes of this thesis, we utilized the luminal domain C of NPC1 only (Deffieu and Pfeffer, 2011). In order to utilize just one luminal domain, modifications had to be made to provide a stable structure to this protein in the absence of transmembrane domains and to facilitate secretion of the protein. The clone was designed from N-terminus to C-terminus as follows: a signal peptide as a secretory signal, a FLAG-tag, and a His-tag, followed by the NPC1-C domain flanked on either side by an anti-parallel α-helix coiled-coil (Deffieu and Pfeffer, 2011). The alpha-helical sequences are characterized by a heptad repeat of ordered amino acid residues lettered A through G and A' through G' on the opposite coil for explanations sake, where A and D are apolar residues, and E and G are charged residues (McClain et al., 2001). The residues that are situated at these four positions are able to participate in interhelical hydrophobic and Coulombic interactions. In an anti-parallel α-helix coiled-coil, G residues interact with G' residues and E residues interact with E' residues (McClain et al., 2001). The specific residues that comprise the α-helices of the coiled-coils used for NPC1-C are described below. Figure 4 depicts a model of the NPC1-C design and how these coiled-coils fold to provide stability to the structure.

Domain C of the NPC1 receptor, residues 372 to 622 (GenBank Accession AAB63372.1), along with an N-terminal DYKDDDDK (Flag) tag and Histidine tag (His-tag) and two anti-parallel flanking alpha helices, (Deffieu and Pfeffer, 2011; McClain et al., 2001) was synthesized including restriction endonuclease sites by Genscript Inc. The exact sequence was as follows: MSALLILALVGAAVADYKDDDDK

LAAANSSIDLMGSSHHHHHHSSGLVPRGSHMKRLEKELAQLEAELEELESKLWHLENE NARLEKELAELEAELAESSS (Deffieu and Pfeffer, 2011). Genscript then subcloned the entire construct into the pCAGGs expression vector, generously donated by Darwyn Kobasa (NML). This construct was designed and ordered by a previous student.

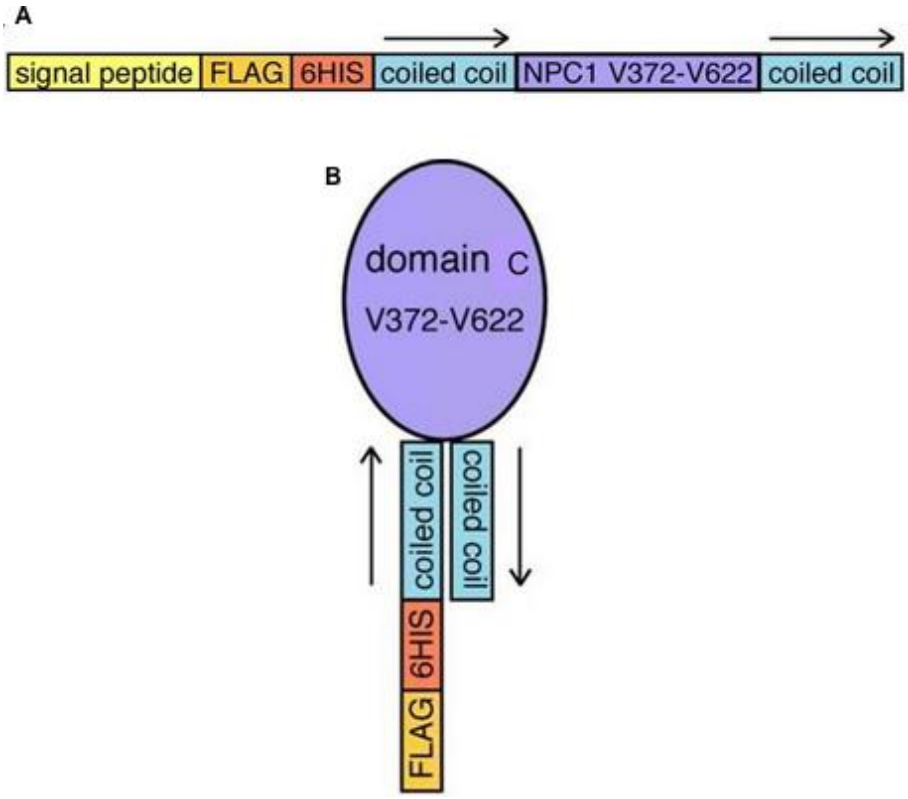

Figure 4. Designing of a soluble NPC1 domain C. (A) depicts the arrangement of the construct, including anti-parallel α-helix coiled-coils for stability. (B) depicts how the construct folds when the anti-parallel α-helix coiled coils interact with one another to provide stability to the soluble NPC1-C. Open-access figure reproduced from **(Deffieu and Pfeffer, 2011)**.

2.2 Plasmids and Cloning

2.2.1 GP

The GP protein of Ebola was cloned into the expression vector pcDNA3.1+ (Thermo Fisher Scientific, Waltham, U.S.A.) using blunt ended cloning. pcDNA3.1+ was first linearized using *EcoRV*. The two versions of the GP, the full GP (GPFull) or the mucin-deleted version of GP (GP∆muc), were produced using the restriction endonucleases indicated in Table 1. The full DNA and amino acid sequence of the GP gene is shown in Supplementary Figure 1, with the glycan cap, MLD, and furin cleavage site indicated. Following gel extraction using the kit Qiaex II® (Qiagen Inc., Hilden, Germany), the gene fragment of interest and the linearized expression vector were ligated overnight at 16°C.

2.2.2 Plasmid verification and propagation

The following protocol was used for plasmids cloned at the NML, as well as plasmids received custom cloned by Genscript. Following ligation or receipt of the plasmids containing the genes of interest, the plasmids were initially propagated using One Shot TOP10 Chemically Competent *E. coli* cells (Thermo Fisher Scientific) using 50 ng of plasmid per 25 µL *E. coli*. Plasmids and *E. coli* were incubated on ice for 30 minutes, followed by a heat shock for 30 seconds at 42°C. After heat shock, the samples were incubated on ice for 2 minutes, S.O.C. medium was added, and the samples were incubated at 37°C for 1 hour with shaking. After initial growth, the samples were spread on Luria Bertani (LB) Lennox agar plates containing 200 µg/mL carbenicilin made by the media department at the NML. Plates were incubated

overnight at 37°C, followed by single colonies being picked and re-streaked onto new LB carbenicillin plates to confirm growth.

Following growth on LB carbenicillin plates, a single colony from a confirmation plate was used to inoculate 3 mL of LB broth containing 100 µg/mL ampicillin, also produced in house. *E. coli* was allowed to grown overnight at 37°C with shaking at ~200 rpm. These 3 mL growth suspensions were then used along with the QIAprep® Spin Miniprep Kit (Qiagen) to prepare plasmids for use in future experiments. Final recovered DNA was eluted into 50 µL nuclease free water (Thermo Fisher Scientific). Concentrations of the isolated DNA samples were determined using the Nanodrop Spectrophotometer ND-1000 and Nanodrop Software (Thermo Fisher Scientific) and sent to the DNA Core facility at the NML for sequence confirmation.

Following sequence confirmation, plasmids were further propagated using the EndoFree® Plasmid Maxi Kit (Qiagen). A single colony from the confirmation plates was used to inoculate 100 mL of LB Ampicillin broth. The suspensions were allowed to grow overnight at 37°C with shaking at ~200 rpm. Bacteria were pelleted at 6,000 xg for 15 minutes at 4°C, followed by resuspension, lysis, and filtration as per the EndoFree Plasmid Maxi kit protocol. Isolated plasmid DNA was finally re-dissolved in 100 µL of nuclease free water (Thermo Fisher Scientific) and stored at -20°C. Final DNA concentrations were determined using the Nanodrop Spectrophotometer ND-1000 and Nanodrop Software (Thermo Fisher Scientific). Plasmids were diluted to 400 ng/ µL and stored at -20°C until further use in transfections.

2.2.3 NPC1-C Clone Production

To obtain NPC1-C receptor in the amounts required for the project, I opted to create a stable cell line expressing NPC1-C. The entire DNA and amino acid sequence of the construct is shown in Supplementary Figure 2. The construct described above (MSALLILALVGAAVADYKDDDDKLAAANSSIDLMGSSHHHHHHSSGLVPRGSHMKRL EKELAQLEAELEELESKLWHLENENARLEKELAELEAELAESSS) was used as template for amplification by the polymerase chain reaction (PCR). Reactions were as listed in Table 2.

Table 2. PCR Components for NPC1-C Cloning

Component	Volume
Water	32.5 ul
10 X iProof buffer	10.0 ul
Primer 1118F (10 uM)	2.5 ul
Primer 1117R (10 uM)	2.5 ul
10 mM DNTP mix	1.0 ul
Template (1ng/ul)	1.0 ul
iProof Polymerase (BioRad)	0.5 ul
Total	**50.0 ul**

Primer 1118F = 5’ CACAtctagaGCCACCATGAGCGCGCTGCTGATTCTGGC) containing an XbaI site (lower case).
Primer 1117R = 5’ ACACggatccTATTCCGCCAGTTTCGCTTTCAGTTC) containing a BamHI site (lower case).

Following PCR cleanup, PCR amplicons and the expression vector, pLentiHygro (pCDH-CMV-MCS-EF1-Hygro) (System BioSciences, cat# CD515B-1), were digested

overnight with XbaI and BamHI. The next day, samples were separated by electrophoresis on a 0.7% TBE agarose gel and the bands were purified using the QIAEX II gel extraction kit (Qiagen). The insert and vector were ligated together overnight at 18°C for 4 hours before storing at 4^{o}C. The following day, ligation products were introduced into One Shot TOP10 Chemically Competent *E. coli* cells (Thermo Fisher Scientific), plated on LB-carbenicillin (200 ug/mL) plates then allowed to grow overnight at 37°C.

Colonies were picked the following morning and streaked onto another plate and used to inoculate 3 mL of LB-Ampicillin broth. *E. coli* was allowed to grow overnight at 37°C with shaking. The next day, the plasmids were isolated from *E. coli* using the QIAprep® Spin Miniprep Kit (Qiagen) and samples were submitted to the DNA Core Facility (NML) for DNA sequence confirmation. Large scale plasmid preparations were prepared by growing the transformed bacteria in LB broth containing ampicillin (100 ug/mL final). Plasmid isolation and purification was performed using the Plasmid Plus Midi Prep system (Qiagen) as described by the manufacturer.

2.3 Cell Culture

2.3.1 Maintenance of 293TN cells

Human embryonic kidney (HEK) 293TN cells were maintained in Dulbecco's Modified Eagle's Medium (DMEM; Thermo Fisher Scientific) supplemented with 10% Fetal Bovine Serum (FBS; Thermo Fisher Scientific) and 1x Penicillin-Streptomycin-L-Glutamine (PSG; Thermo Fisher Scientific) at 37°C with 5% CO_2. Cells were split 1 in 40 approximately every 3-4 days by washing with 1x Phosphate buffered saline (PBS;

Thermo Fisher Scientific), treatment with 2ml of TrypLE Express (Thermo Fisher Scientific), followed by neutralization with 8ml supplemented DMEM.

2.3.2 NPC1-C Stable Cell Line Production

To begin, HEK 293 TN cells (System Biosciences (SBI), Palo Alto, U.S.A.) were plated the day before at $2x10^6$ cells/10 mL in a 15 cm dish in DMEM supplemented with 10% FBS and 1X PSG (Thermo Fisher Scientific). Cells were then transfected with NPC1-C DNA using X-tremeGene HP (Roche Molecular diagnostics, Pleasanton, U.S.A.) along with a packaging mixture (SBI), to make Lentivirus-NPC1-C. The reagent mixture is shown in Table 3. The XtremeGene HP reagent was briefly vortexed, 30 µL was added to the DNA mixture, and the mixture was vortexed for 10 seconds, followed by a 15-minute incubation. The DNA mixture was then added to the cells drop wise and the plates were rocked gently to distribute the DNA, followed by incubating at 37°C for 48 hours.

Table 3. DNA Transfection for Stable Cell Line Production

Reagent	10 cm dish
DMEM (serum and antibiotic free)	1 mL
Lenti Expression Vector containing insert	1.7 µg
Packaging – gag/pol (11100 bp) plasmid rev (5500 bp) plasmid VSV-G (5900 bp) plasmid	2.8 µg 2.8 µg 2.7 µg

The next step in stable cell line formation was to isolate and concentrate the virus particles. The cell supernatant (10 mL) was filtered through a 10 mL syringe fitted with a 0.45 µm cellulose acetate filter. Next, 3.5 mL of RetroX Concentrator (Takara Bio U.S.A.

Inc, Mountain View, U.S.A.) was added to the filtered supernatant and mixed by pipetting up and down. This mixture was parafilmed and left at 4°C overnight to allow virus to precipitate. The following morning, the samples were centrifuged at 1,500 xg in a JS 7.5 rotor (Beckman Coulter, Brea, U.S.A.) for 40 minutes at 4°C. Supernatant was removed, and the Lentiviral pellet was resuspended in 1 mL DMEM supplemented with 10% FBS and 1x PSG (Thermo Fisher Scientific). Virus was then aliquoted in 100-200 µL samples in cryovials and stored at -80°C until further use.

On the day prior to infection, 293TN cells were plated in a 24 well plate at $0.5x10^5$cells/well to result in a density of approximately 50% the following day. The next day, 180 µL DMEM supplemented with 10% FBS and 1x PSG (Thermo Fisher Scientific), 20 µL virus inoculum, and 3.2 µL 0.5 mg/mL polybrene were mixed together. Medium was then removed from the cells and replaced with the virus mixture; plates were rocked every hour to ensure the cells remained in contact with the media. Approximately 8 hours later, 0.8 mL of pre-warmed DMEM supplemented with 10% FBS and 1x PSG (Thermo Fisher Scientific) was added to each well. Plates were incubated at 37°C with 5% CO_2 overnight. The next morning, the virus mixture was removed, cells were washed with medium, and 1 mL of DMEM supplemented with 10% FBS and 1x PSG (Thermo Fisher Scientific) was added to the cells and incubation continued. Three days post-infection, cells stably expressing the selective marker, hygromycin, were selected for by adding 300 µg/mL hygromycin and passaging the cells for 10 days, splitting the cells when they had reached 80% confluency. Surviving cells could now be propagated and NPC1-C could be purified from the cell culture supernatant.

After assessing the amount of secreted NPC1-C, resistant cells were subjected to a second round of selection this time using 600 ug/mL hygromycin for 10 days resulting in a higher level of protein production. These cells were subsequently used to purify NPC1-C and were designated 293TN–NPC1-C-Rx-SC.

To ensure that the stable cell line was created successfully, this experiment was done in conjunction with the creation of a stable cell line expressing Green Fluorescent Protein (GFP).

While retroviral vectors do provide an efficient way of introducing stable DNA to a cell line, retroviral vectors are limiting in that they are only capable of infecting cells that are actively dividing (Reiser et al., 1996). Lentiviral vectors however, a subset of retroviral vectors, are capable of transduction of any cell type, regardless of the current cell cycle stage (Reiser et al., 1996). These vectors are most often constructed using the HIV-1 provirus pseudotyped with the VSV-G protein coat, which due to its binding mechanism, is highly effective when transducing a large variety of cell types (Reiser et al., 1996). For this reason, the production of the NPC1-C stable cell line for this experiment utilized a Lentiviral expression system. According to the NIH, the major safety risk concerning the use of Lentiviral vectors is the potential generation of replication-competent lentivirus (National Institute of Health, 2006). To address the concern of generation of replication-competent lentivirus, the components required for lentivirus production are split across multiple plasmids. Both second and third generation systems use the transfer plasmid containing the gene of interest, but beyond this, the packaging genes are split across 2 (second generation) or 3 (third generation) plasmids (Addgene, 2017). Unless a recombination event occurs between the

packaging, envelope, and transfer vectors, and the subsequent construct is packaged into a viral particle, it is impossible for most viruses produced in this manner to produce more virus after the initial infection (Addgene, 2017). The second generation system involves one packaging plasmid encoding gag, pol, and rev and an envelope plasmid encoding VSV-G, while the third generation system has two packaging plasmids: one encoding gag and pol and the other encoding rev, as well as an envelope plasmid encoding VSV-G (Addgene, 2017). Therefore, third generation systems are considered to be the safest system. While the third generation system can be more difficult since transfection of a total of four plasmids is required (Addgene, 2017), this system was used to produce the NPC1-C stable cell line due to the lowest possible hazard risk from a biosafety standpoint.

For re-cloning NPC1-C into a Lentiviral expression vector, two options were available in the laboratory: pLentiNeo and pLentiHygro. These vectors utilize neomycin and hygromycin resistance, respectively, for selection of recombinants. The vector pLentiHygro was used since the cell line being used (HEK 293TN) – was resistant to neomycin. Thus, hygromycin was used to select for recombinants expressing NPC1-C. The first round of hygromycin selection used 300 μg/mL hygromycin, this concentration was previously determined using a kill curve that showed the lowest dose that kills all of this particular cell line. To produce clones that expressed NPC1-C at higher levels, a second round of hygromycin selection was applied using 600 μg/mL hygromycin.

2.3.3 Maintenance and Harvest of 293TN-NPC1-C-Rx-SC cells

293TN-NPC1-Rx-SC cells were maintained in DMEM (Thermo Fisher Scientific) supplemented with 10% FBS (Thermo Fisher Scientific) and 1x PSG (Thermo Fisher Scientific) at 37°C with 5% CO_2. Cells were split 1 in 40 approximately every 3-4 days by washing with 1x Phosphate buffered saline (PBS; Thermo Fisher Scientific), treatment with 2ml of TrypLE Express (Thermo Fisher Scientific), followed by neutralization with 8ml supplemented DMEM.

In order for scaling up to collect greater volumes of supernatant containing NPC1-C, cells were plated at $1x10^7$cells/plate in DMEM supplemented with 5% FBS and 1x PSG (Thermo Fisher Scientific) in 15 cm dishes. After 4 days of growth, the supernatant was collected and fresh DMEM supplemented with 5% FBS and 1x PSG (Thermo Fisher Scientific) was added back to the plates and the cells were allowed to grow for another 3-4 days, after which the final batch of NPC1-C-containing supernatant was collected.

The supernatant containing NPC1-C was vacuum filtered through a 0.22 µm bottle topped filter apparatus and set aside at 4°C until ready for purification.

2.4 VLP Transfection

Twenty-four hours prior to transfection, 10 mL of HEK 293TN cells were plated at a concentration of $2x10^5$ cells/mL into Corning® CellBIND® 75cm^2 flasks (Corning Inc., Corning, U.S.A.). Transfections were completed using the Effectene Transfection Reagent (Qiagen) and volumes were scaled up for T75 flasks (Table 4). Plasmids were mixed with the required amount of Buffer EC and Enhancer and allowed to incubate for 2-5 minutes at room temperature (Table 4). After the required time had elapsed, the

appropriate amount of effectene was added to the mixture and transfection complex formation was allowed to occur by incubating the mixture for 5-10 minutes at room temperature. During this incubation, the cells were washed with 5 mL DMEM supplemented with 10% FBS and 1x PSG and media was replaced with 10 mL of supplemented DMEM. Next, 4 mL of supplemented DMEM was added to the transfection complexes, and this final suspension was gently added to the flask of cells. Transfected cells were incubated at 37°C with 5% CO_2. After incubating, for 24 hours, a further 10 mL of supplemented DMEM was added to each flask and the cells were incubated another 24 hours. The cell culture supernatant containing VLPs was harvested after a total of 48 hours had elapsed.

Table 4. Effectene Transfection Reagent Volumes for T75 flasks

Qiagen Effectene Transfection Reagent	Volume or Concentration	Example of VP40/GP Transfection
DNA	3.5-7 µg	VP40 3.5 µg GP 3.5 µg
Enhancer	Total DNA (µg) x 8	7 x 8 = 56 µL
Buffer EC	= 500 µL – volume of DNA (µL) – volume of enhancer (µL)	= 500 µL – volume of plasmids – 56 µL
Effectene	Total DNA (µg) x 25	7 x 25 = 175 µL
Media to transfection complexes	4 mL	4 mL
Media to cells	10 mL	10 mL

2.5 VLP Isolation and Purification

48 hours post-transfection, cell culture supernatant containing VLPs was harvested and clarified in a 50 mL centrifuge tube by centrifugation at 1500 rpm (360

xg) for 5 minutes at 4°C. Clarified supernatant (28 mL) was layered onto a sucrose cushion of 20% sucrose in Tris/NaCl/EDTA buffer (TNE buffer) (10 mL) in a 38 mL ultracentrifuge tube. Sucrose cushions were ultracentrifuged at 15,100 rpm (28,000 xg) for 2 hours at 4°C in the SW32 rotor (Beckman Coulter). The pellets of VLPs were gently washed and resuspended in Tris/NaCl/$CaCl_2$ (ThermoBuffer) and stored at 4°C (Melito et al., 2008).

2.6 VLP Thermolysin Digestion

Following VLP isolation and purification, both GPFull and GPΔmuc VLPs were cleaved using thermolysin to expose the receptor binding site. To measure the concentration of the isolated VLPs, a bicinchoninic acid (BCA) assay using the Pierce™ BCA Protein Assay Kit (Thermo Fisher Scientific) was initially done on preparations of the two VLP forms. The concentration was read using the NanoDrop 2000 Spectrophotometer (Thermo Fisher Scientific). The VLPs were cleaved with thermolysin (Sigma-Aldrich) at a ratio of 1 part thermolysin to 8 parts VLPs at 37°C for 5 minutes. Phosphoramidon (Santa Cruz Biotechnology, Dallas, U.S.A.) was then added to a concentration of 500µM and allowed to incubate for 10 minutes at room temperature to stop the reaction.

2.7 NPC1 Purification

2.7.1 Purification by Dynabeads

Before moving on to full-scale purification of NPC1 from cell culture supernatant, we first did small-scale purifications using the Dynabeads His-tag Isolation and Pull-down system (Thermo Fisher Scientific). This was utilized as a quick check to confirm that the initial clone was correctly expressing NPC1-C, and that the His-tag was

functional. Dynabeads were fully resuspended and 50 µL was added to a tube and the tube was placed on the DynaMag (Thermo Fisher Scientific) for 2 minutes, then supernatant was removed. Sample was added to the beads and mixed on the Hula mixer (Thermo Fisher Scientific) for 5 minutes at room temperature. The tube was then placed on the magnet for 2 minutes and supernatant was removed. The beads were then washed 4 times with binding/wash buffer and the purified protein was eluted into 100 µL His-elution buffer. Samples were run by sodium dodecyl sulfate polyacrylamide gel electrophoresis (SDS-PAGE) and Coomassie stained and Western blotted to confirm the NPC1-C had been purified.

2.7.2 Purification by HPLC

The HisPur Co^{2+} affinity column for high performance liquid chromatography (HPLC) was chosen for large scale purifications. This column is a tetradentate chelating agarose resin charged with divalent Cobalt ions to obtain purity without metal contamination (Thermo Fisher Scientific, 2012). Compared to Ni^{2+} columns, His-tagged proteins were bound with greater specificity and could be released with gentler conditions using a lower concentration of imidazole using the HisPur Co^{2+}. Specifically, the HISTrap Excel Affinity column is a Ni^{2+} based column requiring a concentration between 0.5 M and 1 M imidazole to elute bound proteins off of the column (GE Healthcare Life Sciences, 2012), while the HisPur Co^{2+} column only requires a concentration of 0.15 M imidazole to elute proteins off of the column (Thermo Fisher Scientific, 2012). This cobalt column maximizes protein purity without sacrificing protein yield and also binds fewer non-specific proteins and displays less metal leaching (Thermo Fisher Scientific, 2012). While the downstream experiments with NPC1-C will

be using an interaction between Ni and histidine due to the limited options for chelating lipids, it was decided to use a cobalt column for purification due to the benefits over nickel described above. After purifying the NPC1-C using this column, fractions were analyzed by SDS-PAGE silver staining, and western blot to establish purity.

Samples were first purified using the HisPur Co^{2+} column (Thermo Fisher Scientific) by initially diluting the sample in an equal amount of Buffer A plus a small amount of Buffer B (components are as listed in Table 5).

Table 5. HPLC Buffers

Ingredient	HisPur Co^{2+} Buffer A	HisPur Co^{2+} Buffer B	HiTrap Desalt Buffer
$NaPO_4$	50 mM	50 mM	8.06 mM
NaCl	0.3 M	0.3 M	137.93 mM
Imidazole	-	0.15 M	-

The column was washed and the sample was applied to the column using the P-960 pump. The His-tag on the NPC1-C became bound to the Co^{2+} in the column resin, and after the sample was loaded, the percent of Buffer B was increased gradually to allow the imidazole in Buffer B to outcompete the NPC1-C for the Co^{2+} resin, allowing the NPC1-C to be eluted off of the column in buffer consisting of $NaPO_4$, imidazole, and about 300 mM NaCl.

After determining that the product was pure, fractions were pooled and loaded onto the Resource Q Anion Exchange column. This column in particular exhibited quaternary ammonia bound to the column. With the column being positively charged, negatively charged molecules would bind to the column (Duong-Ly and Gabelli, 2014).

Since it was unknown whether or not NPC1-C was positively or negatively charged at that point, both cation and anion exchange columns were initially tried. Once the NPC1-C was bound, it was eluted off of the column by an increasing concentration of NaCl, beginning at 20 mM and ending at 1 M NaCl. The chloride ions compete with the NPC1-C, thereby eluting the NPC1-C off of the column (Duong-Ly and Gabelli, 2014). While this column did increase purity of NPC1-C, because it also resulted in a lower yield of protein, this column was not utilized in any further experiments.

Following the HisPur Co^{2+} column, the eluted fractions containing NPC1-C were desalted using the HiTrap™ desalting column. The HiTrap Desalt column is a desalting and buffer exchange column that is often used as a faster form of dialysis after other chromatographic steps (GE Healthcare Life Sciences, 2014). The column is packed with sephadex G-25 that performs a group separation between high and low molecular weight substances. In this way, proteins are separated from low molecular weight proteins as well as NaCl (GE Healthcare Life Sciences, 2014). Therefore, further purifications were completed using only the HisPur Co^{2+} column, followed by the HiTrap Desalt column to elute the NPC1-C receptor protein in PBS.The column was equilibrated with buffer (Table 5) and the sample was run through the column, resulting in collection of desalted fractions. The finished product was then analyzed for purity by Coomassie and/or Silver stain SDS-PAGE gel.

After completion of all column purifications by HPLC, the NPC1-C receptor was concentrated to a more desirable working concentration using the Amicon Ultra 4 Centrifugal Filter Unit, 30K cut-off (Millipore Canada Ltd., Etobicoke, Canada). The concentration in mg/mL was determined by conducting a BCA Assay on the

concentrated product with the Pierce™ BCA Protein Assay Kit (Thermo Fisher Scientific).

2.8 SDS-PAGE

Samples were prepared by mixing 6.5 µL sample with 2.5 µL NuPAGE LDS sample buffer (4X) (Thermo Fisher Scientific) and 1 µL NuPAGE Reducing Agent (Thermo Fisher Scientific) and heating the samples at 70°C for 10 minutes. Samples were then loaded onto a 4-12% Bis-Tris SDS-PAGE gel (Thermo Fisher Scientific) and run in 1X MES running buffer (Thermo Fisher Scientific) for ~1 hour at 160 volts.

2.8.1 Coomassie staining

Immediately following gel electrophoresis, gels were washed 3 times for 5 minutes each in Milli-Q water and then stained using Coomassie Blue Simply Blue SafeStain (Thermo Fisher Scientific) for 1 hour with shaking. Gels were destained overnight with Milli-Q water and imaged using the Gel Doc™ Easy Imager (Bio-Rad Laboratories Inc., Hercules, U.S.A.).

2.8.2 Silver Staining

Immediately following gel electrophoresis, gels were treated as per the PlusOne Silver staining kit, protein protocol (GE Healthcare Life Sciences, Mississauga, Canada). Gels were fixed in 40% ethanol for 30 minutes, followed by incubations in sensitizing solution for 30 minutes, silver solution for 20 minutes, developing solution for 2 to 5 minutes, stopping solution for 10 minutes, washing with Milli-Q water 3 times for 5 minutes each, and preserving solution for at least 20 minutes. Finally, gels were imaged using the Gel Doc™ Easy Imager (Bio-Rad Laboratories Inc.).

2.9 Western Immunoblotting

Following SDS-PAGE electrophoresis, gels were transferred to polyvinylidene difluoride (PVDF) membranes using the iBlot Gel Transfer System, program 3 (Thermo Fisher Scientific). Over the course of this project, two immunoblotting techniques were used. Proteins were detected using either horseradish peroxidase (HRP) chemiluminescence or infrared (IR) technology. Transfer membranes were blocked for 1 hour at room temperature with either 5% skim milk in Tris Buffered Saline plus 0.1% Tween 20 (TBS-T) or Odyssey Blocking Buffer (Li-Cor Biosciences, Lincoln, U.S.A.) in Tris Buffered Saline (TBS). Blocking buffer was then removed and primary antibody was diluted in fresh blocking buffer, including Tween 20 in both cases, and the membranes were incubated at 4°C overnight with shaking. The next day, membranes were washed 3 times with TBS-T for 5 minutes each and incubated with secondary antibody for 1 hour at room temperature, with the addition of 0.01% sodium dodecyl sulfate (SDS) and kept in the dark during this step if using the infrared method. The membranes were then washed 3-6 times with TBS-T and/or TBS. For the chemiluminescent method, West Pico Super Signal Chemiluminescent substrate (Thermo Fisher Scientific) was added and allowed to incubate for 5 minutes at room temperature, and imaged immediately. For the infrared method, the membrane was wrapped in kimwipes and tin foil after washing and stored at 4°C until imaging. The chemiluminescent system was imaged using either X-ray film and the developer SRX-201A (Konica Minolta Healthcare Americas Inc., Wayne, U.S.A.) or using the Bio-Rad ChemiDoc imager (Bio-Rad Laboratories Inc.).Membranes were imaged using the Bio-Rad ChemiDoc imager (Bio-Rad Laboratories Inc.) when using the infrared detection system.

Throughout the course of this project, four primary antibodies were used: rabbit anti-EBOV GP (Cat #0301-015, IBT Bioservices, Rockville, U.S.A.) at 1 µg/mL, mouse anti-ZEBOV GPdTM mAb (4F3) (Cat #0201-020, IBT Bioservices) at 0.5 µg/mL, rabbit anti-EBOV VP40 pAb (Cat #0301-010) at 0.5 µg/mL, and Mouse anti-DYKDDDDK Tag Antibody, mAb (Genscript Inc.) at 0.5 µg/mL.

For chemiluminescent Western blots, goat anti-mouse IgG2a heavy chain (HRP) (ab98598, Abcam Inc., Toronto, Canada) and goat anti-rabbit IgG H&L (HRP) (ab205718, Abcam Inc.) were used at a 1/5000 dilution. For the IR Western blots, goat anti-mouse IRDye680LT (LIC-926-68020, Mandel Scientific, Guelph, Canada) and goat anti-rabbit IRDye800CW (LIC-926-32211, Mandel Scientific) were used at a ratio of 1/20,000.

2.10 Mass Spectrometry Protein Identification

Following SDS-PAGE and Coomassie staining, bands suspected to be VP40, GP, or NPC1 were sliced out of the gel and aliquoted into separate microcentrifuge tubes containing ddH_2O. In-gel digestion was performed on the bands to reduce and alkylate the protein using dithiothreitol and iodoacetamide (Sigma-Aldrich). The proteins were then digested with trypsin (Promega Corporation, Madison, U.S.A.) and the peptides were run on the Orbitrap XL Mass Spectrometer (MS) (Thermo Fisher Scientific). The resulting output data was then analyzed using Scaffold software (Proteome Software Inc., Oregon, U.S.A.) and proteins were identified using either the full SwissProt database or the virus specific SwissProt database.

2.11 Liposome Preparation

When deciding the composition for the liposomes, in my experiments, the main consideration regarding the phase temperature was that the lipids needed to be in the disordered liquid crystalline stage at all points of the experiment so that manipulations of volumes can be completed. As such, I chose lipids that had relatively low phase transition temperatures, allowing me to work easily with them at room temperature and at 4°C. In regards to the stability of the lipids, I decided to use only monounsaturated lipids. Unsaturation in a lipid results in an increased stability, and a lower phase transition temperature to keep the lipid in the liquid crystalline phase. However, unsaturation also results in a shorter shelf life of the lipid. The use of monounsaturated lipids over polyunsaturated lipids and saturated lipids allows for some stability over saturated lipids, but also ease of use by having a lower phase transition temperature than polyunsaturated lipids (Burgess et al., 1996).

Liposomes were prepared by combining various lipids together in specific ratios, followed by extrusion through a membrane of a defined pore size. Phospholipids in chloroform were ordered from Avanti Polar Lipids Inc., Alabaster, U.S.A., and combined in glass screw capped culture tubes as described in Table 6. After combination, the phospholipid mixture was dried under a gentle stream of argon gas to evaporate the chloroform, and then dried for an additional hour under a speed-vac, using the CentriVap DNA Vacuum Concentrator (Labconco, Kansas City, U.S.A.), at room temperature. Phospholipid mixtures were then stored at -20°C until ready for use.

The structure of the DGS Ni-NTA salt of lipids is shown in Figure 5. The salt of lipids has been widely used to bind a receptor to a liposome via a Ni-His-tag interaction

in experiments studying the interaction of receptors and proteins (Chikh et al., 2002; Tuthill et al., 2006). In this compound, the NTA chelating agent acts as a bridge between the Ni and the fatty acid chains, thereby attaching the Ni to the lipid via the chelator.

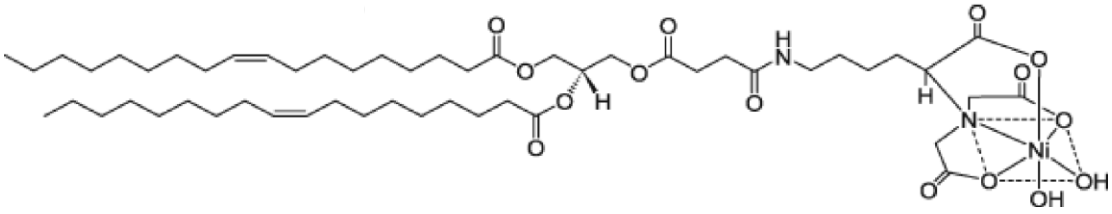

Figure 5. Chemical structure of the DGS Ni-NTA salt of lipids. Figure reproduced with permission from (Avanti Polar Lipids Inc.).

Table 6. Amount of Phospholipids for Phospholipid mixture

Phospholipid	mg or µL	µmole
18:1 (Δ9-cis) phosphatidylcholine (DOPC)	3.95 mg	5.02 µmole
18:1 DGS-NTA (Ni) or 18:1 (Δ9-cis) phosphatidylethanolamine (DOPE)	1.33 mg	1.26 µmole
18:1 Lissamine/Rhodamine phosphatidylethanolamine	0.0411 mg	0.0316 µmole

In order to produce liposomes for this project, there are two main methods to consider. The first method is sonication. Sonication uses ultrasound waves to disrupt LMVs and produce SUVs (Avanti Polar Lipids, 2017). However, the average size and distribution of SUVs obtained using sonication is influenced by many variables, including the composition, concentration, temperature, sonication power and time, volume, and the tuning of the sonicator. Sonication usually results in SUVs of about 15-

50 nm in diameter (Avanti Polar Lipids, 2017). Therefore, there is a large degree of variability between batches when using the sonication method to prepare liposomes (Avanti Polar Lipids, 2017). For this experiment, I needed to produce liposomes with a high degree of consistency in diameter from batch-to-batch, in order to accomplish this, a method other than sonication was needed.

The extrusion method of producing liposomes involves forcing a suspension of lipids through a polycarbonate filter with a defined pore size, the resulting liposomes have an approximate diameter equal to that of the pore of the polycarbonate filter (Avanti Polar Lipids, 2017). However unlike sonication, the size distribution obtained from batch-to-batch is much more uniform and reproducible (Avanti Polar Lipids, 2017). For example, extrusion through pores of 100 nm typically results in large unilamellar vesicles (LUVs) of about 120-140 nm in diameter.

A tube of dried down phospholipid mixture was removed from the -20°C freezer and 2.6 mL of PBS (Thermo Fisher Scientific) was added to the mixture and allowed to incubate overnight with vigorous shaking at room temperature. The following morning, the tube was vortexed vigorously to resuspend the phospholipid in the PBS, resulting in a pink, milky mixture. The suspension was freeze-thawed 3 times by flash freezing in a dry ice/ethanol bath and rapid thawing in a 37°C water bath. The Mini-extruder (Avanti Polar Lipids Inc.) was then assembled according to the instructions and as shown in Figure 6A. The phospholipid mixture was then loaded into a 1 mL gas-tight Hamilton syringe (Hamilton Robotics, Reno, U.S.A.) and the entire volume of the syringe was pushed through the Mini-extruder apparatus into an empty gas-tight syringe on the other end, as depicted in Figure 6B. This process was repeated for 11 passes, until the

mixture was no longer cloudy, as seen in Figure 6C. The suspension was always passed through the Mini-extruder an odd number of times to ensure that the final product did not end up in the original syringe and be contaminated by residual, non-extruded lipids. Extruded liposomes were stored at 4°C until ready to use.

Figure 6. Overview of the Avanti Polar Lipids, Inc Mini-Extruder. A. The order of assembly of the various parts of the mini extruder. Parts are indicated by name in the image. **B.** The assembled extruder with a syringe full of lipid suspension on the left and an empty collection syringe on the right. **C**. Two syringes filled with a suspension of liposomes. The top syringe is pre-extrusion, the bottom syringe is post-extrusion. Notice the improved clarity of the suspension post extrusion (typing is legible through the glass syringe).

2.12 Liposomes NPC1-C Interaction

2.12.1 Liposome-NPC1-C Interaction and Flotation Assay

In order to bind the NPC1-C receptor to the liposome, a nickel-containing lipid salt was included along with the lipid mixture, resulting in exposure of Ni atoms on the surface of the liposome membranes. The NPC1-C receptor was designed with a N-terminal His-tag, allowing NPC1-C to bind to the liposome via an interaction between the Ni atom and the imidazole side chain of the His residues in the His-tag.

Liposomes were extruded as previously described, and were incubated at a concentration of 1 mg/mL with purified NPC1-C receptor at a concentration of 150 µg/mL for 1 hour at room temperature on the Hula mixer (Thermo Fisher Scientific). After incubation, 2 mL of 60% iodixanol (Sigma-Aldrich) was added to 1 mL of sample resulting in a suspension of the sample in 40% iodixanol. Gradients were then constructed in a 13 mL tube by layering 1 mL of 5% iodixanol underneath 1 mL PBS, followed by 8 mL 30% iodixanol underneath the 5%, and finally 3 mL sample in 40% underneath the 30%. Tubes were balanced and then ultracentrifuged at 100,000 xg for 1 hour at 18°C in the SW40 Ti rotor (Beckman Coulter) with moderate level deceleration.

Following ultracentrifugation, 13 fractions of ~1 mL were collected using the Biocomp Fractionator and Fraction Collector (Biocomp Instruments, Fredericton, Canada). Samples of each fraction were analyzed by SDS-PAGE gels and Coomassie stained and Western blotted to confirm NPC1 binding to the liposomes.

Preliminary experiments to detect interaction between the Ni on the liposomes and the His-tagged NPC1-C receptor were done using 100 µg/mL and 200 µg/mL.

Western blots indicated that 100 µg/mL was too little to achieve saturation of the Ni sites, while 200 µg/mL seemed to be too much. Thus, we settled on 150 µg/mL His-tagged NPC1-C receptor was used in all future experiments.

2.12.2 Nanosight

The Nanosight NS500 (Malvern Instruments, Malvern, United Kingdom) particle characterization system was used to analyze the liposome preparation and to confirm that NPC1-C had bound specifically to Ni-liposomes, and had not bound to liposomes lacking Ni. After liposome flotation assays, samples were diluted to 0.25 µg/mL and run on the NS500. Using Brownian motion to track, an output curve was generated with an estimated diameter of the particles in the sample. Samples with and without NPC1-C were compared to determine if the measured diameter had increased when NPC1-C was added to the suspension prior to flotation.

2.13 VLP-NPC1-C Interaction and Flotation Assay

Since VLPs are membrane-bound particles, flotation experiments using iodixanol (Sigma-Aldrich) as a density gradient medium were completed to confirm that the NPC1-C receptor was able to bind to thermolysin-digested VLPs. Uncleaved or cleaved VLPs (100 µg) were mixed with NPC1-C at a concentration of 75-100 µg/mL and allowed to incubate on an orbital shaker Hula mixer (Thermo Fisher Scientific) for 1 hour at room temperature. Samples were then mixed with 60% iodixanol (Sigma-Aldrich) to result in a suspension of sample in 40% iodixanol, as previously done with liposomes. Flotation gradients were assembled as in section 2.12.1, and samples were spun through a flotation gradient by ultracentrifugation at 100,000 xg in an SW40 Ti rotor (Beckman Coulter). Fractions were collected (1 mL) as previously described and

analyzed by SDS-PAGE Western blotting to investigate if the interaction between NPC1-C and GP had occurred.

2.14 TEM Support Grid Preparation

2.14.1 Cleaning

The grids most commonly used for negative staining purposes are 400 mesh copper hexagonal grids (Electron Microscopy Sciences, Hatfield, Pennsylvania, U.S.A.). The cleaning of the grids consists of sequential washing with acetic acid, acetone, 70% ethanol, and then 100% ethanol for 2 minutes each. The grids were placed in a 50ml beaker and washed with approximately 1ml of acetic acid. The acetic acid was carefully decanted off and this step was repeated with the next three solutions. After all washes were complete, the grids were transferred to a glass petri-plate with a Whatman filter paper (Whatman PLC, Maidstone, Kent, United Kingdom) and were allowed to dry.

2.14.2 Formvar Support Film

Formvar plastic support films were made to support the samples being applied to the EM grids. A solution of 1% formvar in chloroform (Electron Microscopy Sciences) was poured into a previously cleaned Coplin jar. A clean glass slide was dipped into the solution and pulled out immediately, but slowly to ensure that the film of plastic on the glass slide was as thin as possible. The plastic was allowed to dry on the slide while holding the slide at an incline. At this point, the slide was removed from the fume hood. Next, all of the edges of the slide were etched with a razor blade so that the plastic would come off of the slide more easily in the next step. The glass slide was gently and slowly immersed in a bowl of water letting the plastic film come off the slide and float on top of the water. The cleaned grids were individually placed on the sheet of plastic film,

frosty side down. Once the film was full of grids, a piece of cardstock was plunged into the water bath to pick up the grids and plastic. The grids were allowed to air dry in a covered Petri dish.

2.14.3 Carbon Coating

After sufficient drying, the grids, along with the sheet of cardstock and plastic they are stuck to, are placed formvar side up in a filter paper lined glass Petri plate and weighed down by washers. The Petri plate was then placed on the stage of the Agar 208 Turbo Carbon Coater (Agar Scientific Ltd., Stansted, U.K.) in such a way that the grids were positioned directly underneath the carbon rods. One carbon rod was sharpened into a point using the electric sharpener, while another carbon rod was shaped into a sphere at the tip using sand paper. The pointed rod on the right was tightened using a thumb screw and centered using the spot on the cover plate. The second carbon rod was inserted by pressing back the spring as far as possible, making the two carbon rods touch and tightening with a thumb screw; the shield was then put in place. The lid was closed to ensure the seals were tight. The machine was turned on and once the vacuum was established, the carbon rods were degassed by slowly turning up the voltage in the manual setting for about 30 seconds. The voltage was then turned back down and the machine was switched to the automatic setting, with a voltage of 4.2V and a time of 4 seconds to give sufficient carbon coating. The shield over the carbon rods was removed and the 4 second evaporation was started by pressing start. After the process was complete, the Penning gauge was put back into the off position and the machine was turned off. The resulting grids consisting of a layer

carbon on top of a layer of formvar were then carefully peeled off of the cardstock and placed in a storage boxes for future use.

2.14.4 Glow Discharging

Prior to use, grids were glow discharged to render the surface of the grid hydrophilic, thus allowing sample to adsorb to the grids more evenly. The process is the same regardless of what type of grids being used as long as the grids are discharged with the carbon side facing up; 400 mesh copper grids coated with carbon and Formvar for negative staining, or Quantifoil® for cryo-EM. Carbon coated grids were placed carbon side up around the center hole of the glow discharge lid of the evaporator. The lid was placed on the evaporator and the machine was turned on. After the vacuum had established and the ready light had turned on, the large needle valve switch was switched down into the on position. The needle valve, or knob, at the back of the machine was used to adjust the vacuum until it read 0.2 mbar. The auxiliary power unit was turned on and the timer was set to 30 seconds of glow discharging; the start button was pressed to initiate the process. While the grids were being glow discharged, the needle valve knob at the back of the machine was used to maintain the vacuum at 0.2 mbar. Once the process was complete, the auxiliary power unit was turned off and the needle valve knob was used to return the vacuum to its original state in order to remove the lid from the evaporator. The large needle valve was switched up into the off position and the evaporator was turned off. The grids were stored in grid boxes until use within approximately 2 hours.

2.15 Negative Staining

Negative staining is a process used to visualize biological samples by using heavy metals (in the stain) to scatter electrons. The samples appear light on a dark background. The negative staining process was done using 400 mesh copper grids coated in carbon and formvar support film. An EM grid was held using a pair of forceps, carbon side up to ensure that the carbon side (that had been previously glow discharged) is the side that gets the sample and stain applied to it. First, 3µL of well mixed sample was applied to the grid using a pipette and was allowed to adsorb to the grid for 1 minute. The grid was then washed with 3µL of Milli-Q water and gently agitated by expelling the water onto the grid and sucking it back up about 5 times. A total of three washes were done, each with a fresh aliquot of 3µL of Milli-Q water. After the final wash, the water was wicked off of the grid using a piece of filter paper. Next, 3µL of methylamine tungstate – MT (Nanoprobes, Yaphank, New York, U.S.A.) stain was applied to the grid and allowed to adsorb for 30 seconds. After the 30 seconds had elapsed, another piece of filter paper was used to wick the excess stain off of the EM grid. The grids were allowed to air dry and then stored in a grid box until viewing under the TEM.

2.16 Vitrobot

The Vitrobot™ is a plunge-freezing device used to prepare EM grids of samples that are frozen in a thin layer of vitreous ice. First, we filled the water reservoir, turned on the Vitrobot™ and then set the temperature of the Vitrobot™ to 5°C and the humidity of the blotting chamber to 100%. To cool the Vitrobot™ cup, the vessel was filled with liquid nitrogen in the outer circle of the vessel; next, ethane gas was allowed to flow

slowly into the inner circle of the vessel. As the ethane is cooled by the metal of the vessel and the surrounding liquid nitrogen, the ethane slowly condenses into a liquid state, suitable for plunge freezing. The ethane will not go all the way to the solid phase because there is a plastic insulator surrounding the inner circle of the vessel that regulates how cold the inner circle gets from the surrounding outer circle of liquid nitrogen. Quantifoil grids with 2 µm holes and 2 µm spacing had been glow discharged previously. Samples were prepared by combining 4 parts of the sample with 1 part 10 nm BSA Gold tracer (Electron Microscopy Sciences, Hatfield, U.S.A.) to aid in focusing. A sample of 3 µL was applied to the grid inside the blotting chamber and the grids were blotted for 2 seconds, before being plunged into the liquid ethane. The plunge frozen grids were then stored in grid boxes inside cryo boxes in the racks of the liquid nitrogen Thermolyne Locator JR. cryo storage tank (Thermo Fisher Scientific), until viewing on the TEM.

2.17 Liposome-NPC1-C-VLP Experiment

In the final experiment, liposomes were combined with NPC1-C and floated as described previously. However, instead of fractionating the gradient, the pink band of liposomes was extracted from the gradient from the top of the centrifuge tube using a 1 mL Hamilton syringe (Hamilton Robotics Inc.) in order to avoid dilution of the liposomes that would occur by collecting 1 mL fractions.

This liposome fraction was then combined with VLPs that had been previously cleaved with thermolysin (Sigma-Aldrich) at a ratio of 1 part liposomes-NPC1-C to 2 parts VLPs. This mixture was incubated on the orbital shaker Hula mixer (Thermo

Fisher Scientific) for 1 hour at room temperature, followed by plunge freezing of specimens into liquid ethane as described previously.

2.18 TEM Alignments

At the beginning of the day, the microscope and computers are turned on and liquid nitrogen is put in the dewar for the cold trap to cool the cryoblades that minimize contamination during specimen exchange. This should be left to cool for 20 minutes. When inserting the holder, the column valves must be closed, the gun should be in the low 20s (Log units), and the column should be at 6 (Log units). If viewing a negatively stained grid, the holder is put directly into the microscope and is ready for viewing. When doing cryo-EM, the holder comes equipped with a dewar flask insulated thermos on the end of it that is filled with liquid nitrogen to keep the sample under cryo conditions during viewing. Before the grid is put into the cryo-holder, the holder is placed into a cryo transfer stage that both cools the holder and allows you to put the grid into the holder while in a bath of liquid nitrogen. Once the grid is in the holder, the holder can be inserted into the microscope; however with cryo-EM, the holder needs time to stabilize in the microscope due to the expanding and contracting of the metal in the cryo-holder. After a sufficient amount of waiting to allow the specimen chamber to reach sufficiently high vacuum or for the temperature to stabilize, the column valves are opened and aligning the microscope can begin. The dose of electrons is set depending on the type of EM being done, usually 10 $e^-/Å^2$, the camera is calibrated, and the beam is aligned. Next, we tried to find an area of the grid that is sufficient for our purposes; we want it to be roughly centred in the grid square, and the grid square should have hazy circles indicating that there is frozen sample present inside the circle. Finally, the eucentric

height and focus of the microscope must be set to ensure accurate magnification and focusing of the specimen, as well as primary focusing of the image in search mode and centering the target for images.

2.19 Negative Stain Imaging

All imaging was done using the Tecnai F20 transmission electron microscope (FEI Company, Hillsboro, Oregon, USA). Once a sample has been applied to a carbon and formvar coated 400 mesh copper grid, the grid placed in the holder, inserted into the microscope and alignments are completed, imaging of the sample can begin. When imaging negatively stained samples, the microscope is running at 200 kV and the side-mount AMT Advantage XR 12 CCD camera (AMT, Danvers, MA, USA) was used to obtain images. First, we use the translation function of the stage controlled by a joystick to search for a grid area that looks to have an optimum amount of VLPs present, between 25 and 50 VLPs of various shapes and sizes in the field of view at 5000x magnification. Once an ideal grid square is found, the magnification is increased and the area of interest is centered in the field of view. Focusing of the microscope was done manually using the wobbler function and then the picture was taken. The Tecnai User Interface software is running and AMT camera software were both used for negative stain imaging. The digital images are automatically saved to a folder created previously and are ready for analysis.

2.20 Cryo-EM Single-Particle Imaging

This method is called low dose imaging where to reduce beam damage, focusing takes place in an area adjacent to the area to be imaged. For single particle imaging, once the grid containing the sample was put into the holder, the holder was inserted into

the microscope and alignments were done. After alignments, the dose of electrons, the defocus, and the magnification need to be set in the Tecnai User Interface Low Dose software. Under the search category, the exposure time was set to 3 seconds, the defocus was set to -3.5 µm and the magnification of the microscope was set to 5,000x; and under the focus category, the exposure time was set to 3.0sec with a magnification of 29,000x or 50,000x. Under the exposure category, the dose of electrons was set 10e/Å^2/s or 1000 electrons/nm^2/s with an exposure time of 1 second. The magnification of the microscope was set to 29,000x or 50,000x; and in the tomography software, the defocus was set to -3 µm. Once a good grid area is found, one with a sufficient amount of sample and where the ice is not too thick, imaging can begin. First in “Search” mode, the VLP or liposome of interest was centered in the field of view by aligning it with the red “X” across the image; if the sample is difficult to see, the “preview” mode can aid in centering the virus before you focus the image. Next, we changed to “Focus” mode and clicked “Start”; once the image appears, we pressed “Proceed” in the tomography software to autofocus the image; we can tell when the image has focused correctly by watching the correlation plot. Once focused, we pressed “Expose” in the TIA software to take the picture. After the first picture is taken, it is saved into a folder that indicated what the sample is and the date it was collected on and the auto-save function is turned on. The auto focus done by the tomography software is sufficient for a few pictures when collecting images. Once all pictures in the grid circle have been taken, we hit “Search” and then “Start” to continue moving to the next circle. All images were collected using the Tecnai 20 transmission electron microscope and samples were prepared on Quantifoil® grids.

3. Results

A liposome-VLP model system was successfully developed. Liposomes exhibiting expressed and purified receptor NPC1-C on their surface were made by combining a HIS-tagged engineered version of NPC1-C with liposomes made with nickel ion containing lipids. Binding occurred between the imidazole headgroup of the histidine amino acid and the nickel ions on the surface of the liposome to result in NPC1-C receptor decorated liposomes. I also showed that the GP of Ebola as expressed in non-infectious VLPs, will only bind to NPC1-C when both removal of the mucin-like domain and further cleavage of GP1 by proteases has been carried out.

3.1 VLPs

3.1.1 Cloning of GP

Both versions of the GP protein, GPFull and GPΔmuc were cloned in the lab, whereas custom synthesized VP40 was ordered directly from The Genscript Company. The two GP genes of interest were cloned out of the pUC57 vector by restriction digestion and following cloning, minipreps were sent for sequencing. I analyzed the sequence data to check the clones and all of the sequences were an exact match to the Ebola Zaire consensus sequence. A selection of the quality of sequence data collected is shown in Figure 7. A selection of the nucleotide Basic Local Alignment Search Tool (BLAST, NCBI, Bethesda, U.S.A.) outputs of the two successful clones are shown in Figure 8. Most notable in this figure is Figure 8A depicting that the GPΔmuc form was detected as two fragments surrounding the now deleted MLD. Supplementary Figure 1 shows the DNA and protein sequence of the Ebola glycoprotein, highlighting the key regions of interest including the glycan cap and MLD.

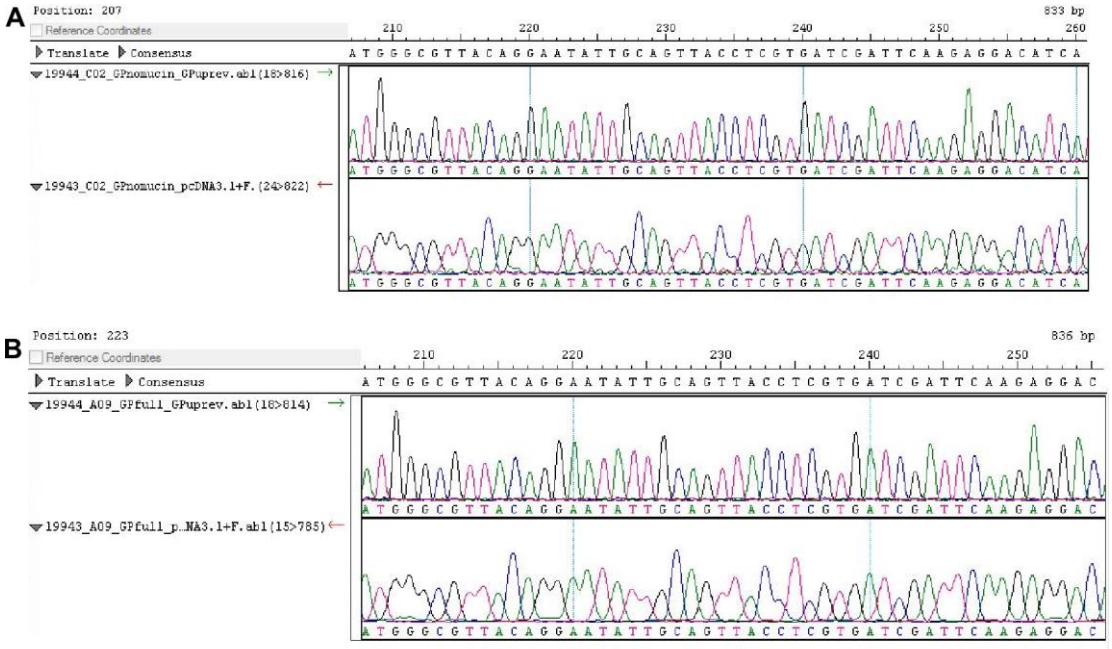

Figure 7. Lasergene output of sequence data. Mini-preps were sent to the DNA Core Facility (NML) for sequence confirmation. **A.** A selection on sequence data of GPΔmuc mini-preps. **B**. A selection of sequence data of GPFull mini-preps.

Figure 8. BLAST output of the mini-preps of plasmids. Following sequencing by the DNA Core Facility, sequences were compared by BLAST (NCBI) **A.** Data for GPΔmuc mini-prep. **B.** Data for GPFull mini-prep. Both clones showed 100% identity to Zaire Ebola virus with the GPΔmuc construct consisting of 2 fragments surrounding where the sequence corresponding to the MLD had been located.

3.1.2 VLP Expression and Isolation

In order to study the interactions between the GP spike protein and the NPC1 receptor, I first needed to synthesize VLPs. The genes for VP40 and GP were expressed by co-transfection of 293TN cells in order to produce VLPs.

To purify the VLPs from cell culture media, 28 mL supernatant was ultracentrifuged through a 20% sucrose cushion (10 mL). During the first attempts, the yield of VLPs was poor. In subsequent experiments, the VLPs seemed to be caught in the interphase between the cell culture supernatant and the 20% sucrose in TNE buffer. Therefore, instead of simply layering the cell culture supernatant over the 20% sucrose, I mixed 5 mL of the supernatant with the 20% sucrose, so that the sucrose was only slightly diluted at the interphase, and to produce a small gradient, instead of a sharp interphase between the supernatant and the 20% sucrose. After ultracentrifugation, the pellet was easily visible, indicating that VLPs had likely been released into the supernatant.

To confirm expression of VP40 and GP after VLP purification, resuspended samples of the pellet were run on SDS-PAGE and stained with Coomassie blue or by Western blot, as seen in Figure 9. I noticed that the anti-GP antibody only detected the GPFull version of GP, not the GPΔmuc version in the Western blot (Figure 9). In order to visualize GPΔmuc, a different antibody against GP was tried, but this also failed to detect GPΔmuc (Figure 10). The GP positive control shown in Figure 9 and Figure 10 was purchased from IBT Bioservices and was produced in Sf9 insect cells using baculovirus for expression. This expression system results in a differentially glycosylated form of GP as shown by multiple bands in lane 5 of Figure 9B.

The next endeavour was to confirm proper assembly of expressed VP40 and GPFull/ GPΔmuc into VLPs. The different VLP types were analyzed by negative stain for TEM (Figure 11). The VLPs produced were highly filamentous with a diameter of about 50nm, loosely resembling Ebola virus particles, however lacking a nucleocapsid. Some VLPs were also “check-mark” shaped or had bulbous ends to the filaments (Figure 11c, d). The GPΔmuc construct was also expressed successfully as shown in Figure 11b, d).

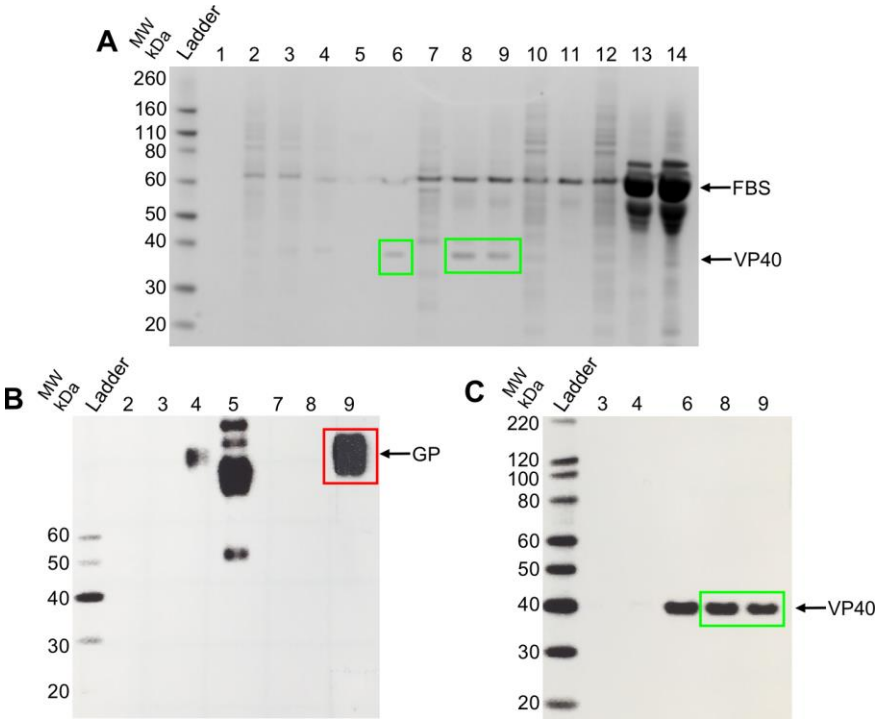

Figure 9. Coomassie blue stained SDS-PAGE gels and Western blots of VP40 and GP expression. A. Coomassie blue stained gel with Novex Sharp Prestained Protein Standard. **B.** anti-GP Western blot with Magic Mark Ladder. **C.** anti-VP40 Western blot with Magic Mark ladder.Green boxes indicate VP40, red boxes indicated GP. Legend: Lane 1. Blank; Lane 2. GPΔmuc cell lysate; Lane 3. VP40/ GPΔmuc cell lysate; Lane 4. VP40/GPFull cell lysate; Lane 5. GP positive control; Lane 6. VP40 positive control; Lane 7. GPΔmuc VLP; Lane 8. VP40/ GPΔmuc VLP; Lane 9. VP40/GPFull VLP; Lane 10. pCAGGs vector cell lysate; Lane 11. pCAGGs vector supernatant; Lane 12. Cells only cell lysate; Lane 13. Cells only supernatant; Lane 14. pcDNA3.1+ cloning vector supernatant.

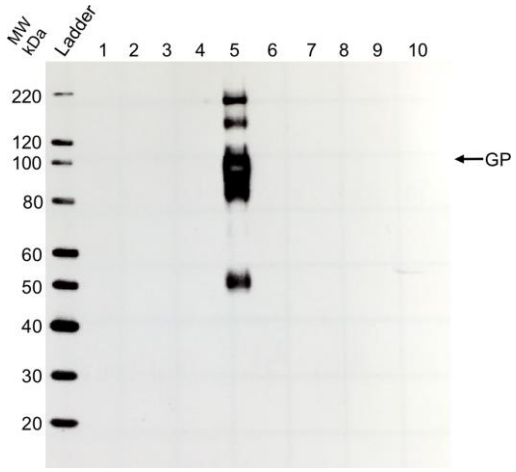

Figure 10. Western blot using an alternative anti-GP antibody in an attempt to visualize GPΔmuc. Legend: Lane 1. GPΔmuc cell lysate; Lane 2. VP40/ GPΔmuc cell lysate; Lane 3. pcDNA3.1+ vector cell lysate; Lane 4. Cells only cell lysate; Lane 5. GP positive control; Lane 6. GPΔmuc VLP; Lane 7. VP40/ GPΔmuc VLP; Lane 8. pcDNA3.1+ vector supernatant; Lane 9. Novex Sharp Prestained Protein Standard; Lane 10. Cells only supernatant.

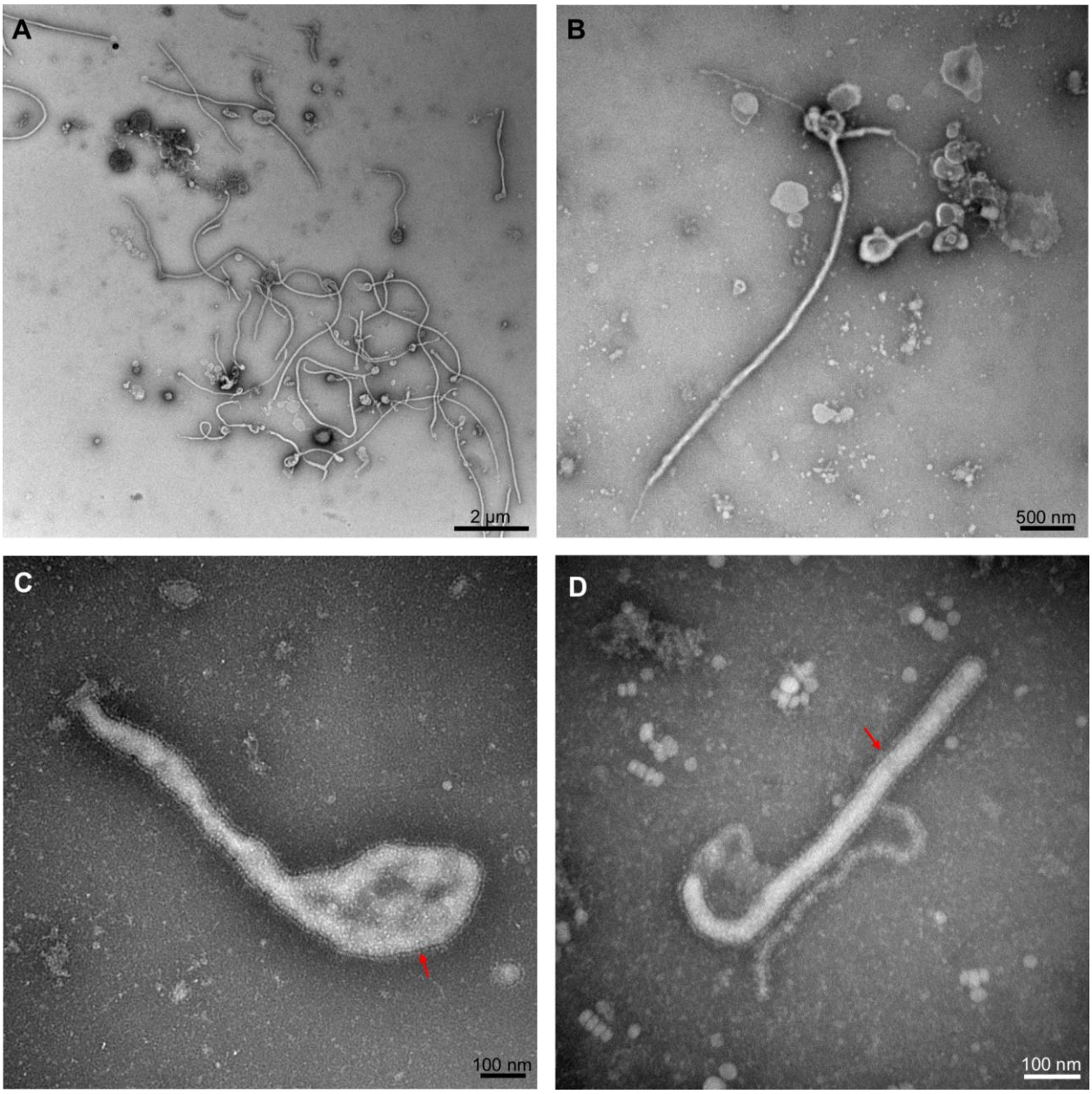

Figure 11. Confirmation of VLP assembly by negative staining and TEM. A. Low magnification image of VP40/GPFull VLPs. **B.** Low magnification image of VP40/ GPΔmuc VLPs. **C.** High magnification image of VP40/GPFull VLPs. **D.** High magnification image of VP40/ GPΔmuc VLPs. Notice the characteristic filamentous structure of Ebola virus driven by the VP40 matrix protein budding from the cell. The GP spikes are clearly visible in the two high magnification images as indicated by the red arrows.

3.1.3 VLP thermolysin digestion

In order for the GP on the VLPs to bind to NPC1, there is evidence that GP must first be cleaved to expose the receptor-binding site. During an Ebola infection, it is likely that this step is completed by endosomal cathepsins. Thermolysin was used *in lieu* of cathepsins since the former is inexpensive and readily available and has been widely used in Ebola GP studies (Brecher et al., 2012; Kaletsky et al., 2007). Initially, digestion of ~0.5 mg/mL VLPs with different concentrations of thermolysin ranging from 0.1 to 0.3 mg/mL at 37°C for 1 hour was attempted. The reaction was stopped by the addition of 500 µM phosphoramidon. By western blot, the GP was no longer detectable after treatment and by EM, the envelope of the VLPs had been disrupted. It was concluded that the VLPs had been overdigested. Based on the previous results, it was decided to try a greatly reduced concentration of thermolysin, 100 and 1000-fold less, using the same temperature of 37°C at various time points. This resulted in thermolysin concentrations of 0.01 mg/mL and 0.001 mg/mL. At these lower concentrations, there was no cleavage of VLP proteins under any of the conditions. By TEM, the VLPs appeared unaffected by these digestion conditions.

Based on the previous results showing either no cleavage or excessive proteolysis, intermediate conditions in between these two extremes were tried. Varying concentrations of thermolysin, between the minimum and maximum concentrations that were used previously, were attempted, with stopping the reaction with 500 µM phosphoramidon. At 0.1 mg/mL thermolysin, the GPFull was hardly detected, and an additional VP40 band appeared at ~10 kDa in size (Figure 12C, lane 5); while at 0.25 mg/mL, the GPFull was completely undetectable (Figure 12C, lane 6). Examination by

negative stain TEM showed that the 0.1 mg/mL treatment preserved the structure of the envelope (Figure 13B, C), while the latter had become indistinct and mostly lysed at 0.25 mg/mL (Figure 13D).

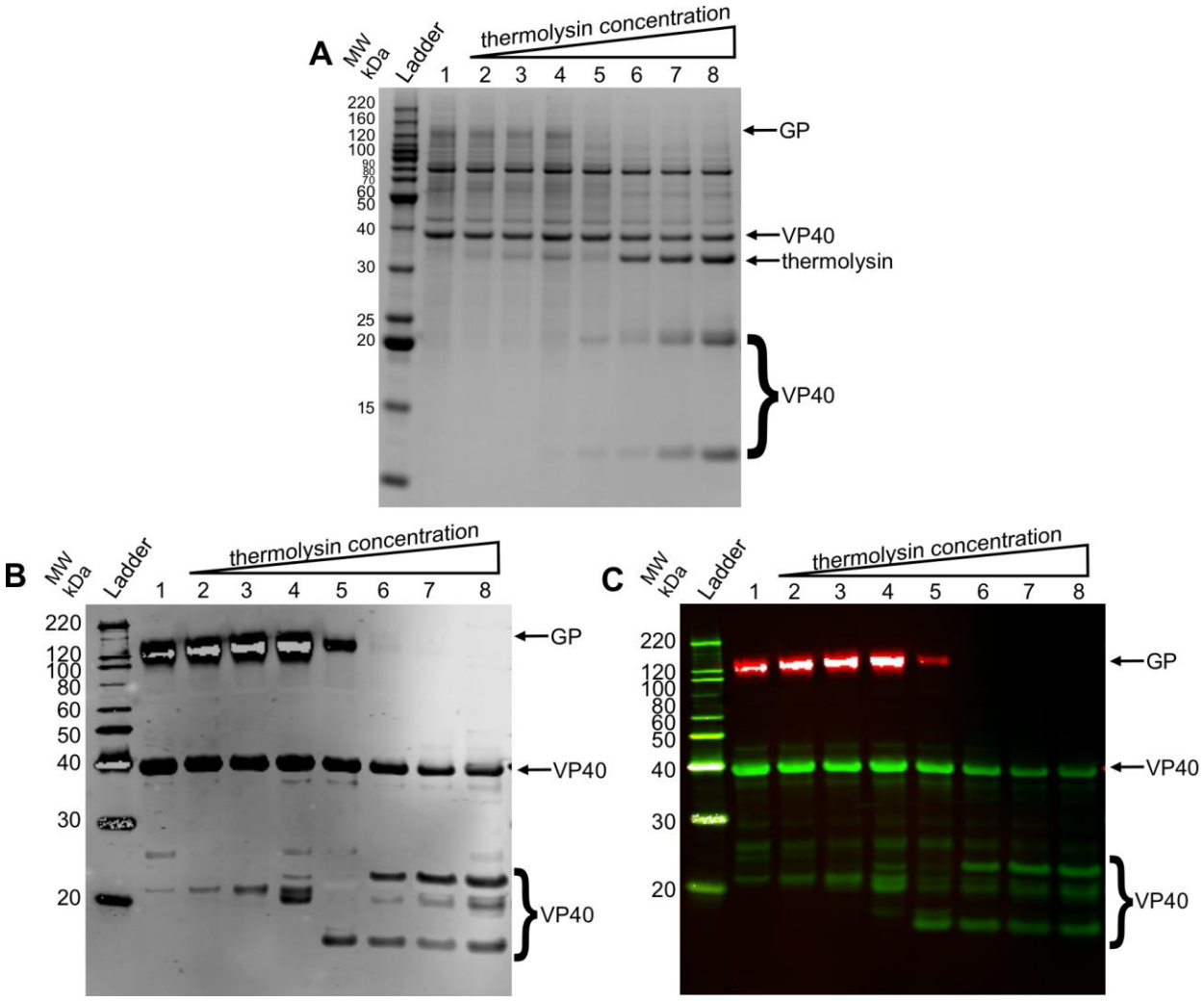

Figure 12. Optimum cleavage of both GP and VP40 in VLPs by thermolysin. Coomassie blue stained SDS-PAGE (A) and anti-VP40/anti-GP Western blot (B – grey scale)/(C – VP40=green, GP=red) of VP40/GPFull VLPs digested for 5 minutes at 37°C with various concentrations of thermolysin. Legend: Lane 1. VP40/GPFull diluted and undigested; Lane 2. 0.025 mg/mL thermolysin; Lane 3. 0.05 mg/mL thermolysin; Lane 4. 0.075 mg/mL thermolysin; Lane 5. 0.1 mg/mL thermolysin; Lane 6. 0.25 mg/mL thermolysin; Lane 7. 0.5 mg/mL thermolysin; Lane 8. 0.75 mg/mL thermolysin. At 0.1 mg/mL the GP signal is decreasing, indicating that the MLD is being digested. By 0.25 mg/mL, the GP signal has disappeared.

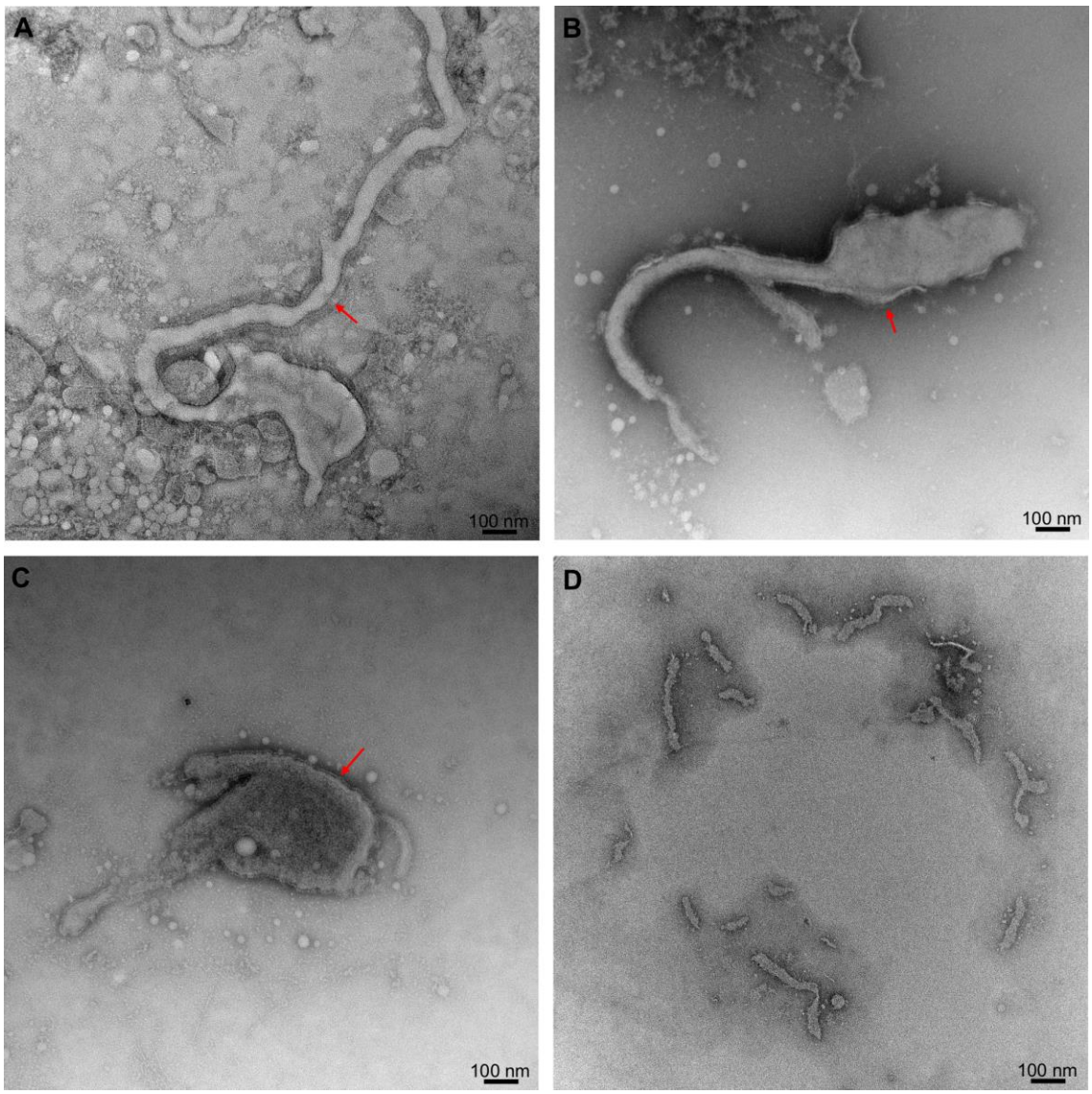

Figure 13. TEM of VP40/GPFull VLPs digested with thermolysin for 5 minutes at 37°C at various concentrations. A. 0.075 mg/mL thermolysin. **B and C.** 0.1 mg/mL thermolysin. **D.** 0.25 mg/mL thermolysin. As shown above, the GP spikes are indicated by the red arrows, and the VLPs at 0.1 mg/mL appear intact, yet digested with some GP spikes visible while some are missing having been cleaved.

3.2 NPC1-C

3.2.1 NPC1-C Transient Expression

To produce pure NPC1-C receptor, expression of the NPC1-C protein was carried out by transfection of 293TN cells using both the attractene transfection reagent and the X-tremeGene HP transfection reagent to optimize which kit would have the best yield. The relative expression of NPC1-C in both kits is shown in (Figure 14). The expression vector causes secretion of NPC1-C into the supernatant, however, the yield was higher in the cell lysates than in the supernatant. Based on this outcome, it was decided to develop a stable cell line expressing NPC1-C where NPC1-C was continuously secreted into the cell culture medium by the growing 293TN cells.

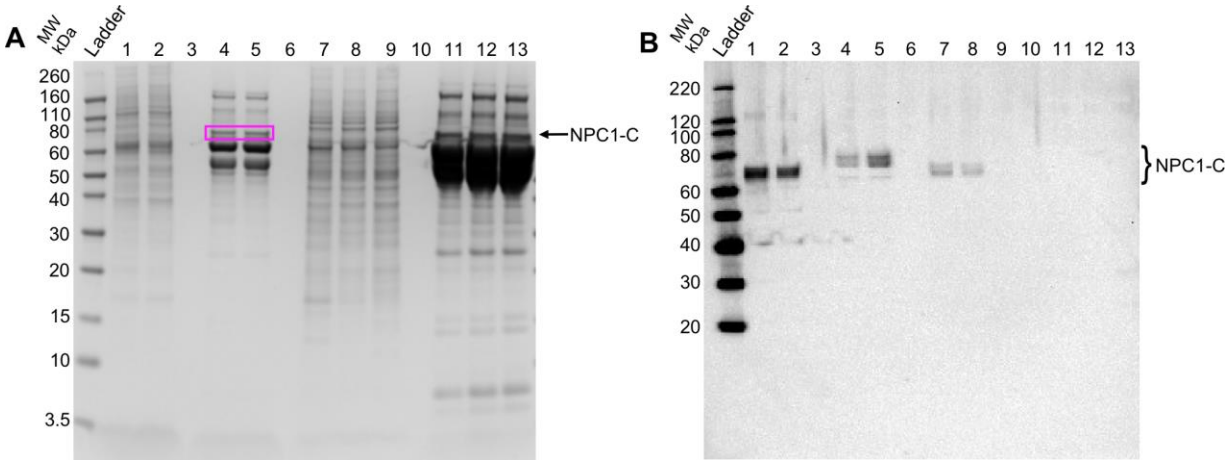

Figure 14. Transient Expression of NPC1-C with attractene or X-tremeGene HP transfection reagent. Coomassie blue stained SDS-PAGE (A) and Western blot (B) of transient NPC1-C expression with various transfection reagents. Legend: Lane 1. Attractene cell lysate, dynabead purified; Lane 2. X-tremeGene cell lysate, dynabead purified; Lane 4. Attractene supernatant, dynabead purified; Lane 5. X-tremeGene supernatant, dynabead purified; Lane 7. Attractene cell lysate; Lane 8. X-tremeGene cell lysate; Lane 9. pcAGGS cells lysate; Lane 11. Attractene supernatant; Lane 12. X-tremeGene supernatant; Lane 13. pCAGGs supernatant.

3.2.2 NPC1-C Cloning and Stable Cell Line Production

In order to produce a stable transformed NPC1-C expressing cell line, the gene was cloned into a Lentiviral expression vector. Upon analysis, the clone that had been obtained previously was shown to have an unnecessary sequence coding for Hemoglobin subunit beta-1/2. This portion was therefore excluded when cloning the gene into the pLenti-Hygro expression vector. The full sequence of the construct is shown in Supplementary Figure 2. A restriction map of the clone is shown in Figure 15.

The correct NPC1-C sequence of the new clone was checked, and expression was confirmed by transient transfection using XtremeGene HP before production of the stable cell line. Successful expression of the protein is shown in Figure 16.

A stable cell line expressing GFP as a control was also produced in parallel. Upon infection of the cells with the GFP-Lentivirus, if GFP expression is visible, production of the stable cell line was successful. Since this virus and inoculation were completed in parallel to the NPC1-C-Lentivirus, the infection of the cells with the NPC1-C-Lentivirus was most likely successful as well. After inoculation of the 293TN cells with GFP-Lentivirus (and infection of another well of cells with NPC1-C-Lentivirus), fluorescence was visible 3 days post-infection.

Three days post-infection, cells stably expressing NPC1-C and thus exhibiting hygromycin resistance, were selected for by adding hygromycin (300 μg/mL) and passaging the cells for 10 days, splitting when the cells reached 80% confluency. To optimize NPC1-C yield, cells expressing hygromycin resistance were subject to a second, stronger round of hygromycin selection, at a higher concentration (600 μg/mL),

resulting in higher levels of protein production. Figure 17 shows the relative difference in amounts of NPC1-C produced by NPC1-C-Rx and NPC1-C-Rx-SC produced by applying increased hygromycin selection pressure.

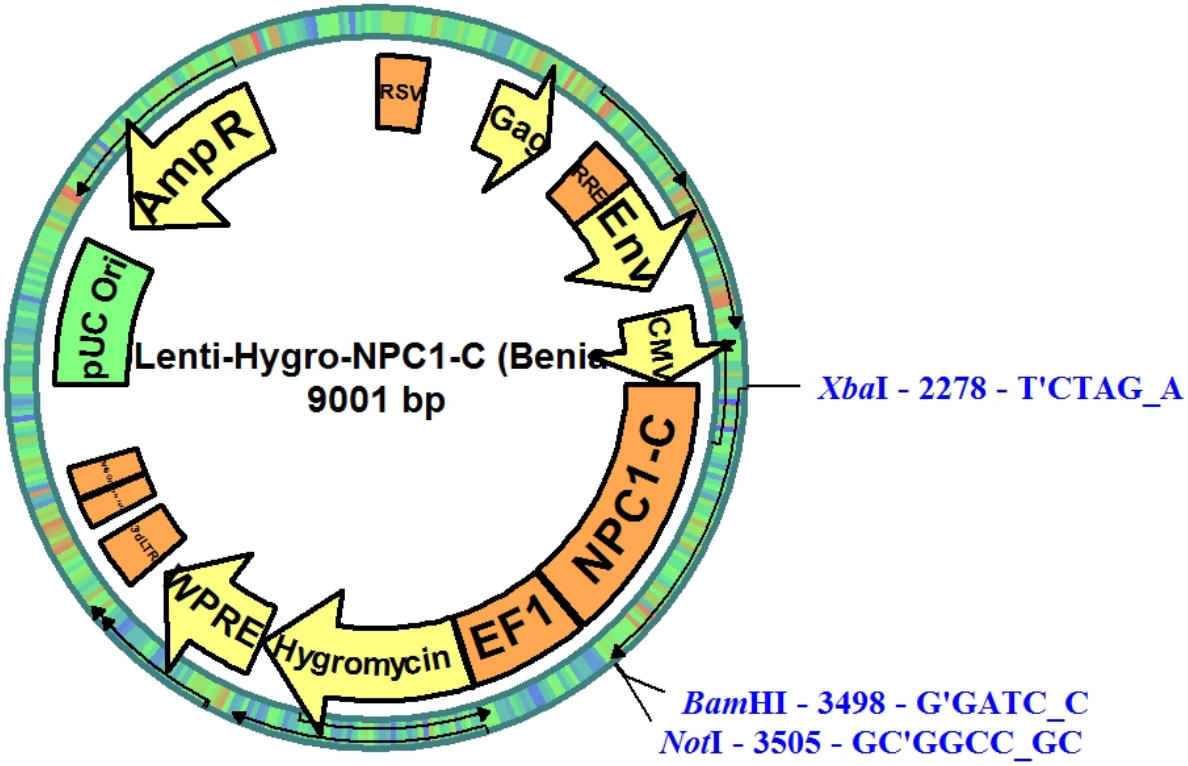

Figure 15. pLenti-Hygro vector map containing NPC1-C construct. Features of note: the NPC1-C gene is positioned next to the CMV promotor for expression; XbaI and BamHI, as indicated on the map, were the restriction sites used for gene insertion; AmpR for selection of clones during the cloning process; and the Hygromycin resistance marker for selection of 293TN cells stably expressing our clone.

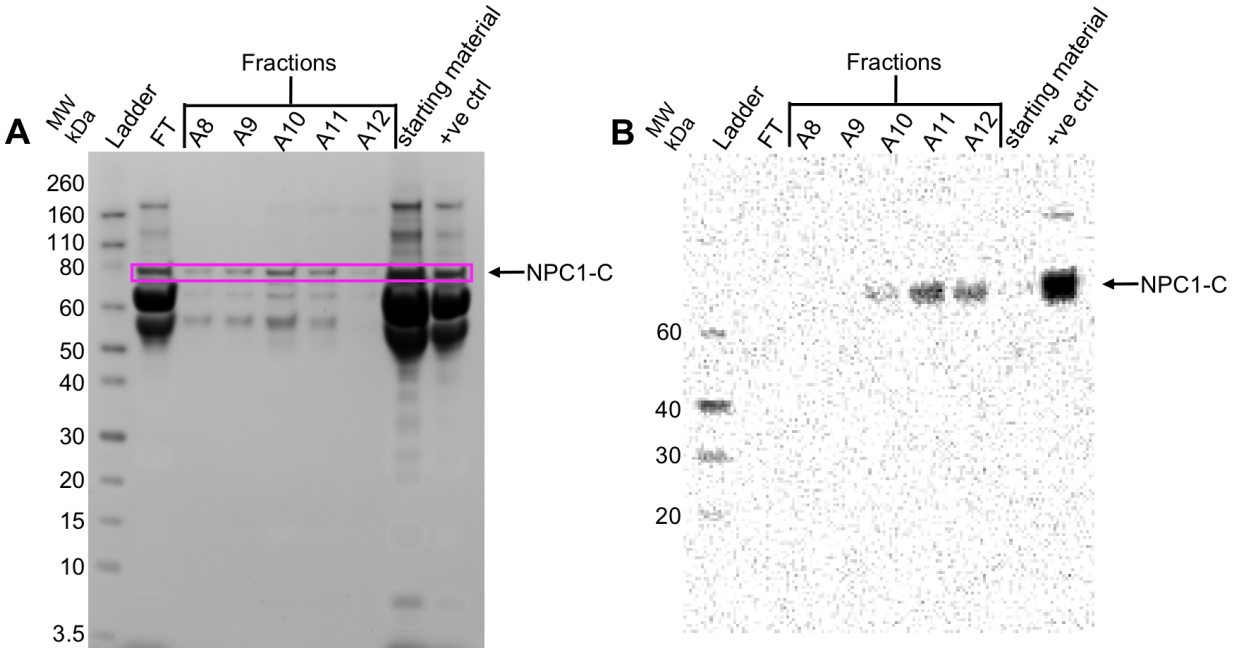

Figure 16. Coomassie blue stained SDS-PAGE (A) and anti-Flag Western blot (B) of HISTrap excel affinity fractions. 293TN cells were transiently transfected with NPC1-C in pLenti-Hygro and were purified on the HISTrap excel column. Legend: Lanes labeled as sample or fraction numbers.

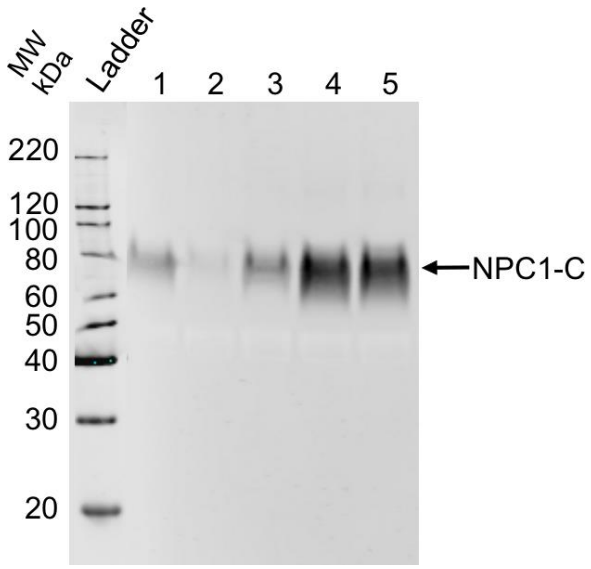

Figure 17. anti-Flag Western blot of NPC1-C-Rx vs NPC1-C-Rx-SC. Legend: Lane 1. NPC1-C-Rx 7 days; Lane 2. NPC1-C-Rx-SC 3 days; Lane 3. NPC1-C-Rx-SC 5 days; Lane 4. NPC1-C-Rx-SC 7 days; Lane 5. NPC1-C-Rx-SC 9 days. An aliquot of sample was collected on each day as indicated, and the remaining cells in media were left to continue to grow undisturbed until the next sample collection day.

3.2.3 NPC1-C Purification

To ensure that the His-tag was functional, prior to scaling up the purification, Dynabeads were used to conduct small scale purifications. (Figure 14) depicts the difference in expression levels detected before and after purification with Dynabeads.

Several different purification columns were tested in order to determine the best combination of columns to produce the highest yield of pure product. The HisPur Co^{2+} column was always used as the primary step in every purification. The output curve from the HPLC and the Silver stained SDS-PAGE gels and Western blots of the resultant fractions are shown in (Figure 18). After pooling and desalting the NPC1-C fractions from the 1^{st} column, the sample was then run on the Q-Resource Anion Exchange Column. The resulting output curve from the HPLC and the Silver stained SDS-PAGE gels and Western blots of the resultant fractions are shown in (Figure 19). It was apparent that the second column was not necessary and subsequent purifications were done in one step using the HisPur Co^{2+} column, followed by the HiTrap Desalt column. This single step produced pure NPC1-C receptor that was then concentrated prior to use in experiments (Figure 20).

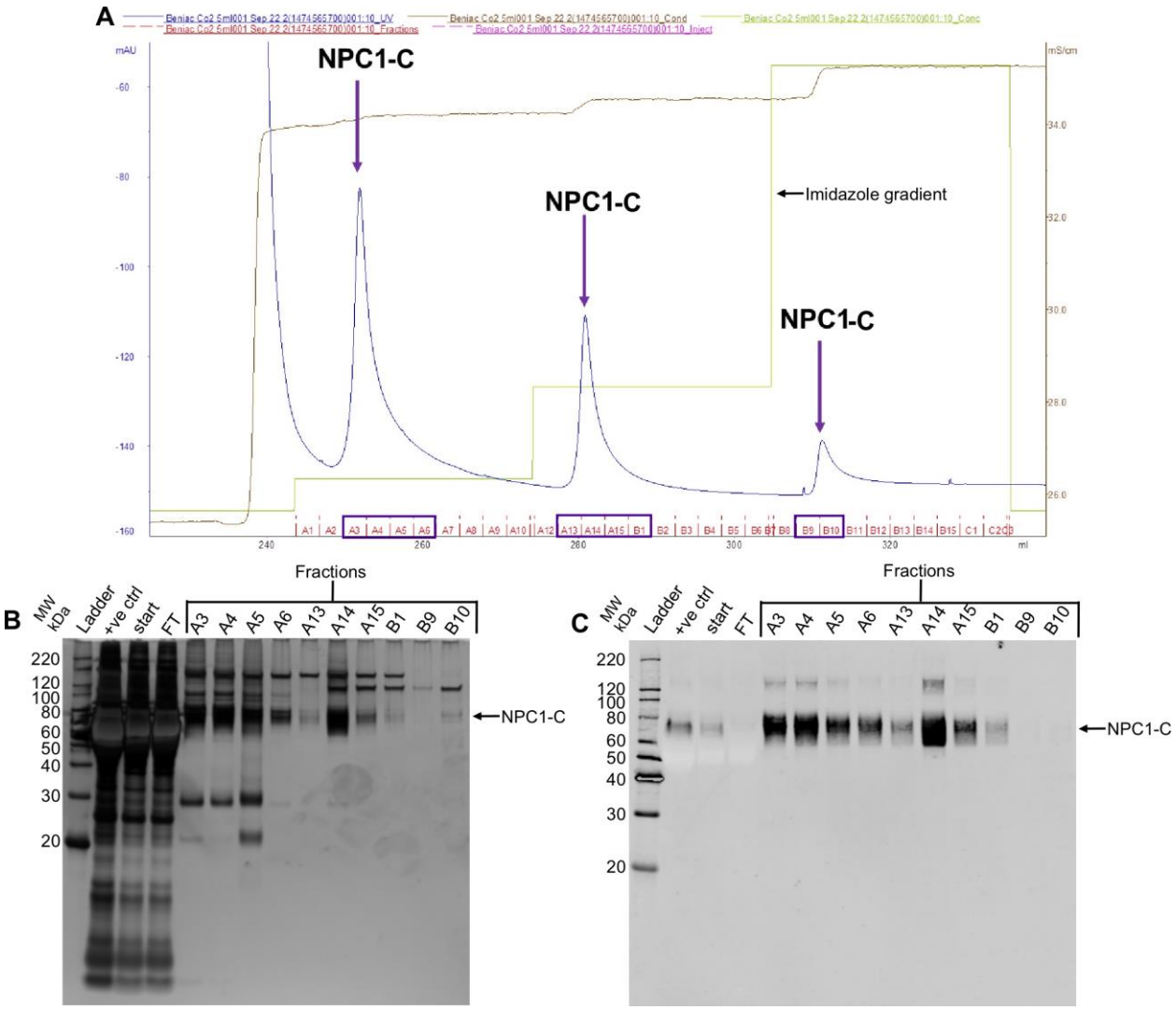

Figure 18. Output curve from HisPur Co^{2+} column (A), Silver stained SDS-PAGE of select fractions (B), and anti-Flag Western blot of the same select fractions (C). (A) NPC1-C in the cell culture supernatant binds to the column, and upon addition of increasing imidazole, is progressively released from the column into the collected fractions. (B)/(C) Legend: Lanes labeled with sample name. Fractions A3-A6 and A12-A15 were pooled and desalted for the next column.

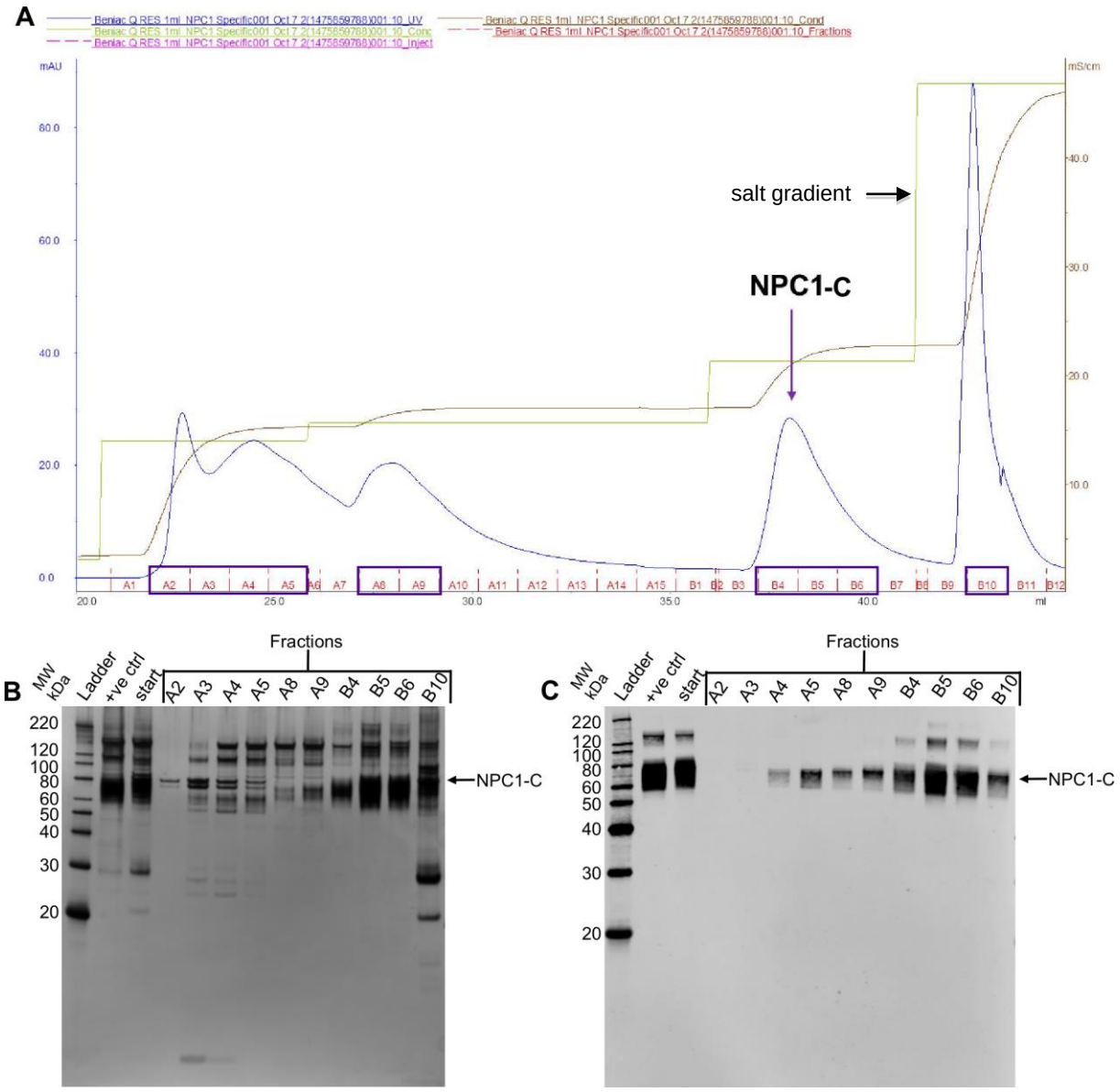

Figure 19. Output curve from Q-Resource Anion Exchange column (A), Silver stained SDS-PAGE of select fractions (B), and anti-Flag Western blot of the same select fractions (C). (A) NPC1-C is eluted off of the column by increasing salt concentration. (B)/(C) Legend: Lanes labeled with sample name. Samples B4-B6 were pooled and desalted for use.

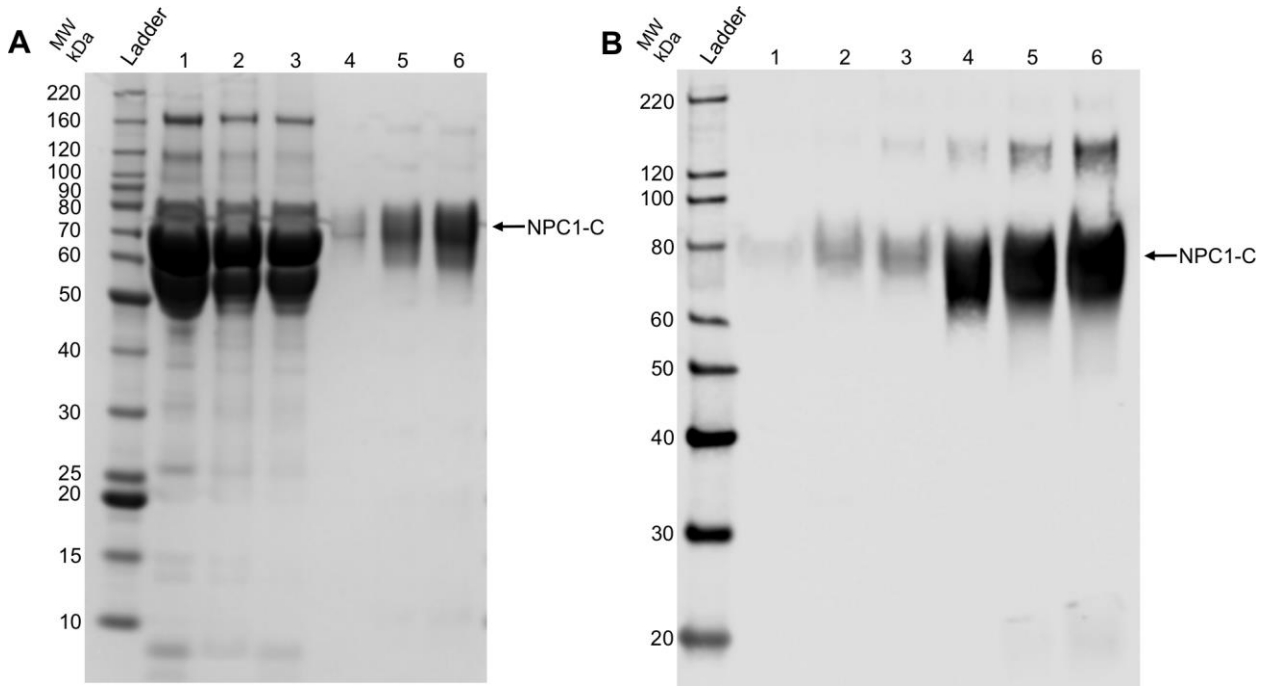

Figure 20. Coomassie blue stained SDS-PAGE (A) and anti-Flag Western blot (B) of the stages in purification NPC1-C from cell culture supernatant. Legend: Lane 1. Untransfected 293TN supernatant; Lane 2. Starting material; Lane 3. Flow-through; Lane 4. Sample collected pre-concentration; Lane 5. Sample concentrated once; Lane 6. Sample concentrated further. It was necessary to concentrate the sample further for ease of volume required in future experiments.

3.3 Confirmation of Expression and Purification by Mass Spectrometry

In-gel digestion and mass spectrometry were used to confirm that particular bands on the SDS-PAGE gels were indeed our proteins of interest (Figure 21). Bands 1 and 2 were identified as NPC1-C, Bands 3 and 4 were identified as GP, and band 5 was detected as VP40. This particular experiment was used to confirm successful expression of VP40, GP, and NPC1-C.

During the experiment to optimize thermolysin digestion, in-gel digestion of Coomassie blue stained SDS-PAGE gels were sent for MS analysis to determine if the thermolysin was digesting the VP40 as well as the GP. (Figure 22) shows the SDS-PAGE gels and the summary of which samples were detected as VP40 and GP. Bands 1, 2, 3, and 8 were detected as GP, bands 4 and 6 were detected as VP40, bands 5 and 9 were detected as both GP and VP40, while band 7 was detected as thermolysin only. From these data, it was concluded that the thermolysin digestion conditions in this experiment were too harsh and the thermolysin had also digested the VP40 protein of the VLP.

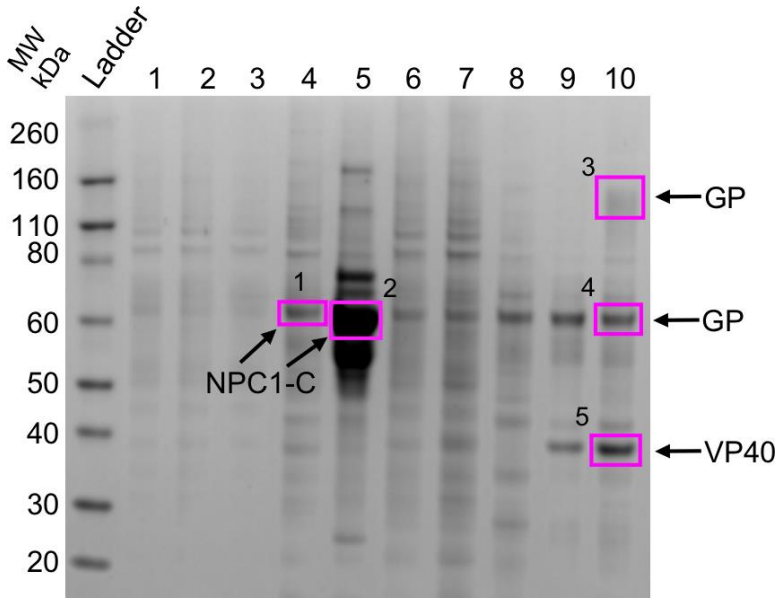

Figure 21. SDS-PAGE gel used for MS analysis of samples for expression of GP, VP40 and NPC1-C. Coomassie blue stained SDS-PAGE of samples suspected to contain GP, VP40, or NPC1-C. Legend: Lane 1. Transient NPC1-C cell lysate using attractene; Lane 2. Transient NPC1-C cell lysate using effectene; Lane 3. Transient NPC1 expression cell lysate using X-tremeGene; Lane 4. Transient NPC1-C cell lysate using X-tremeGene flask volume; Lane 5. Transient NPC1-C supernatant using X-tremeGene flask volume; Lane 6. GPΔmuc cell lysate; Lane 7. VP40/GPFull VLPs; Lane 8. GPΔmuc VLP; Lane 9. VP40/ GPΔmuc VLP; Lane 10. VP40/GPFull VLP. Outlined bands were excised from the gel and analyzed by in-gel digestion MS. Identities of the excised bands are as indicated in the figure.

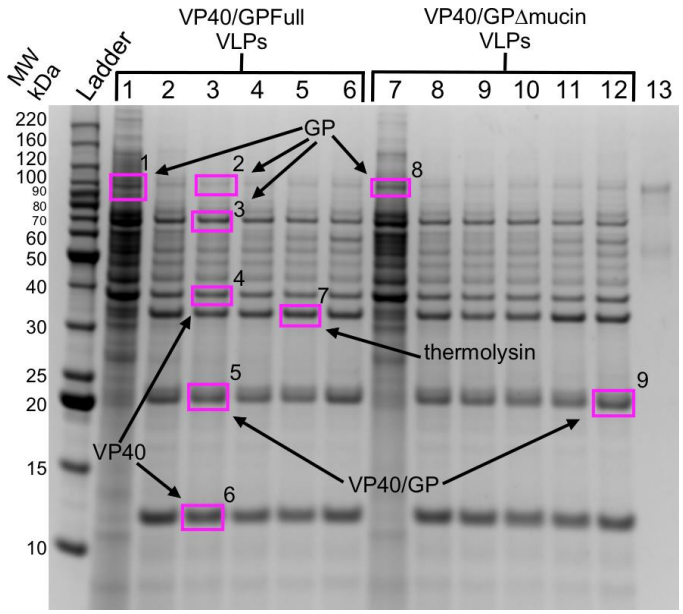

Figure 22. MS analysis of samples for expression of GP, VP40 and thermolysin. Coomassie blue stained SDS-PAGE of samples suspected to contain GP, VP40, or NPC1. Legend: Lanes 1-6 are VP40/GPFull; Lanes 7-12 are VP40/GPΔmuc; Lane 1. VP40/GPFull undiluted and undigested; Lane 7: VP40/GPΔmuc undiluted and undigested; Lane 13: GP positive control; Lanes 2,8: 2.5 minutes thermolysin; Lanes 3,9: 5 minutes thermolysin; Lanes 4,10:10 minutes thermolysin; Lanes 6,11: 30 minutes thermolysin; Lanes 6,12: 60 minutes thermolysin. Outlined bands were excised from the gel and analyzed by in-gel digestion MS. Identities of the excised bands are as indicated in the figure.

3.4 Liposomes

3.4.1 Optimization of Lipid Suspension

The starting protocol for making liposomes involved using 2.6 µmoles lipids (2.34 µmole DOPC and 0.26 µmole Ni-NTA or DOPE) and rehydrating the dried down lipids with 2.6 mL PBS, which corresponded to a lipid concentration of 0.823 mg/mL. This concentration was used in initial experiments and is similar to that used in previous nickel-binding experiments with liposomes containing Ni-lipids (Tuthill et al., 2006). In (Tuthill et al., 2006), liposomes were used at a concentration of 1 mg/mL and receptor at a concentration of 200 µg/mL.

Once the receptor NPC1 was incorporated into the experiment, the concentration of NPC1 began to limit the concentration of liposomes that could be added; if either the liposomes or NPC1 were kept at the desired concentration, the other ended up being at too low a concentration. In order to circumvent this issue, I decided to produce the liposomes at a concentration of 2 mg/mL by using 6.32 µmoles lipids (5.02 µmole DOPC, 1.26 µmole Ni-NTA or DOPE, and 0.0316 µmole Lissamine/Rhodamine PE) and continuing to rehydrate in 2.6 mL PBS.

Another recommendation from the literature, was to add a specific phospholipid to the suspension, PE with a lissamine/rhodamine labeled headgroup at 0.5% w/v (Tuthill et al., 2006). The addition of this head group gives the liposomes a pink hue, which allowed for easy visualization of liposome bands when optimizing the liposome flotation assay.

3.4.2 Extrusion of Lipid Suspension and Confirmation of Diameter

Once the lipids had been combined in the ratio stated above, the lipid suspension was extruded to produce liposomes. Initially, the suspension of lipids was cloudy and pink in colour. Successful extrusion of the suspension to form liposomes produced a clear pink liquid. Figure 6C shows the suspension becoming clear and less turbid after extrusion.

The extruded liposomes were diluted and run through the Nanosight NS500 to measure sizes of the liposomes produced. The Nanosight output curve of the extruded liposomes is shown in (Figure 23A). This is just one example of the many replicates that were run, and the peaks of the diameters measured was from 101-117 nm, with a mean of 113 nm and a standard deviation of 22.5 nm, while the base of each peak shows a range of 60-180 nm (Figure 23A). Confirmation of sizes measured by Nanosight were done by cryo-EM of the liposomes (Figure 23B). Measurements of 139 liposomes were taken using ImageJ and the images taken by cryo-EM. The results of the measurements were a mean of 108 nm and a standard deviation of 33 nm. Overall, these results were very similar to the numbers the Nanosight estimated at the top of the peak.

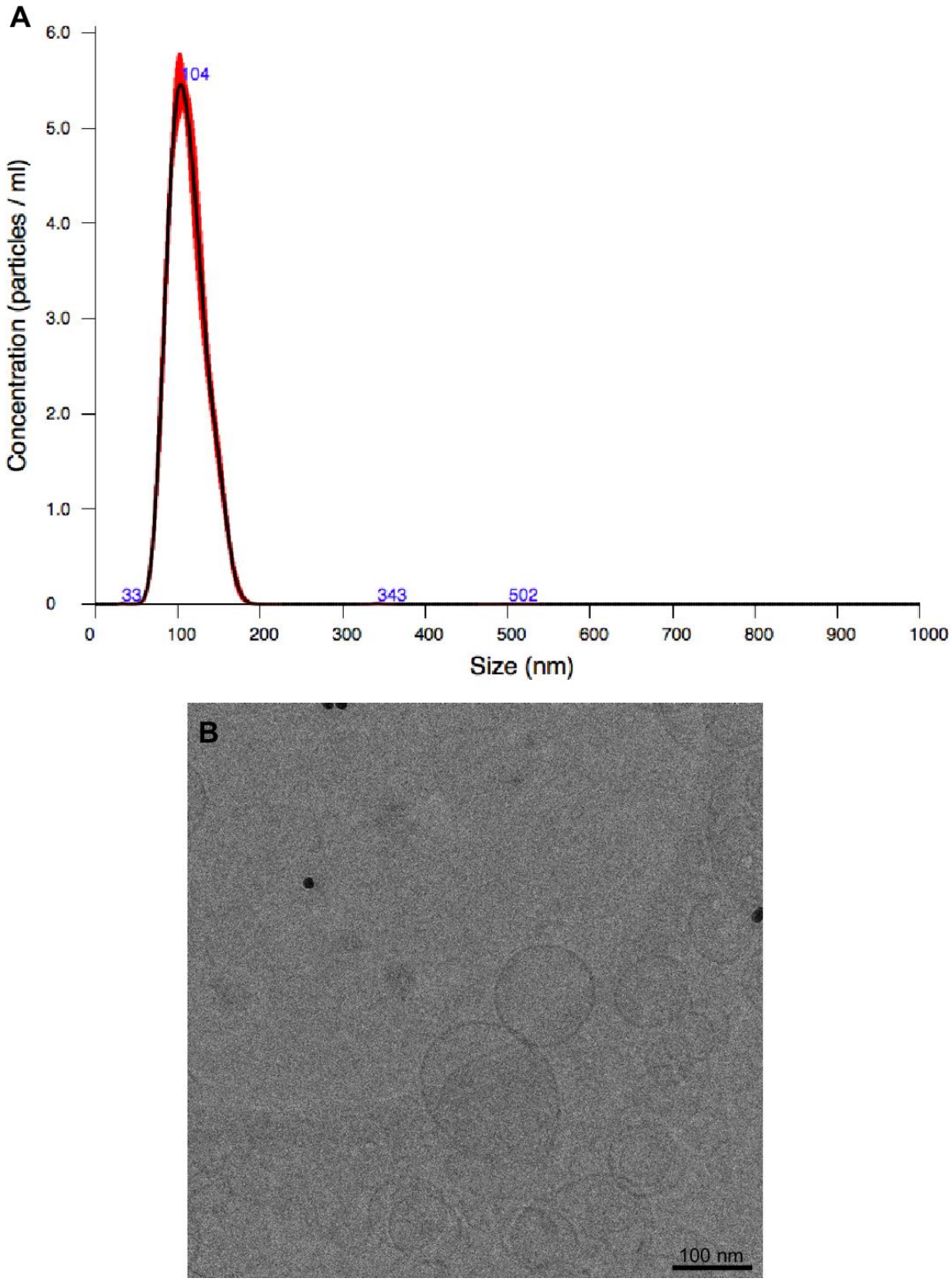

Figure 23. Nanosight output of DOPC:Ni-NTA liposomes (A) and a cryo-EM micrograph depicting DOPC:Ni-NTA liposomes. The lipid suspension was extruded through a membrane with 100 nm pores resulting in a nanosight output with liposomes measuring 104 nm (A) and liposomes measuring approximately 100 nm in diameter by cryo-EM (B).

3.4.3 Development of Liposome Flotation Assay

As a starting point for the flotation assay, a previously published method was adopted (Tuthill et al., 2006). The liposome suspension was adjusted to contain 20% Ficoll and 10% Ficoll was layered on top, followed by buffer in a centrifuge tube (Tuthill et al., 2006). Following centrifugation, the gradient fractions, collected from the top, were analyzed by Western blot (Figure 24). After several attempts using this method, it was apparent that the liposomes remained mostly at the bottom of the tube in fractions 9-11 (Figure 24). Thus, there was not enough separation between NPC1-C bound to liposomes and the excess unbound NPC1-C remaining at the bottom of the tube.

As a next step, a different density gradient medium, Optiprep^{TM} (iodixanol) was tried. A gradient was designed in a 13 mL ultracentrifuge tube with the sample adjusted to contain 40% iodixanol (3 mL), then 30% iodixanol layered on top (8 mL), followed by 5% iodixanol (1 mL), and finally PBS as the top layer (1 mL) (Weaver et al., 2007). The liposomes before and after ultracentrifugation are shown in (Figure 25A and B). Western blots of the collected fractions are shown in (Figure 25C-E), where C is NPC1-C alone, D is DOPE+NPC1, and E is Ni+NPC1-C. This protocol proved ideal to float the liposomes, with the unbound NPC1-C remaining at the bottom of the tube, while the NPC1-C-bound liposomes floated up to fraction 2-3 (Figure 25E). Cryo-EM images are shown in Figure 25F and G.

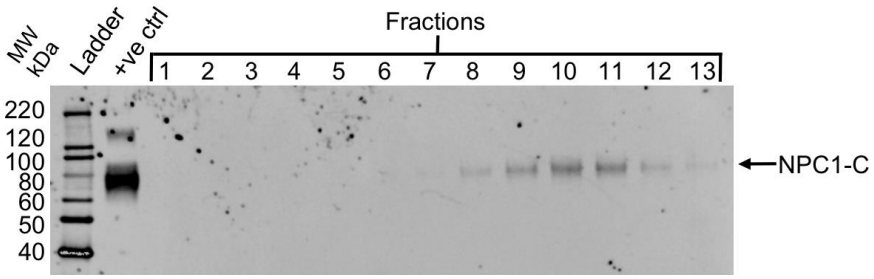

Figure 24. anti-Flag Western blot of fractions collected from Ficoll gradient liposome-NPC1-C flotation assay. Legend: Lanes labeled as ladder, NPC1-C positive control and fraction numbers. The liposomes did not float very far since the NPC1-C bound to liposomes is detected mostly in the bottom fractions.

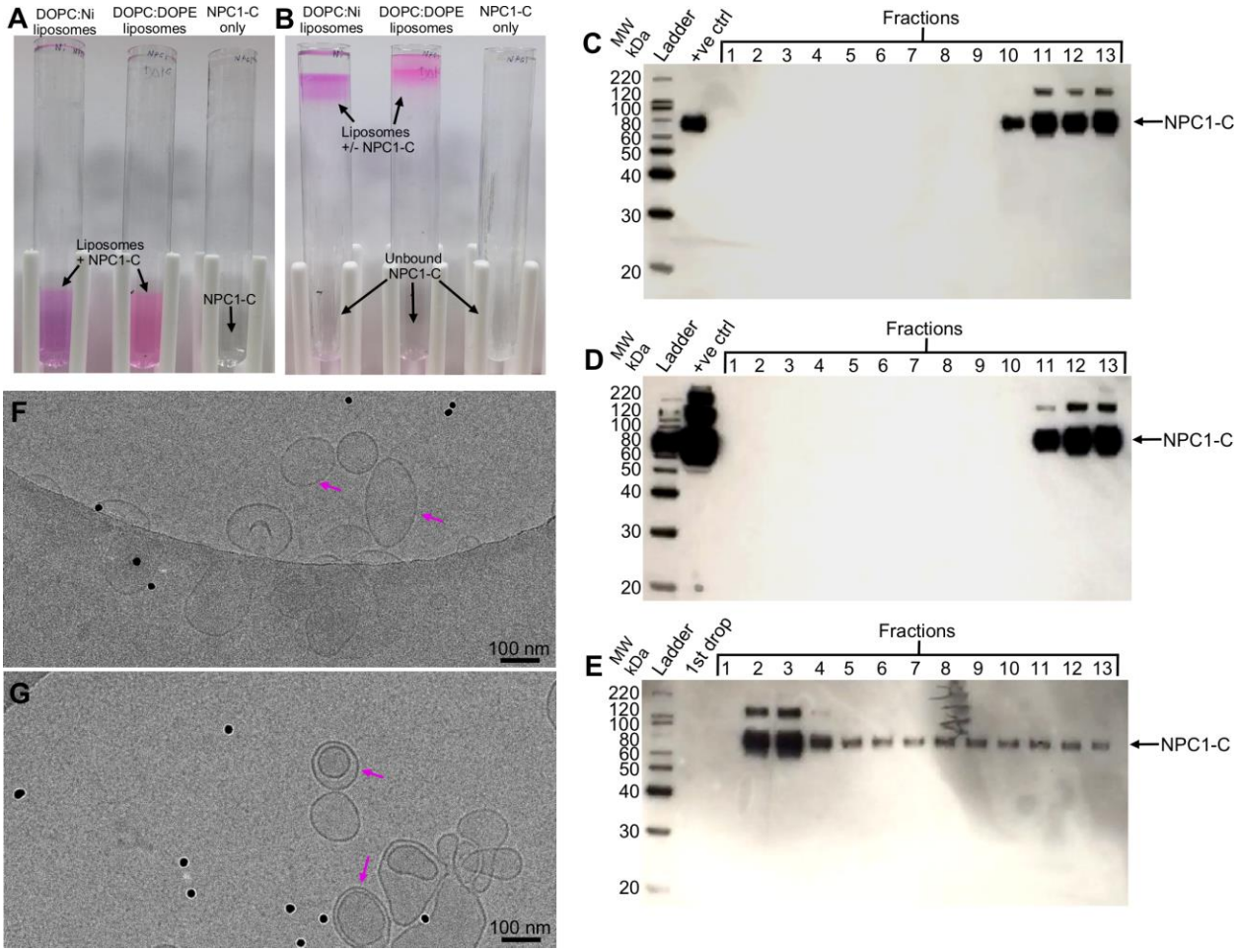

Figure 25. Analysis of liposome-NPC1-C flotation gradients. Liposomes + NPC1-C before (A) and after (B) ultracentrifugation, samples as indicated. (C-E) anti-Flag Western blots of fractions collected from gradients. Legend: Lanes labeled as samples loaded (C) NPC1-C only; (D) DOPC:DOPE + NPC1-C; (E) DOPC:Ni + NPC1-C. As seen above, NPC1-C only bound when Ni was present, and NPC1 did not float without liposomes. (F-G) cryo-EM micrographs of DOPC:Ni liposomes bound by NPC1-C.

3.5 Liposomes + NPC1-C

3.5.1 Conditions Required for Liposome-NPC1-C Interaction

The liposome flotation assay developed above was next used to determine whether the NPC1-C receptor was binding to the liposome via a His-tag to Ni interaction. The following combination of flotations were completed: DOPC:Ni: Lissamine/ Rhodamine PE liposomes (5.02 µmole DOPC, 1.26 µmole Ni-NTA, and 0.0316 µmole Lissamine/Rhodamine PE) with NPC1-C, DOPC:DOPE Lissamine/ Rhodamine PE (5.02 µmole DOPC, 1.26 µmole or DOPE, and 0.0316 µmole Lissamine/Rhodamine PE) with NPC1-C, and NPC1-C without lipids. As shown in (Figure 25C-E), only when liposomes and nickel were included, did the NPC1-C float to the top of the centrifuge tube along with the liposomes. Thus, this protocol proved ideal to separate NPC1-C-bound liposomes from unbound NPC1-C. As a control, an additional gradient was run consisting of DOPC:Ni:Lissamine/Rhodamine PE (5.02 µmole DOPC, 1.26 µmole DOPE, and 0.0316 µmole Lissamine/Rhodamine PE) with BSA. As shown in (Figure 26), the BSA remained at the bottom of the tube in fractions 11-14, and did not bind to the liposomes. This indicates a specific interaction with a His-tagged protein (NPC1-C) but not BSA.

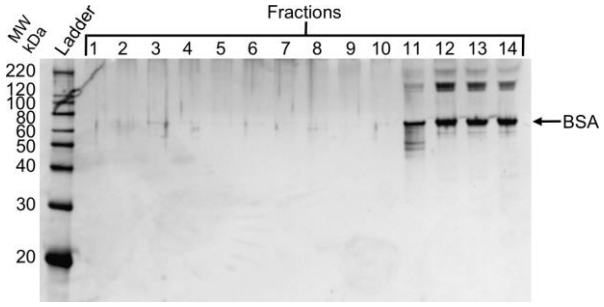

Figure 26. Silver stained SDS-PAGE of DOPC:Ni liposomes + BSA. Legend: Lanes labeled as fraction numbers. As shown, a protein lacking a His-tag will not bind to the DOPC:Ni liposomes.

3.5.2 Nanosight indication of NPC1-C binding

In addition to Western blotting, the Nanosight was also used to analyze NPC1-C binding to liposomes (Figure 27). An apparent increase in diameter observed by Nanosight measurements was consistent with NPC1-C binding. The peak measured increased from 110 nm to 142 nm in the example shown below. As previously described, the mean of the liposomes lacking NPC1-C was 113 nm with a standard deviation of 22.5 nm. The mean diameter of the liposomes with NPC1-C on the surface was 142.2 nm with a standard deviation of 35.7 nm, while the tops of the peaks ranged from 11-142 nm and the base of the peaks ranged from 80-250 nm. Since NPC1-C protrudes about 5 nm from the plasma membrane, as is deduced from a calculation using the NPC1 molecular weight of 80 kDa and an assumed protein density of 0.8Da/Å^3 (Henderson, 1995), this is consistent with the liposomes being coated with a 5-10 nm layer of protein on the outside.

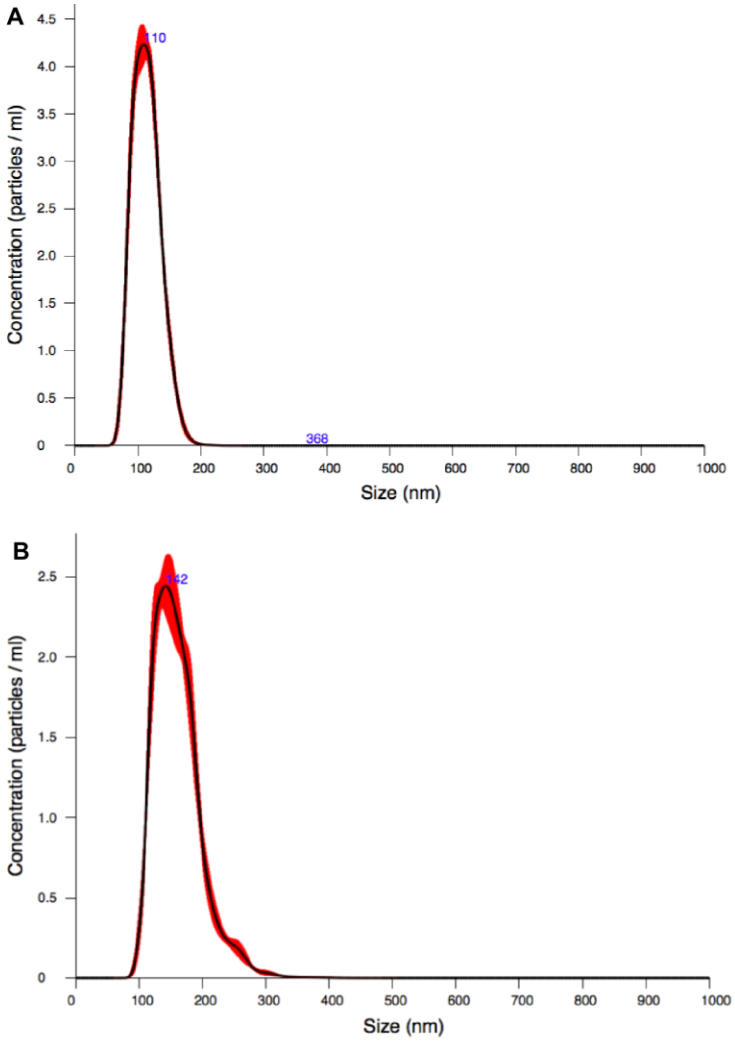

Figure 27. Nanosight outputs of DOPC:Ni liposomes without NPC1 (A) and with NPC1 (B). As shown, the measured diameter of the liposomes increases once the NPC1 has been added and allowed to bind.

3.6 VLPs + NPC1-C

3.6.1 Development of VLP Flotation Assay

Attempts were made to isolate VLPs bound to NPC1-C-liposomes. Purified NPC1-C-bound liposomes were added to VLPs and a second ultracentrifuge spin was done to remove unbound VLPs from this mixture. It was hoped that this would demonstrate NPC1-C binding to the VLPs. However, this was not successful since the VLPs floated and migrated to the top of the centrifuge tube in a similar manner to the liposomes (Figure 28). Western blot and Coomassie blue stained gels revealed GP, VP40, and NPC1-C at fractions corresponding to the floated VLP-NPC1-C-Liposomes, while nothing was detected at the bottom of the tube (data not shown).

In order to further analyze the interaction of NPC1-C with the VLPs, a flotation assay was developed to study the GP-NPC1-C interaction. The following combination of flotations were tested: VP40 GPFull VLPs + NPC1-C, VP40 GP∆muc VLPs with NPC1-C, and VP40 VLPs with NPC1-C. Figure 29 depicts the VLP flotations pre- (A) and post-ultracentrifugation (B) and the Coomassie stained SDS-PAGE (C, E, and G) and Western blots (D, F, and H) of the collected fractions. The result failed to explain the hypothesis that only the VP40 GP∆muc VLPs should interact with NPC1-C. Since the NPC1-C did not bind to any VLP form, a proteolytic cleavage event must be necessary to allow for NPC1-C binding to GP.

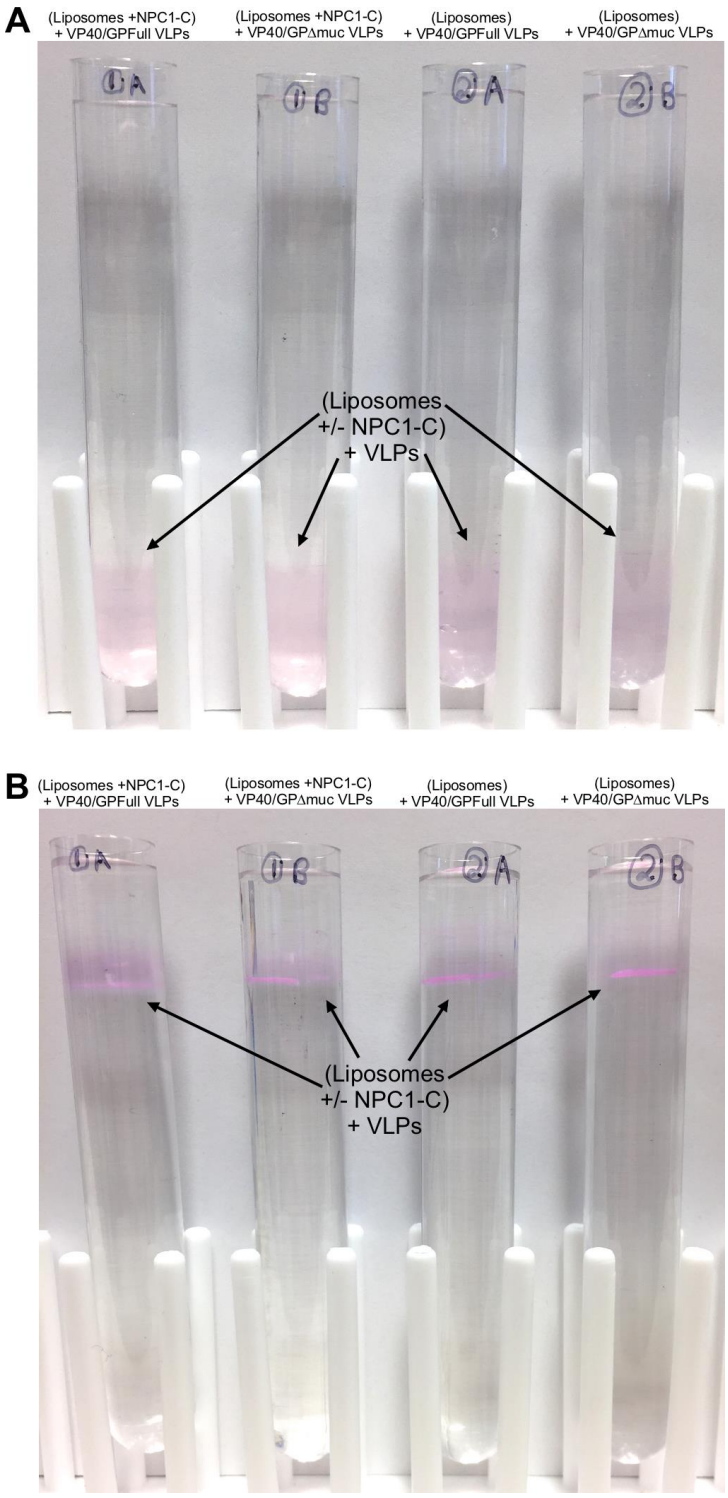

Figure 28. (Liposomes+NPC1-C) + VLPs pre- (A) and post-ultracentrifugation (B). This experiment depicted that the VLPs float along with the liposomes and allowed the design of a VLP flotation assay to confirm GP-NPC1-C interaction.

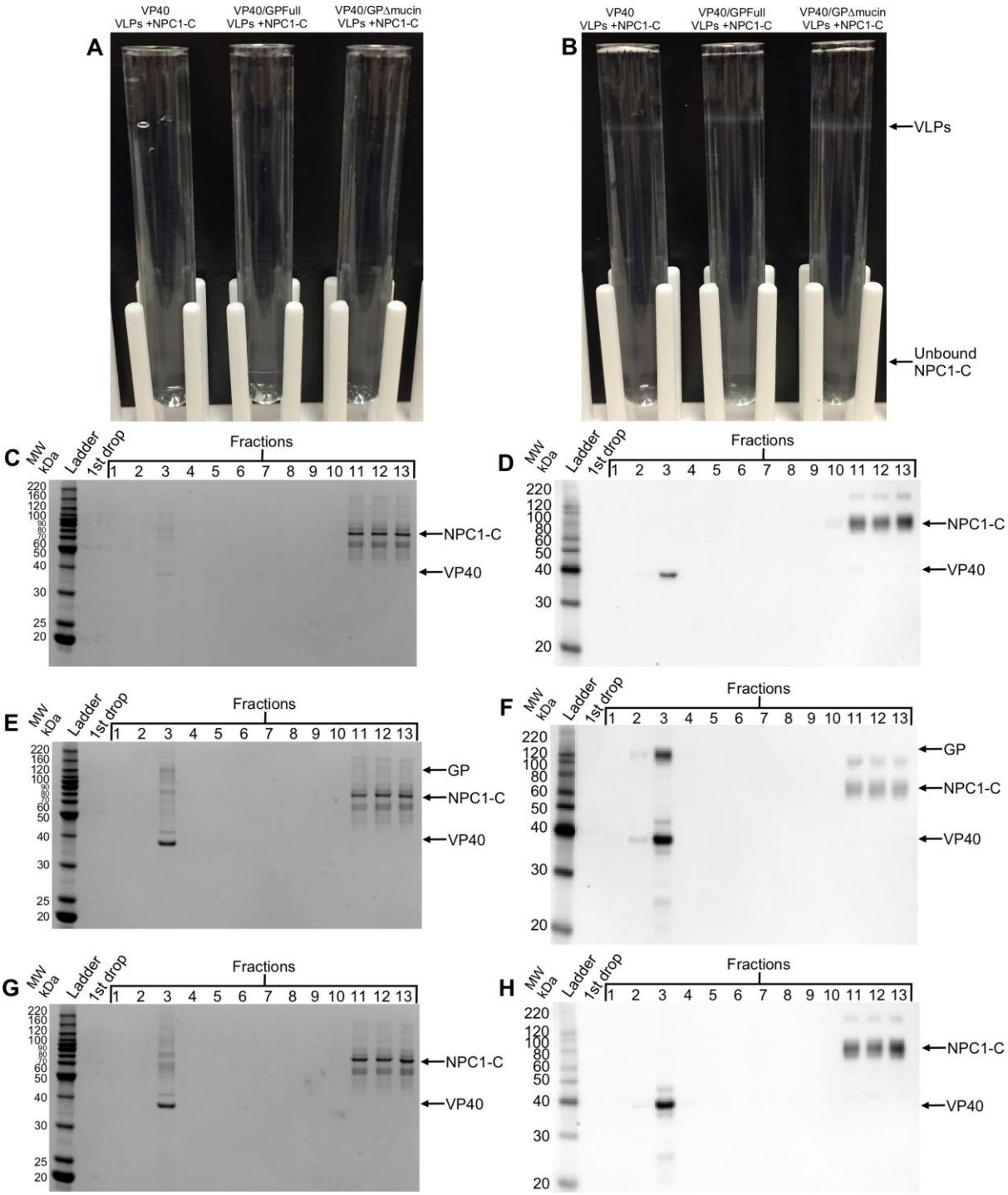

Figure 29. VLP flotation assay showing the lack of interaction between NPC1-C and GP. Gradients pre- (A) and post-ultracentrifugation. Coomassie blue stained SDS-PAGE (C, E, G) and anti-Flag Western blots (D, F, H) of VP40 VLPs (C, D), VP40/GPFull VLPs (E, F), and VP40/GPΔmuc VLPs (G, H). Legend for all gels and westerns: Lanes labeled as fraction numbers.

3.6.2 Conditions Required for VLP-NPC1-C Interaction

The previous experiment indicated that NPC1-C did not interact with any of the VLP forms. Recently it was suggested that it was necessary to treat the GPΔmuc mutant with thermolysin before binding with NPC1-C can occur (Wang et al., 2016). Therefore, the previous experiments were repeated but with VLPs that had been previously cleaved with thermolysin: VP40 VLPs with NPC1-C (Figure 30), VP40 GPFull VLPs with NPC1-C (Figure 31), and VP40 GPΔmuc VLPs with NPC1-C (Figure 32). The results showed that NPC1-C only bound to the VP40 GPΔmuc VLPs that had been previously cleaved by thermolysin treatment (Figure 32). Since the Coomassie blue stain was not sensitive enough to detect the NPC1-C in fraction 3, silver staining of select fractions was done to visualize NPC1-C by SDS-PAGE (Figure 33). Thus, it was shown conclusively that both deletion of the MLD of the GP protein as well as thermolysin cleavage, are needed before the GP on the surface of the VLPs will bind with NPC1-C-liposomes.

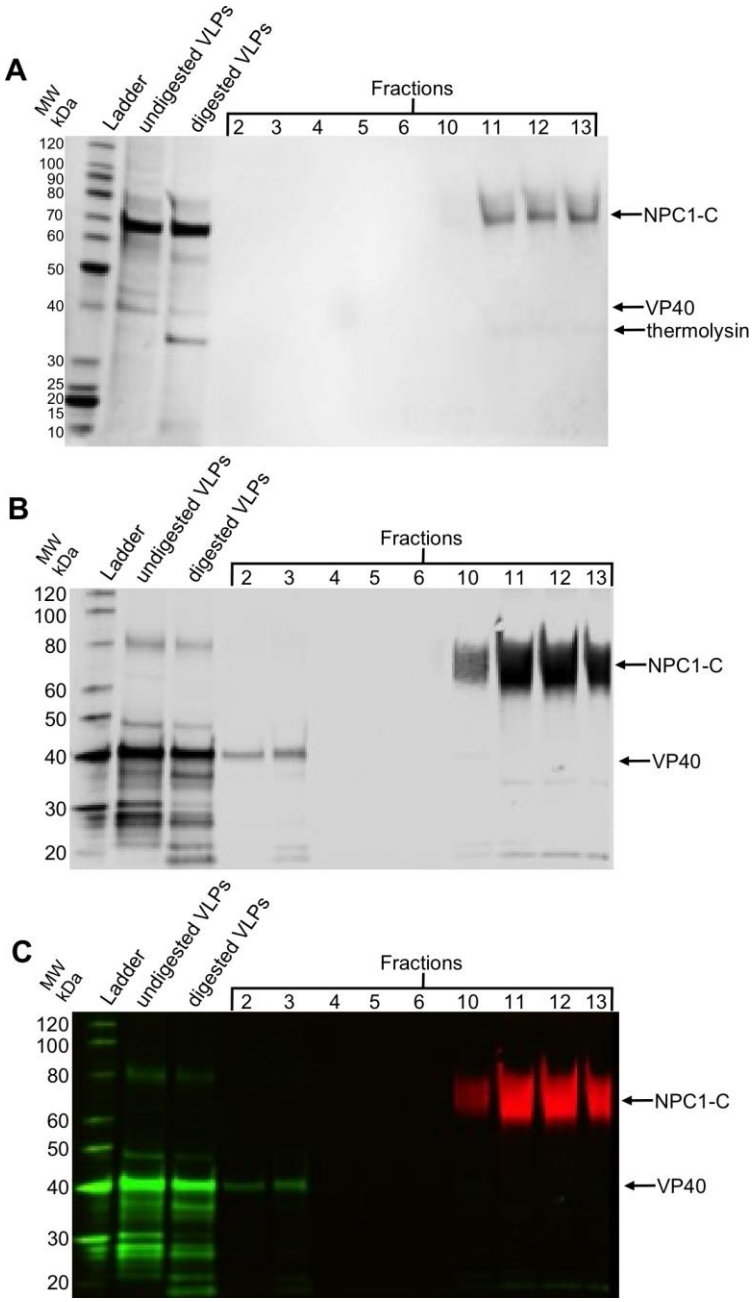

Figure 30. Coomassie blue stained SDS-PAGE (A) and anti-VP40/anti-Flag Western blots (B, C) of thermolysin digested VP40 VLPs-NPC1-C flotation experiments. Legend for all gels and blots: Lanes labeled as sample or fraction numbers. The Western blot is shown twice: once in grayscale (B) and once in colour (C) to depict the anti-VP40 detection in green, and the anti-Flag detection of NPC1-C in red. As shown, NPC1-C did not bind thermolysin digested VP40 VLPs.

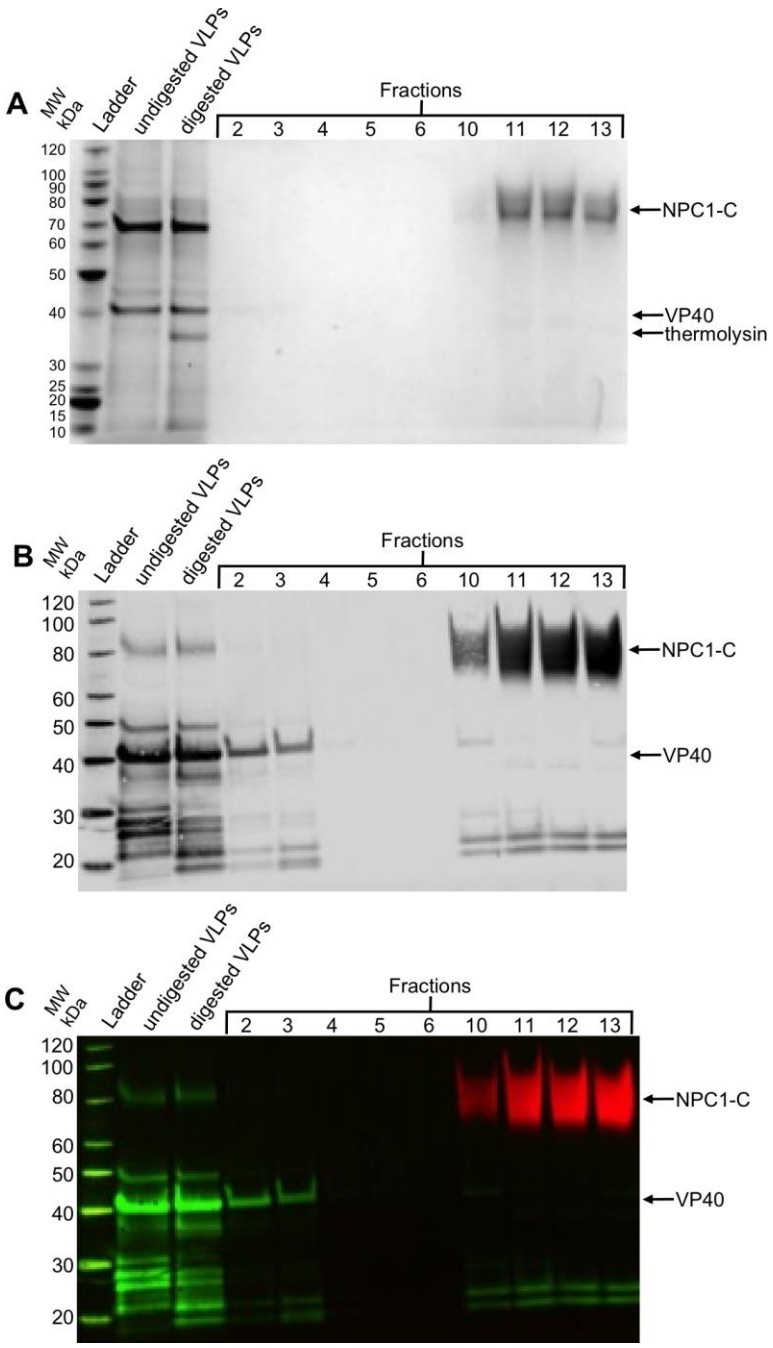

Figure 31. Coomassie blue stained SDS-PAGE (A) and anti-VP40/anti-Flag Western blots (B, C) of thermolysin digested VP40/GPFull VLPs-NPC1-C flotation experiments. Legend for all gels and blots: Lanes labeled as sample or fraction numbers. The Western blot is shown twice: once in grayscale (B) and once in colour (C) to depict the anti-VP40 detection in green, and the anti-Flag detection of NPC1-C in red. As shown, NPC1-C did not bind thermolysin digested VP40/GPFull VLPs.

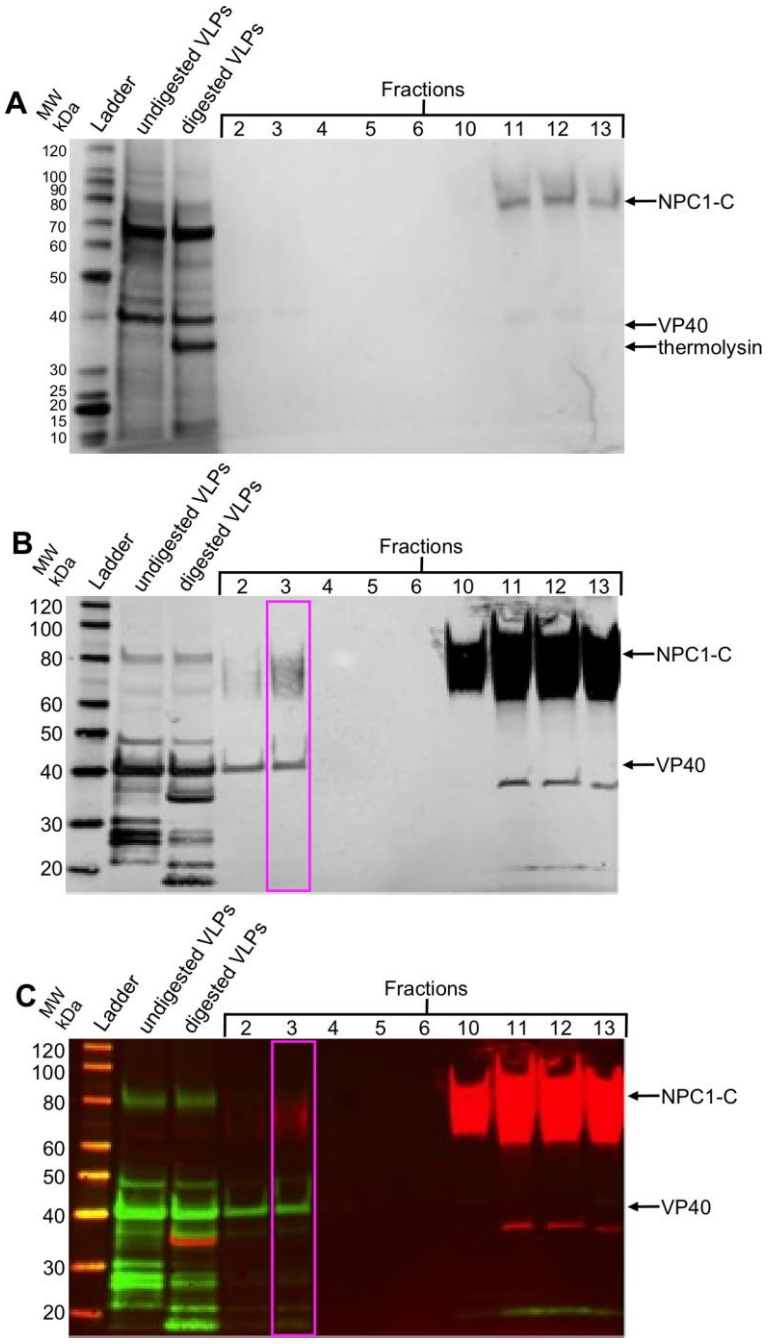

Figure 32. Coomassie blue stained SDS-PAGE (A) and anti-VP40/anti-Flag Western blots (B, C) of thermolysin digested VP40/GPΔmuc VLPs-NPC1-C flotation experiments. Legend for all gels and blots: Lanes labeled as sample or fraction numbers. The Western blot is shown twice: once in grayscale (B) and once in colour (C) to depict the anti-VP40 detection in green, and the anti-Flag detection of NPC1-C in red. As shown by the pink box, NPC1-C only bound in this scenario, when VP40/GPΔmuc VLPs were digested with thermolysin.

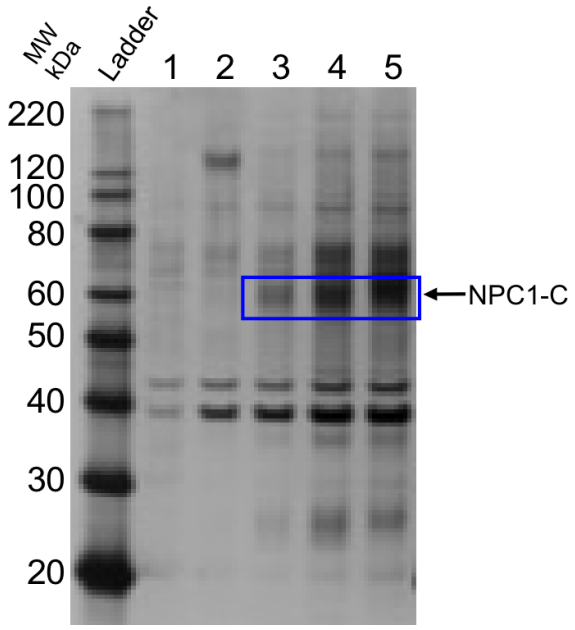

Figure 33. Silver stained SDS-PAGE of various fractions that were either positive for NPC1-C or negative for NPC1-C. Legend: Lane 1. VP40 VLPs+NPC1-C fraction 3; Lane 2. VP40/GPFull VLPs+NPC1-C fraction 3; Lane 3. VP40/GPΔmuc VLPs+NPC1-C (at 75μg/mL) fraction 3; Lane 4. VP40/GPΔmuc VLPs (from 170720)+NPC1-C (at 115 μg/mL); Lane 5. VP40/GPΔmuc VLPs (from 170629)+NPC1-C (at 115 μg/mL). The blue box indicates the NPC1-C bands that are only visible when NPC1 is incubated, and binds to thermolysin treated VP40/GPΔmuc VLPs.

3.7 Interactions Observed Between (Liposomes + NPC1-C) + VLPs

Finally, the interaction of NPC1-C liposomes with VLPs was analyzed by cryo-EM. Liposomes were prepared and incubated with NPC1, followed by flotation to remove unbound NPC1-C as shown in (Figure 34). The addition of NPC1-C seems to result in a more defined band of liposomes. Meanwhile, VP40 GPΔmuc VLPs were digested with thermolysin. The following combinations of VLPs and liposomes were incubated together, followed by plunge-freezing in liquid ethane for observation by cryo-EM:

- VP40 GPFull VLPs + NPC1-C-Liposomes
- Cleaved VP40 GPΔmuc VLPs + Liposomes
- VP40 GPΔmuc VLPs + NPC1-C-Liposomes
- Cleaved VP40 GPΔmuc VLPs + NPC1-C-Liposomes

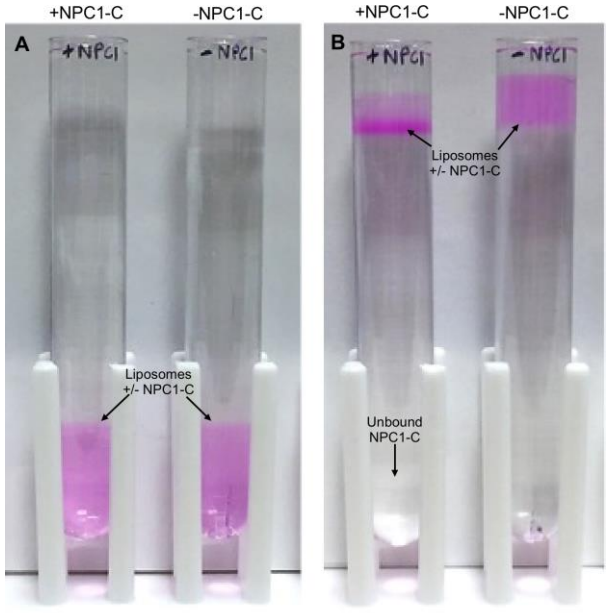

Figure 34. DOPC:Ni liposomes with and without NPC1 shown both pre- (A) and post-ultracentrifugation (B).

Cryo-EM micrographs of VLPs without the addition of liposomes are shown in low magnification in Figure 35 and in high magnification in Figure 36. These images depict the wide array of sizes and shapes that the VLPs form when produced. Cryo-EM micrographs of cleaved VP40 GPΔmuc VLPs + liposomes are shown in Figure 37. As shown in this figure, there are very few liposomes immediately surrounding the VLPs due to the lack of NPC1-C in this particular experiment. Cryo-EM micrographs of uncleaved VP40 GPΔmuc VLPs + NPC1-C decorated liposomes are shown in Figure 38. As shown in this figure, there are again very few liposomes surrounding the VLPs due to the lack of thermolysin treatment on the VLPs in this experiment. Cryo-EM micrographs of cleaved VP40 GPΔmuc VLPs + NPC1-C decorated liposomes are shown in Figure 39. As shown in this figure, the number of liposomes surrounding the VLPs has increased greatly, due to the interaction of the cleaved GP on the VLPs with the NPC1-C on the surface of the liposomes.

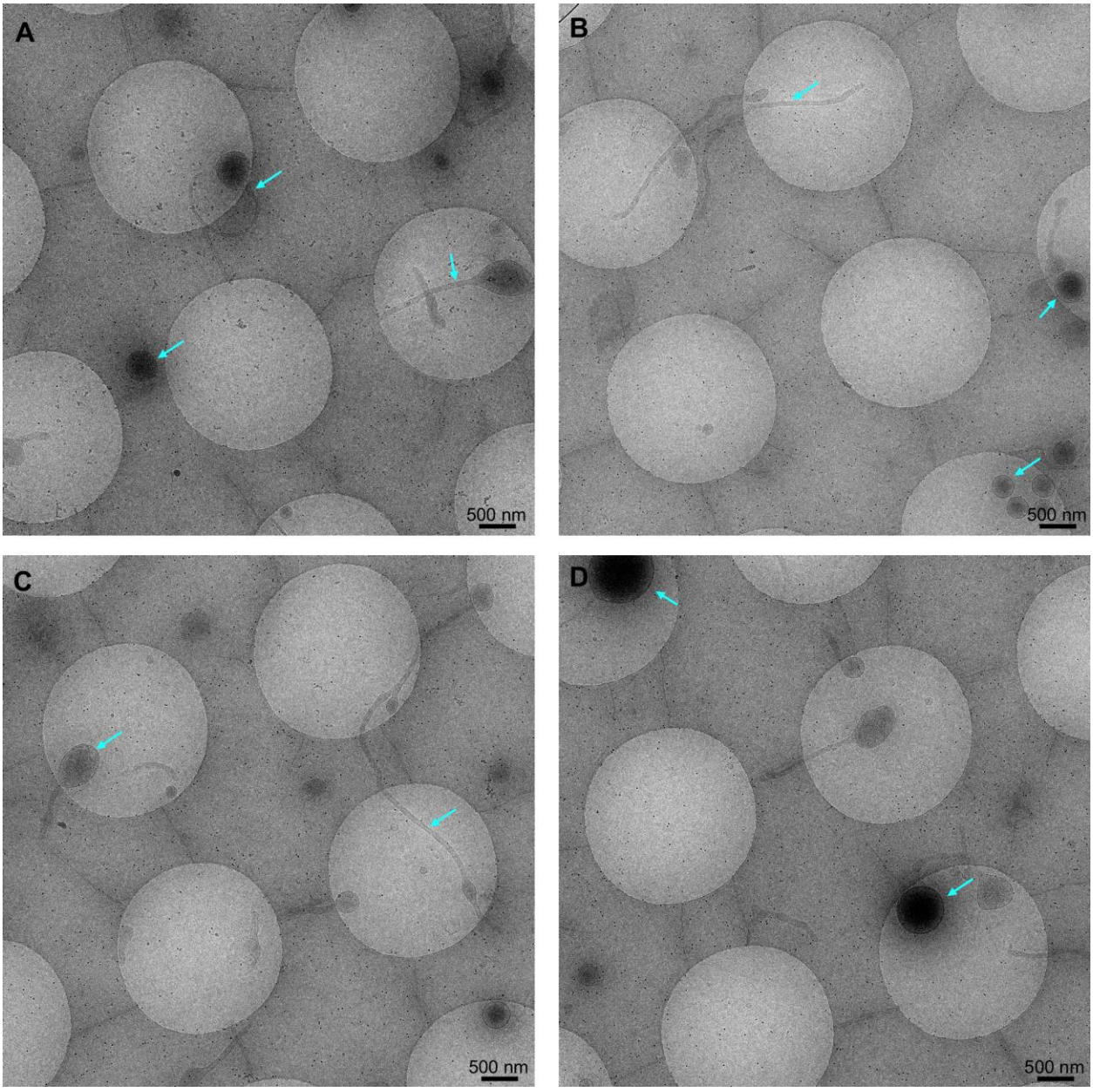

Figure 35. Cryo-EM micrographs of undigested VP40/GPΔmuc VLPs at 5000x magnification. These micrographs depict the wide variation in shape and size of the VLPs. Select VLPs are indicated by blue arrows.

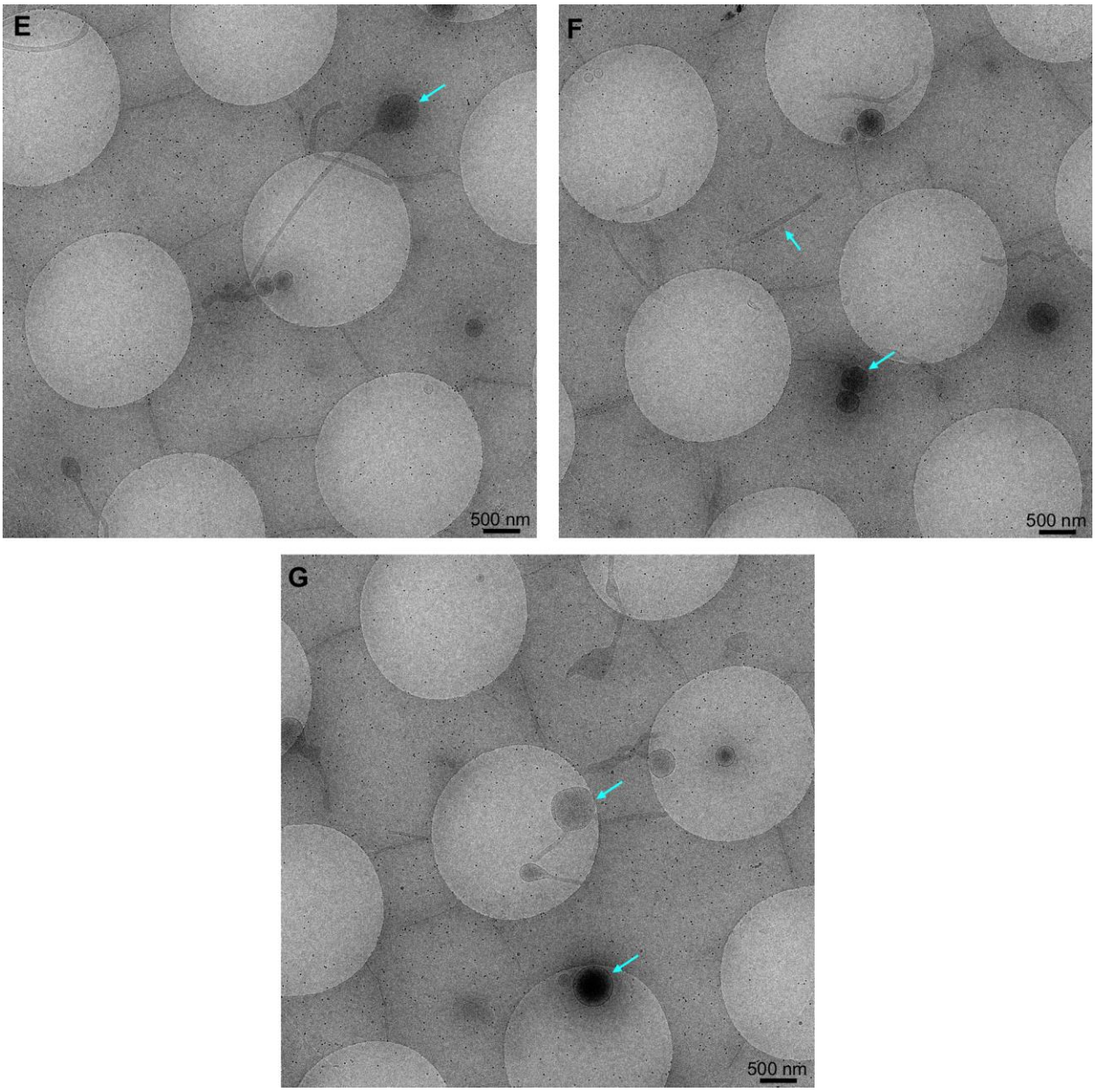

Figure 35 continued.

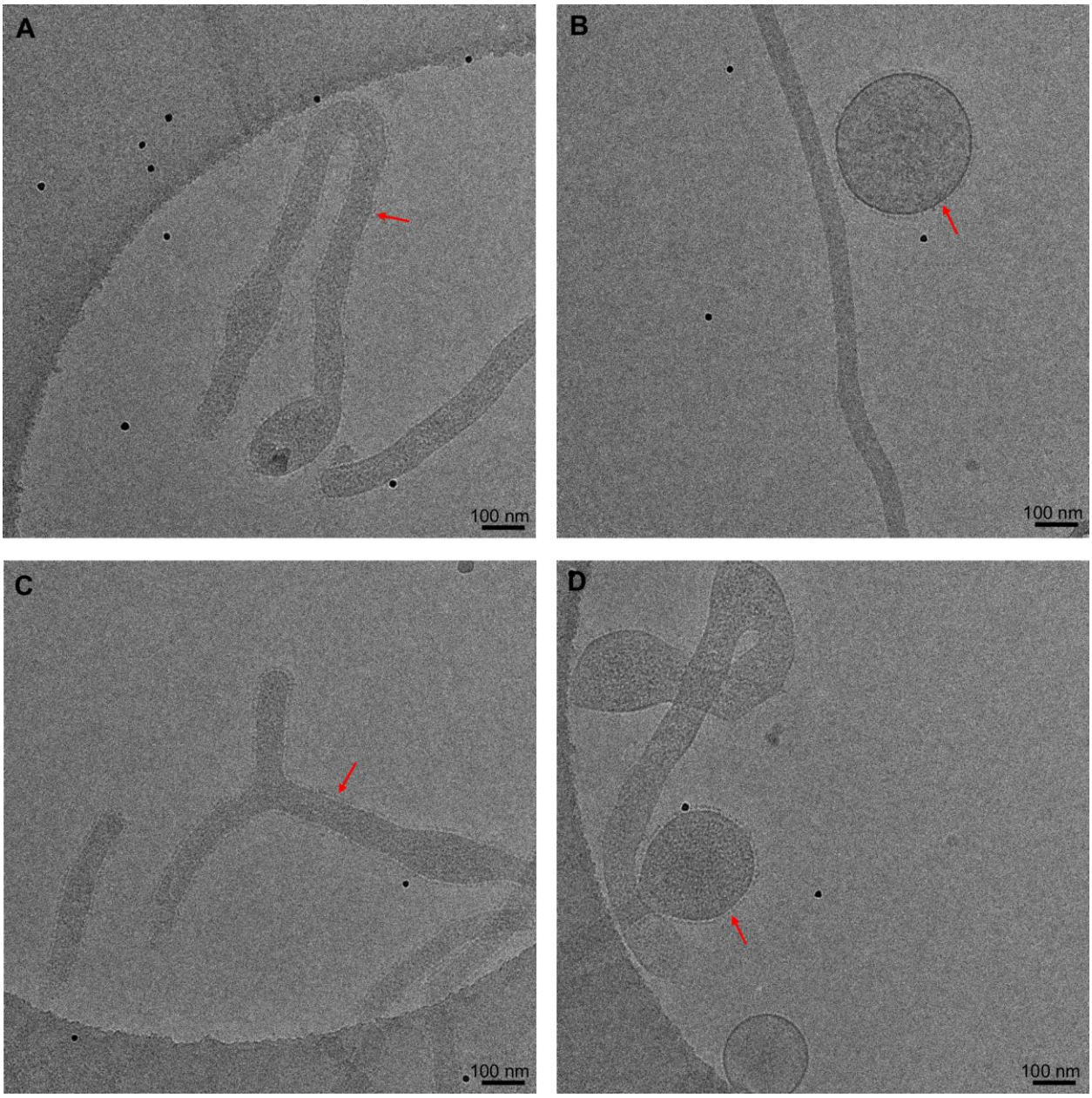

Figure 36. Cryo-EM micrographs of undigested VP40/GPΔmuc VLPs at 29,000x magnification. The wide variation of shape and size of the VLPs is once again depicted in these micrographs. The GP spikes on the surface of the VLPs are indicated by red arrows.

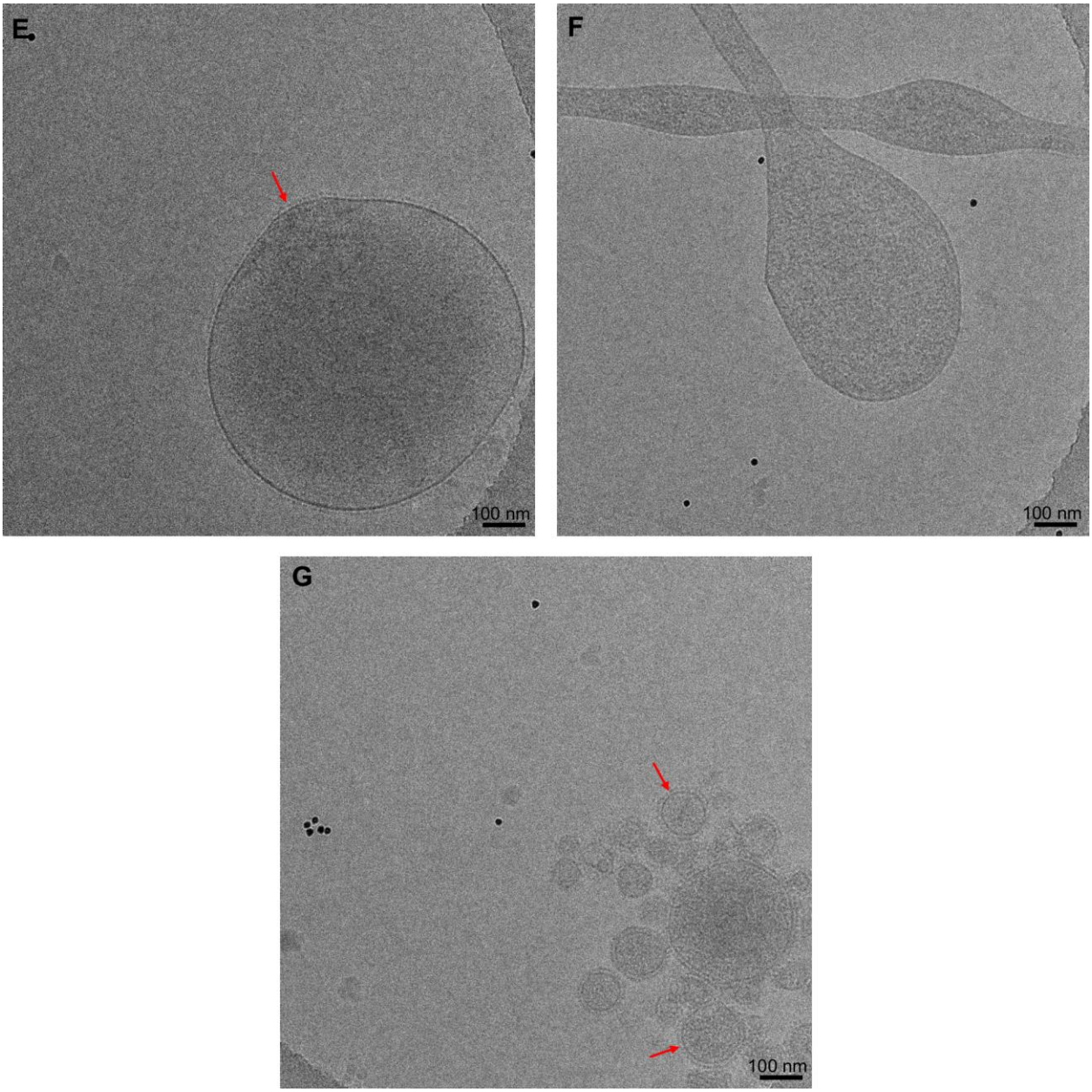

Figure 36 continued.

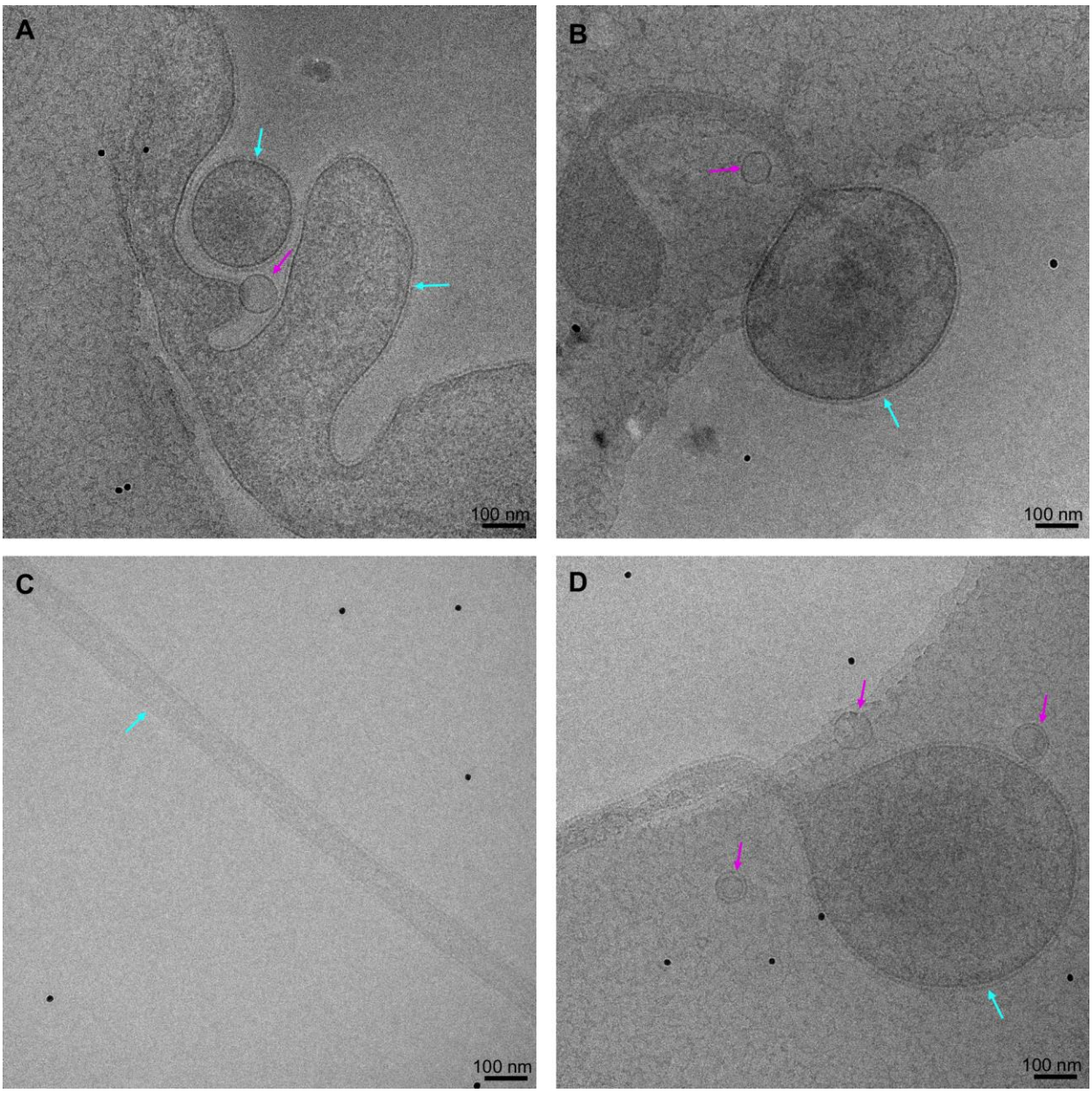

Figure 37. Liposomes without NPC1-C + thermolysin cleaved VP40/GPΔmuc VLPs. As shown, very few liposomes appear to associate with the VLPs when NPC1-C is absent. Liposomes are indicated by pink arrows and VLPs are indicated by blue arrows.

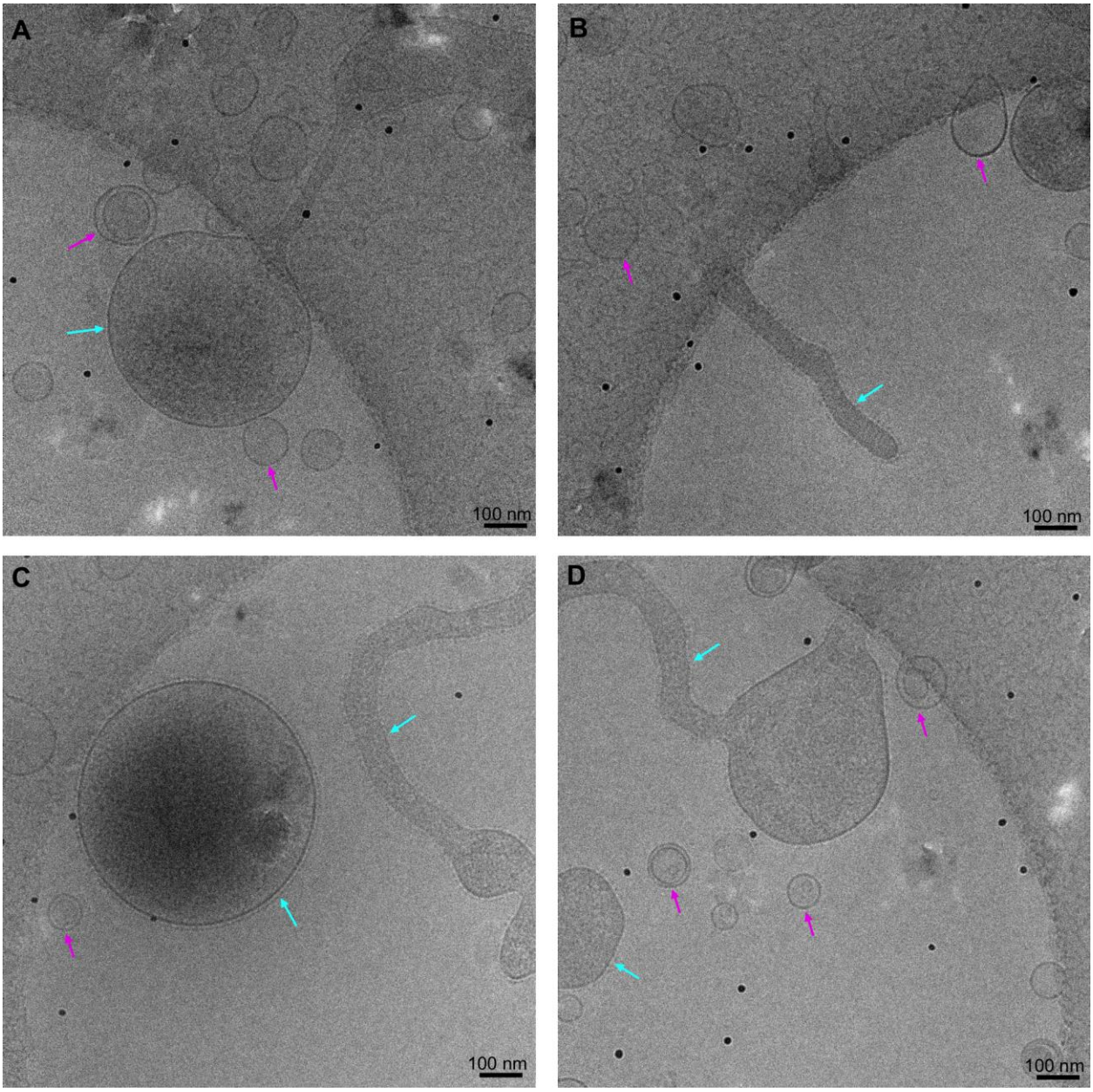

Figure 38. Liposomes + NPC1-C with untreated VP40/GPΔmuc VLPs. As shown, very few liposomes appear to associate with the VLPs when the VLPs have not been digested with thermolysin. Liposomes are indicated by pink arrows and VLPs are indicated by blue arrows.

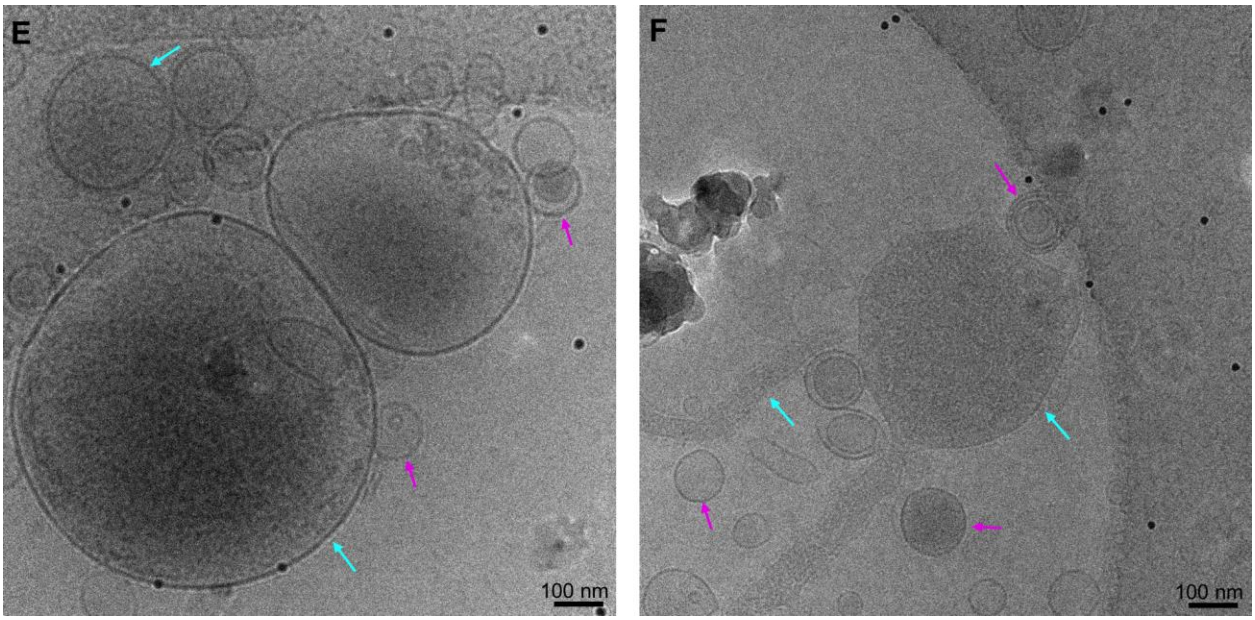

Figure 38 continued.

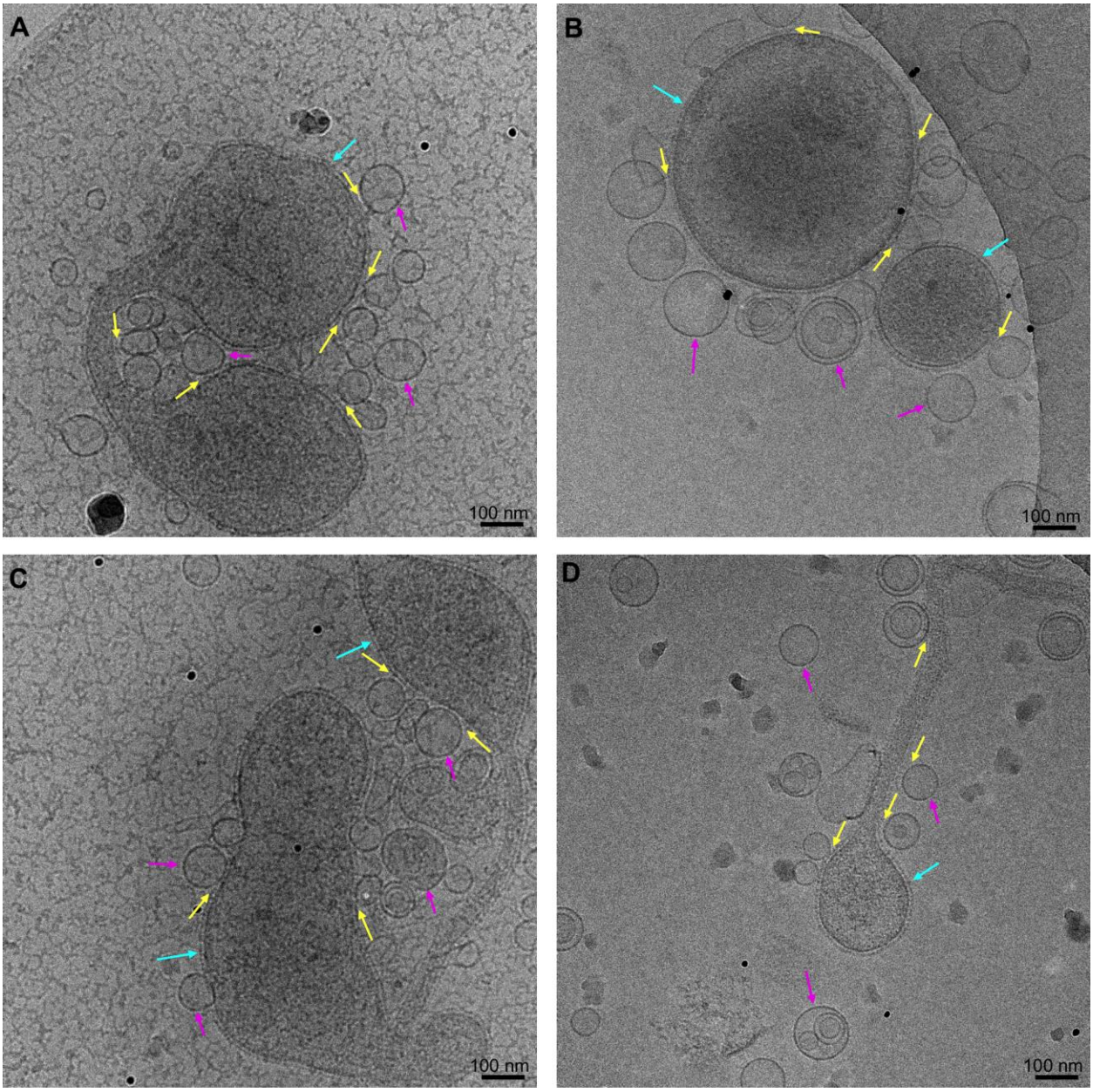

Figure 39. Liposomes + NPC1-C with thermolysin treated VP40/GPΔmuc VLPs. As seen in the figure, the NPC1-C-decorated liposomes (pink arrows) associated with the VLPs (blue arrows) very closely when the VP40/GPΔmuc VLPs have been thermolysin digested, in agreement with the findings above that NPC1-C only interacts with thermolysin digested VP40/GPΔmuc VLPs. Interaction is shown by the yellow arrows.

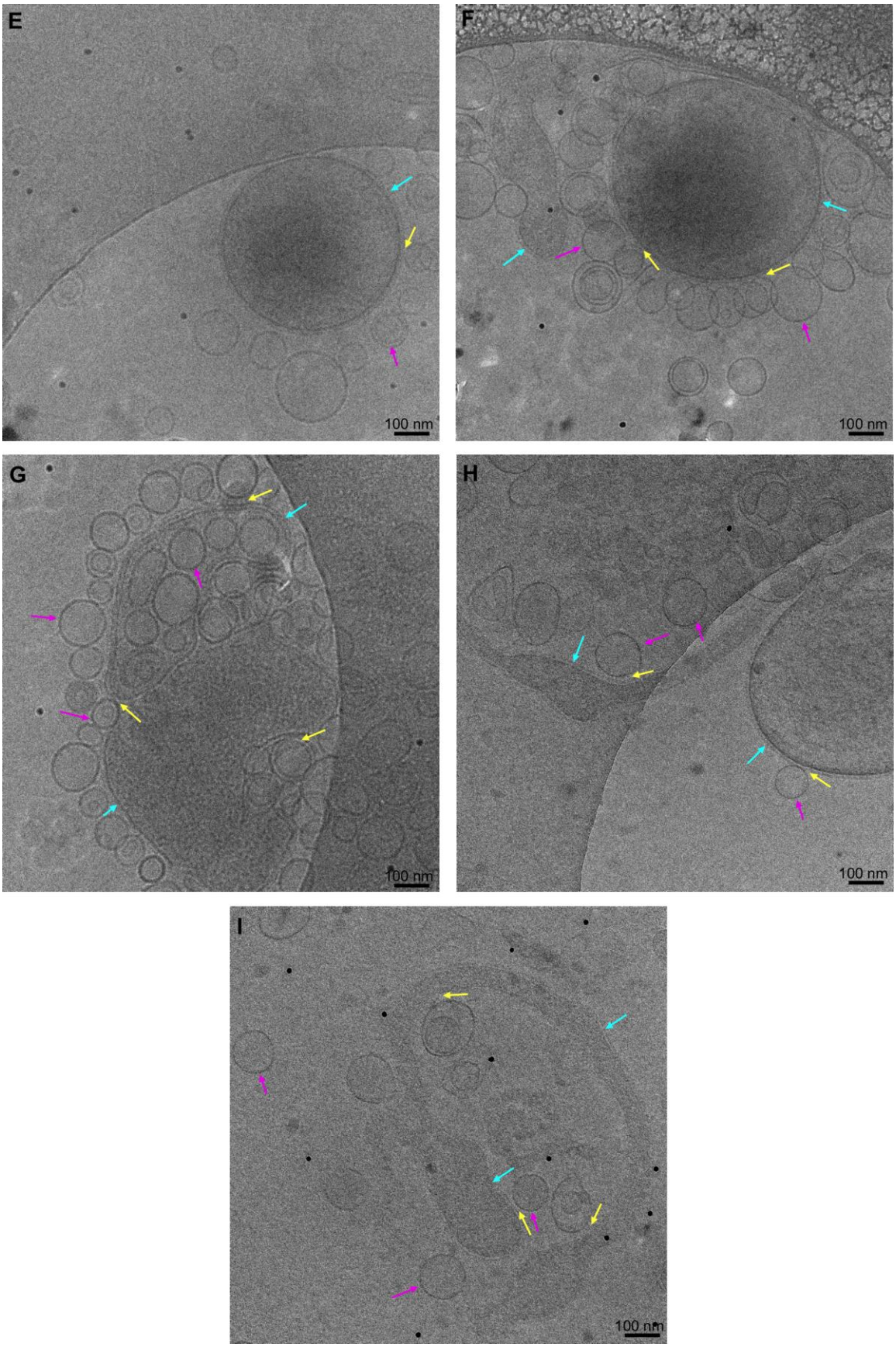

Figure 39 continued.

4. Discussion

This project investigated Ebola VLPs and receptor-decorated liposomes in order to develop a model system to allow further studies on attachment and fusion of enveloped viruses and their cell entry mechanisms. The successful attachment shown between the NPC1-C on the liposomes and the VLPs (Figure 39) demonstrates that this approach for studying attachment will be useful in further studies for how any enveloped virus attaches and fuses with their host cells. Implementation of this method in other viral studies could lead to elucidation of future targets for antivirals and vaccine development.

Utilizing a cell free system gives the researcher an immense amount of control over all of the variables in the experiment. Liposomes can be constructed from almost any lipid combination that is applicable to a specific experiment. Variables that could trigger fusion can also be controlled, be it the addition of receptor or a change in the pH of the system. It is an *in vitro* system that reduces the amount of complex interactions that would be present if the study were conducted on a whole cell. This system also uses VLPs instead of live virus. This aspect of the system greatly reduces the biosafety risks involved in conducting the experiment. In this particular case, Ebola VLPs can be handled in level 2 laboratories, whereas a level 4 containment laboratory would be necessary to conduct this experiment with the virus itself.

From a structural biology perspective, I have shown that this model system is capable of specific binding (Figure 32, Figure 39), but demonstration of fusion must await future studies. This system is ideal to investigate structural aspects of receptor-protein interactions, conditions, and intermediates that may occur during the fusion

process. Previous studies of viral fusion proteins have mostly used x-ray crystallography to obtain structures of molecules, with transmembrane domains having been deleted (McLellan et al., 2011). These studies have shown the molecules in pre- and post-fusion conformations, and details of structural intermediates are mostly speculation. Future applications of the model system developed in this thesis could aid in elucidating the details of these structural intermediates. The use of cells often results in a lot of debris from the cell culture medium. Whereas, the use of liposomes instead of cells diminishes the amount of background noise visualized in the specimen. Liposomes can also be made in a matter of hours as compared to the length of time it would take to express a membrane bound protein on the surface of a cell.

4.1 Ebola VLPs

The use of VLPs in this model system allowed the manipulation of the proteins involved. There was no need to include proteins, such as the proteins involved in nucleocapsid structure when all that was being studied was the GP interaction with the receptor. The liposome-VLP model system allows for the study of only factors of interest in any particular experiment.

4.1.1 GP cloning

Two versions of the Ebola GP protein were designed and cloned by myself using the NCBI and LaserGene software programs. At the beginning of my project, there were some challenges and setbacks with the cloning. These were solved by using the pcDNA3.1+ expression vector, which proved successful. Following transfection along with VP40, GPFull was detected as being expressed via Western blot (Figure 9). However, the GPΔmuc version of GP was not detected by Western blot. According to

the manufacturer, both of these antibodies bind a linear epitope on the MLD, hence the reason I was never able to detect the GPΔmuc version of the protein, since it does not have the MLD. Instead, our confirmation of expression is shown by the clearly visible spikes on the VLPs surface observed by TEM in Figure 11, as well as through the MS data Figure 21 and Figure 22.

Throughout the experiment, it was always difficult to detect GP expression via Coomassie blue stain SDS-PAGE. In SDS-PAGE, the sample is first boiled in a buffer containing SDS. Each protein in the mixture becomes fully denatured resulting in a more open structure with negatively charged SDS molecules along the polypeptide chain (Walker, 2009). The resulting proteins exhibit a similar shape, ensuring that the proteins separate exclusively due to their differing masses (Nelson and Cox, 2008c). While common methods of staining SDS-PAGE, including Coomassie blue or silver stain, work well for most proteins, they are much less sensitive when used for detection of glycoproteins, leading to weak staining or sometimes failure to detect the protein at all (Møller and Poulsen, 2009). This is due in part from the SDS molecules only binding the polypeptide part of the molecule (Walker, 2009), and steric interference by the carbohydrates present (Møller and Poulsen, 2009). Therefore, I concluded that these were the reasons for the difficulty in detecting GP on SDS-PAGE. In the future, staining kits specifically formulated for the visualization of glycoproteins may be of use to depict GP expression by SDS-PAGE.

Also of note are the different banding patterns shown for the full glycoprotein as compared to the positive control GP (Figure 9). The GP protein that I expressed was conducted using 293TN cells, a mammalian expression system. The GP positive control

obtained from IBT Bioservices was conducted using Sf9 cells, an insect expression system. As seen in Figure 9, the GP expressed in the mammalian system is about 140-160 kDa, while the GP expressed in the insect system is 120 kDa with multiple bands above and below the major band. These results are in agreement with experiments conducted by (Clarke et al., 2017) that showed GP expressed in mammalian systems to be 160 kDa and GP expressed in insect systems to be 110 kDa. This discrepancy in size between the two systems is due to key differences in the types of glycosylation imparted to the GP in both systems (Clarke et al., 2017). Glycoproteins as a whole are carbohydrate-protein conjugates. The carbohydrate is attached to the –OH of a serine or threonine residue (O-linked) or through an N-glycosyl link to the amide nitrogen of an asparagine residue (N-linked) (Nelson and Cox, 2008d). Mammalian expression systems result in a high percentage of complex N-linked glycans as well as O-linked glycans, while insect systems result in simple N-linked glycans, simple O-linked glycans and high mannose structures (Clarke et al., 2017). It has also been shown that mammalian systems have the ability to impart sialylation to proteins while most insect systems are unable to do this (Clarke et al., 2017). Taken together, the differences between these two expression methods are the reason for the discrepancy in molecular weight observed in the GP expressed in the mammalian system and the GP purchased as a positive control.

4.1.2 VLP Isolation

In order to isolate VLPs from cell culture supernatant, preparations were subject to ultracentrifugations through a 20% sucrose cushion as per (Jasenosky et al., 2001; Johnson et al., 2006). Initially, the VLPs failed to pellet and remained at the interphase

between the culture medium and the 20% sucrose in TNE buffer. Mixing the first 5 mL of medium with the 20% sucrose already in the tube appeared to give good results, rather than layering the medium over the 20% sucrose solution. This method produced a short density gradient, rather than a sudden step in density, and was successful in pelleting the VLPs. This was surprising since it has been shown that VLPs can be sedimented through 20% sucrose, I find this very odd that I was unable to pellet the VLPs through 20%. By definition, the density of 20% sucrose is 1.081 g/mL (Heidcamp, 2015), I measured the 20% sucrose in TNE used for this project to have a density of 1.078 g/mL. The density of a VP40 VLP is 1.102 g/mL, and a VP40 GPFull VLP is 1.091 g/mL (Johnson et al., 2006), while the density of the VLPs used in this project were 1.089 g/mL. Although the VLPs should pellet through 20% sucrose because the particles have a higher density, it is possible that the VLPs would not pellet through 20% sucrose due to the viscosity of the sucrose. Sucrose has a problem in that one needs a high molarity solution to get sufficient density for separation. This means the medium becomes quite viscous. Hence the reason for the development of high-density gradient media such as iodixanol: you can achieve a higher density with lower viscosity since each molecule is more dense. Perhaps a future option for purifying VLPs is to try using a 20% iodixanol cushion instead or to continue with sucrose but ultracentrifuge the cushion for a longer amount of time. I measured the density of 20% iodixanol in TNE by weighing out the volume of 60% iodixanol that would be required to produce a 20% solution and found the density to be 1.072 g/mL.

4.1.3 Thermolysin vs Cathepsins

As seen from electron microscopy analysis (Figure 13), 0.1 mg/mL for 5 minutes, or about a ratio of 1 part thermolysin to 8 parts VLPs appeared to be the optimal concentration of thermolysin to cleave the GP as analyzed by gel electrophoresis (Figure 12), yet leaving the VLPs intact (Figure 13). In order to successfully cleave GP with thermolysin, I first had to find the optimum buffer to resuspend the VLPs in. When the VLPs were purified by sucrose cushion, the VLPs were initially resuspended in PBS. However, when adding the thermolysin to the VLPs, although the thermolysin was resupended in the appropriate buffer at the optimum pH of 8.0 and containing the Ca^{2+} cofactor (ThermoBuffer: 50 mM Tris 8, 150 mM NaCl, 0.5 mM $CaCl_2$), the first attempts were unsuccessful. When the VLPs were resuspended in ThermoBuffer instead of PBS, the cleavage of GP was successful. Therefore, since so little thermolysin was required to cleave the VLPs, the optimum buffer for thermolysin activity was being diluted out by the PBS that the VLPs were in. Resuspending the VLPs in ThermoBuffer resulted in successful cleavage by thermolysin.

While searching for recommendations for thermolysin treatment, in most of the literature that I was able to find as described above, the thermolysin treatment was being applied to GP alone (Brecher et al., 2012; Miller et al., 2012a). In this experiment, the use of VP40 and EM likely provided a unique set of conditions that needed to be met. Since the VP40 drives budding and the formation of VLPs (lipid bilayer structure), the conditions that may have worked when treating GP alone seemed to be too harsh to maintain the structural integrity of the VLPs, especially for visualization of the VLPs by EM. Our requirements of forming VLPs and observing the experiment by EM, resulted in

the need to optimize the thermolysin conditions in a specific way for the needs of this experiment.

There are several differences between thermolysin and cathepsins, and their activities on Ebola GP. While thermolysin, a metalloprotease that functions at neutral pH cleaved the GPΔmuc version of GP to the 19kDa subunit necessary for fusion when used at a concentration between 0.1 and 0.25 mg/ml, cathepsin L and B (cysteine proteases) needed to be combined together, at a concentration of 5 µg/ml and at acidic pH in order to cleave this 19kDa fragment (Brecher et al., 2012). Otherwise, thermolysin digestion and cathepsin digestion appear to cleave the GP in a similar fashion (Brecher et al., 2012).

One aspect of note regarding cleavage with thermolysin are the known differences in specificity between thermolysin and cathepsin (Figure 40). Although literature on the effects of thermolysin on VP40 is sparse, I was unable to find any literature on treatment of VLPs with thermolysin, it is known that thermolysin is less specific, and this experiment showed proteolytic activity on the VP40 of the VLPs as indicated in the MS data (Figure 21 and Figure 22). Perhaps cathepsins, the enzymes that cleave GP during an EBOV infection, might not affect the VP40 protein at higher concentrations or longer exposures to the enzyme.

Cathepsin L:

Preferential cleavage:

P6	P5	P4	P3	P2	P1	↓	P1'	P2'	P3'	P4'
Xaa	Xaa	Xaa	hydrophobic	Phe	Arg	↓	Xaa	Xaa	Xaa	Xaa
Xaa	Xaa	Xaa	aromatic	Phe	Arg	↓	Xaa	Xaa	Xaa	Xaa
Xaa	Xaa	Xaa	hydrophobic	Arg	Arg	↓	Xaa	Xaa	Xaa	Xaa
Xaa	Xaa	Xaa	aromatic	Arg	Arg	↓	Xaa	Xaa	Xaa	Xaa

Xaa = any amino acid residue

hydrophobic = Ala, Val, Leu, Ile, Phe, Trp, Tyr

aromatic = Phe, Trp, His, Tyr

↓ = cleavage site

Thermolysin:

Preferential cleavage:

P6	P5	P4	P3	P2	P1	↓	P1'	P2'	P3'	P4'
Xaa	Xaa	Xaa	Xaa	Xaa	Xaa	↓	Leu	Xaa	Xaa	Xaa
Xaa	Xaa	Xaa	Xaa	Xaa	Xaa	↓	Phe	Xaa	Xaa	Xaa

Xaa = any amino acid residue

↓ = cleavage site

Figure 40. Cleavage sites for Cathepsin L and Thermolysin. As shown, cleavage sites for Cathepsin L are much more specific than for thermolysin. Figure reproduced with permission from Sigma Aldrich Inc.

4.2 NPC1-C

4.2.1 NPC1-C is Post-Translationally Modified

In Figure 14, it can be seen that there is a molecular weight discrepancy between NPC1-C in the cell lysate vs in the supernatant. This is due to the fact that NPC1 is a glycoprotein (Davies and Ioannou, 2000). In the lumen of the endoplasmic reticulum, newly synthesized proteins are post-translationally modified in many ways, such as the addition of glycosylation to form glycoproteins (Nelson and Cox, 2008b). In experiments conducted by (Davies and Ioannou, 2000)it was determined by treatment with N-glycosidase F, that domain C was 16 kDa larger when left untreated than it was after having been treated with N-glycosidase F. Therefore, domain C was concluded to be a glycosylated loop and was thus located in the lumen. Due to glycosylation, NPC1-C appears as a smear on most gels and Western blots (Figure 17).

4.2.2 Production by Stable Cell Line

Production of sufficiently pure NPC1-C was essential in order to model its activity in development of the VLP-liposome model system. A construct was ordered from Genscript based on a previously designed construct (Deffieu and Pfeffer, 2011). This is a soluble NPC1-C containing an N-terminal His-tag for purification and a FLAG-tag for Western blot detection. The results for transient expression showed insufficient yields of NPC1-C. These yields were impractical for the amounts required for cryo-EM and biochemical analyses. Numerous transfections would be needed which would take too much time and be very costly (Figure 14). A solution to the problem was found after discussions with Dr. Michael Carpenter: we would re-clone this construct to produce a stable cell line constitutively expressing the NPC1-C (Figure 15). In this way, one initial transfection, followed by infection with the Lentivirus expressing NPC1-C and hygromycin selection was successful in producing a stable cell line. Successive subculturing and saving of low-passage stocks was all that was needed. Harvesting of the cell culture supernatant, followed by purification, gave a substantial yield of protein for analysis in further experiments.

4.2.3 NPC1-C Purification

The NPC1-C construct was previously designed as described above, in such a way that interaction studies and purification could be completed with ease via the N-terminal His-tag. Since the His-tag is relatively small at 0.84kDa for a hex-His tag, and the fact that it exhibits a net neutral charge at physiological pH, His tags do not usually affect folding of the protein, nor the structure and function of said proteins (Carson et al.,

2007). For these reasons, the His-tag was the appropriate choice for downstream experiments in this project.

Large scale purifications of NPC1-C were completed using the HisPur Co^{2+} column. After this column, the fractions were pooled and run on the Resource Q Anion Exchange column. While this column did purify NPC1, upon review of the yields, it was clear that attempting to further purify the sample after the HisPur Co^{2+} column was resulting in less protein yield due to inevitable sample loss with each column, with no significant increase in purity.

4.2.4 Stability of NPC1 Domain C-His

As previously mentioned, NPC1 plays an essential role in cholesterol transport in mammalian cells (Davies and Ioannou, 2000). Only the luminal domain C of NPC1 is required for Ebola virus infection (Miller et al., 2012a). NPC1 deletion mutants lacking one of each of the 3 luminal domains was constructed and expressed in NPC1-null cells (Miller et al., 2012a). Upon infection with wild-type Ebola or rVSV-GP, the cells that were expressing the NPC1 construct with the domain C deletion remained uninfected, while the cells expressing NPC1 with the deletion in either domains A or I became infected (Miller et al., 2012a).

As seen in Figure 3, domain C of NPC1 is flanked by two transmembrane domains for membrane anchoring of the protein. While the NPC1-C construct could have been made in this way, and been arguably a more accurate representation of what is naturally occurring, working with proteins that have a transmembrane domain can be challenging. The benefits of constructing the NPC1-C with a His-tag and α-helical coiled coils for stability instead of the two transmembrane domains, is that we have generated

a soluble form of the receptor protein. Experiments would be extremely complex to attempt to visualize interaction between Ebola VLPs and cells expressing a membrane bound version of the NPC1-C on their surface. Production of this soluble form of NPC1-C allows the investigation of receptor-glycoprotein interactions in a focused, liposome model system without the presence of other cellular proteins that could hinder the investigation of the interaction. This model system, though not a completely accurate depiction of reality, is just that, a model. Once an understanding has been gained of the specific receptor-protein interaction, this model system can then be applied to experiments in the future that more accurately depict reality.

As far as the literature has shown, as long as there is some form of stability given to the NPC1-C construct, the NPC1-C functions normally in regard to the receptor activity for Ebola virus infection (Deffieu and Pfeffer, 2011). However, whether or not deletion of all but domain C impairs NPC1's ability to transport cholesterol remains unknown. Further studies are required to understand how NPC1 acts as a receptor during EBOV infection. An intriguing possibility is that NPC1 could be used as a target for antiviral drugs preventing or treating Ebola virus infection that would not adversely affect NPC1s prime function of cholesterol transport.

4.3 Liposomes

The use of liposomes as opposed to cells allowed for the experiment to be completed without all of the complications that a cell brings with it. When studying the interaction between a receptor and a protein, the rest of the organelles and proteins involved in maintaining the cell are irrelevant. Using liposomes provided a simple model

membrane that can be adapted to any size and phospholipid composition that is desired by the researcher.

4.3.1 Phospholipid Composition of Liposomes

In order to simplify the number of variables involved in this project, I decided to utilize a well established formula for liposomes. I chose to use phosphatidylcholine as the constant component of the liposomes, since it is the most prominent phospholipid present in cell membranes (Nelson and Cox, 2008a). In addition to phosphatidylcholine (5.02 μmole), I used Lissamine/Rhodamine phosphatidylethanolamine (0.0316 μmole) to impart a pink colour to the floated liposomes, phosphatidylethanolamine (1.26 μmole) in the control liposomes, while I used the Ni-NTA salt of lipids (1.26 μmole), to produce liposomes capable of binding a his-tagged protein.

While utilizing phosphatidylcholine (80% or 5.02 μmole) and phosphatidylethanolamine (20% or 1.26 μmole) worked well for this experiment, it may be worthwhile conducting the experiment with a different composition of lipids. The total lipid composition of bovine liver cells for example is 42% phosphatidylcholine, 22% phosphatidylethanolamine, 8% phosphatidylinositol, 7% cholesterol, and 20% other phospholipids (Avanti Polar Lipids, 2017). The bilayer of endosomes, the membranes that Ebola virus will fuse with in mammalian cells, are made up of phosphatidylcholine (50.7%), phosphatidylethanolamine (25.7%), as well as phosphatidylserine (9.5%), phosphatidylinositol (3.0%), cardiolipin (1.0%), and sphingomyelin (9.5%) (Urade et al., 1988) and exhibit a net negative charge (Nelson and Cox, 2008a). The addition of these lipids may mimic reality more closely. Cholesterol for strength may also be a good addition, perhaps the cholesterol providing stability would allow for the liposomes to last

longer in the fridge and experiments would not need to be completed within one day of extruding the liposomes.

An example cryo-EM image taken of the liposomes containing the Ni-NTA salt of lipids is shown in (Figure 23B). As analyzed by EM and by dynamic light scattering analysis with the Nanosight (Figure 23A), the liposomes constructed out of phosphatidylcholine and Ni-NTA were of similar shape and sizes. By EM, the diameter of 139 liposomes were measured and found to have a mean of 107.89 nm with a standard deviation of 32.99 nm. By dynamic light scattering with the Nanosight, the mean diameter was 113 nm with a standard deviation of 22.5 nm while the tops of the peaks measured from 101-117 nm and the bases of the peaks measured 60-180 nm. Therefore, this standard recipe for liposomes was settled on, and it was not necessary to experiment with a different combination of lipids at this stage.

4.3.2 Flotation Assay and Density Gradient Media

In developing a flotation assay to purify the receptor-decorated liposomes from unbound receptor, the literature was consulted for suitable protocols that could be adapted (Tuthill et al., 2006). Most membrane flotation assays that have been reported involve adjusting the sample to contain 20% Ficoll, and layering 10% Ficoll on top of that, followed by buffer in a centrifuge tube (Tuthill et al., 2006). I tried the following combinations: (3 mL sample in 20% Ficoll, 6 mL 10% Ficoll, and 4 mL PBS), (3 mL sample in 20% Ficoll, 5 mL 10% Ficoll, and 5 mL PBS) along with ultracentrifugation times ranging from 30 minutes to 2 hours at 100,000 xg in the SW40 rotor. However, I found that there was insufficient separation between the receptor-decorated liposomes and the unbound receptor no matter the volume of each layer used. For example, with a

centrifuge tube measuring 95 mm from the bottom to the top, the floated liposomes rose by only 25 mm, then the receptor would have been present in only the last 3 out of 13 one milliliter fractions. Ideally, good separation would result in the receptor being at the top of the tube (bound to liposomes), absent in the middle, and with unbound receptor being left at the bottom of the tube. Minor adjustments, as above, of the Ficoll volume each time, had no affect on improving the separation.

After discussions it was decided to try a different density gradient medium that was readily available in the laboratory, iodixanol, and a protocol based on that which was designed by (Weaver et al., 2007) was used. Iodixanol gradients resulted in much improved separation (Figure 25). The sample was adjusted to contain 40% iodixanol (3 mL), followed by 30% iodixanol (8 mL), 5% iodixanol (1 mL), and finally PBS (1 mL) on top. The gradient was centrifuged for 1 hour at 100,000 xg in the SW40 rotor. In a centrifuge tube with a height of 95 mm, the liposomes floated to about 88 mm height in the tube compared to the 25 mm obtained with Ficoll. This resulted in successful removal of unbound receptor producing liposomes that were saturated with NPC1-C. A higher specific binding activity is desirable for future GP-NPC1-C binding and fusion experiments.

It remains unclear as to why liposome flotation experiments were successful using iodixanol but not with Ficoll when research has shown Ficoll to be suitable for a liposome flotation assay (Tuthill et al., 2006). While Ficoll is marketed toward research involving the isolation of mononuclear cells from blood (GE Healthcare Life Sciences, 2011), it is a density gradient medium and should have resulted in floated liposomes. Both iodixanol and Ficoll are endotoxin free, aqueous, ready-to-use solutions, however

Iodixanol is less viscous than Ficoll (Sigma Aldrich, 2018), and the two have notably different densities with Ficoll having a density of 1.077 g/mL and iodixanol having a density of 1.32 g/mL. The theory behind the liposome flotation assay is that the liposomes float in the density gradient medium because they are less dense than the medium itself (Philippot and Schuber, 1995). Perhaps the liposomes floated more easily in the iodixanol because the iodixanol exhibits a higher density than Ficoll.

4.4 Liposomes + NPC1-C

After combining the DOPC:Ni-NTA liposomes with the purified his-tagged NPC1-C receptor, I conducted liposome flotation assays as described above to separate the receptor-decorated liposomes from the unbound receptor. The utilization of an affinity interaction between nickel and the his-tag allowed for the design of this liposome model system by creating an alternative to having a membrane bound receptor protein expressed on the surface of a cell. Following ultracentrifugation, the samples as shown in Figure 25 were fractionated and run on SDS-PAGE gel and Western blotted. The Western blot results are shown in Figure 25 and Figure 26. As can be seen by these Western blots, the NPC1-C receptor only bound to the liposomes that were made by incorporating the Ni-NTA into them, not to the DOPE control liposomes; therefore, as expected the Ni was necessary to interact with the His-tag. As another control and to prove that a His-tag was producing specific affinity binding to the liposome, and that no other interactions were taking place, I combined the DOPC:Ni-NTA liposomes with BSA (that has no poly-His sequence) and conducted a liposome flotation assay. All of the BSA pelleted to the bottom of the tube (Figure 26), and no BSA remained bound to the

floated liposomes. Therefore, the NPC1-C was binding to the DOPC:Ni-NTA liposomes specifically through a Ni-His-tag affinity interaction.

As stated previously, His-tagged proteins bind cobalt columns with greater specificity, but with a weaker interaction than with nickel (Thermo Fisher Scientific, 2012). While during purification of the NPC1-C, a cobalt column was used since the resulting interaction is more specific, for binding NPC1-C to the liposomes, nickel was used since the affinity interaction between histidine and nickel is greater, resulting in NPC1-C being bound to the liposome more strongly.

4.5 VLPs + NPC1-C

The experimental plan was to produce liposomes containing NPC1-C on their outside surface, float the liposomes to remove unbound NPC1-C, and observe the interaction of the NPC1-C-coated liposomes with VLPs. In order to confirm NPC1-C binding to the VLPs, a flotation experiment, with VLPs and the NPC1-C receptor without the liposomes was carried out. I had already established that NPC1-C bound specifically to the liposomes, so now it was necessary to show that the NPC1-C bound to the VLPs. As shown in Figure 29, the NPC1-C was not binding to the GPΔmuc VLPs. The next experiment we tried was to digest the GPΔmuc VLPs with thermolysin as was done by (Wang et al., 2016). Figure 30 shows the results of this experiment that proved successful binding of the NPC1-C to the thermolysin cleaved GPΔmuc VLPs.

The next question was, why did the NPC1-C not bind to the GPΔmuc VLPs without thermolysin cleavage? Previously published data indicated that cleavage of the MLD was required for NPC1-C to bind (Cote et al., 2011; Schornberg et al., 2006). Not only does cathepsin activity cleave the MLD, but also the glycan cap (Bale et al., 2011;

Hood et al., 2010; Lee et al., 2008). Since the glycan cap is still on the GPΔmuc construct we made, this result shows that cleavage or removal of the glycan cap is also required for NPC1-C to bind, and is consistent with other published studies (Cote et al., 2011; Wang et al., 2016). Perhaps the use of cathepsins L and B in future studies would yield a result more closely mimicking reality. Interestingly, thermolysin cleavage of the VLPs containing the GPFull version did not result in binding to NPC1-C (Figure 28). Thermolysin treatment of the MLD deleted version was necessary for NPC1-C to bind to the VLP. Therefore, it is likely that a two-stage cleavage of GP is needed to remove the MLD and the glycan cap, to allow NPC1-C to bind and Ebola infection to proceed, otherwise, thermolysin cleavage of the GPFull version (what is present upon infection) should have worked. Previous studies have alluded to the fact that both the MLD and the glycan cap must be cleaved in order for infection to proceed (Bale et al., 2011; Brecher et al., 2012), however, I was only able to find one other paper speculating that a “double cleavage” of the Ebola GP must happen (Wang et al., 2016). This research supports the “double cleavage” theory and that perhaps there is a two step process of cleaving GP that is required for successful infection.

One such component that may be missing from this model system is acid sphingomyelinase (ASMase) (Miller et al., 2012b). This enzyme converts the lipid sphingomyelin into phosphatidylcholine and ceramide and has been shown to play a role in rhinovirus and measles infections. Previous work to investigate if ASMase plays a role during Ebola infection showed that Ebola virus particles strongly associated with the sphingomyelin rich region of the cell membrane, and that depletion of the sphingomyelin in this region, greatly reduced Ebola virus infection (Miller et al., 2012b).

It was also found that Ebola VLPs strongly associated with surface-localized ASMase and sphingomyelin-rich regions. It was concluded that ASMase activity is necessary for efficient infection of cells by Ebola virus (Miller et al., 2012b). It would be interesting to investigate how the addition of sphingomyelin to the liposome mixture as well as the addition of ASMase to the experiment might affect the interaction observed between NPC1-C and the GPFull VLP. Maybe ASMase is the piece of the puzzle that has been missing to help solve the condundrum of how fusion between the Ebola virus envelope and the target membrane to occur.

4.6 Liposomes + NPC1-C + VLPs

When the NPC1-C decorated liposomes were added to the GPΔmuc VLPs that were thermolysin treated, samples were prepared for cryo-EM analysis to investigate possible interactions, and/or fusion (Figure 35). As can be seen from these images, binding of the receptor to the VLPs is occuring, but fusion is not.

One reason why fusion did not occur could be because this experiment was conducted at neutral pH. Low pH has been proven to play a role, but the only role it has strictly been proven to play during Ebola infection is to provide an acidic environment for cathepsin activity to occur (White et al., 2008). Perhaps this thesis is proof that low pH is not only required for endosomal cathepsin activity, but also for fusion to occur.

One other reason the fusion may not have occurred could have to do with the phospholipid composition of the liposomes. I decided to keep the liposomes simple by just utilizing phosphatidylcholine and phosphatidylethanolamine, and ending up with a net positive charge due to the Ni^{2+} atoms on the liposome surface to bind the his-tag. However, the bilayer of endosomes, the membranes that Ebola virus will fuse with in

mammalian cells, are made up of phosphatidylcholine, phosphatidylethanolamine, as well as phosphatidylserine, phosphatidylinositol, cardiolipin, and sphingomyelin (Urade et al., 1988) and exhibit a net negative charge (Nelson and Cox, 2008a). Since the phospholipid composition of the liposomes I used did not exactly mimic the phospholipid composition of endosomes, maybe this was not an exact depiction of how fusion would occur. During fusion experiments involving influenza, it was found that fusion with liposomes composed of phosphatidylcholine was dependent on the presence of cholesterol, whereas fusion with negatively charged liposomes such as phosphatidylserine or of phosphatidylcholine and phosphatidylethanolamine was able to occur in the absence of cholesterol (Nussbaum et al., 1992). In the experiments of this thesis, the control liposomes were composed of phosphatidylcholine and phosphatidylethanolamine, which in the case of influenza, fusion would have occurred. Perhaps, the addition of cholesterol would allow for fusion to occur spontaneously as it does for the influenza virus (Nussbaum et al., 1992).

The Nanosight particle characterization system was used to confirm the size of the liposomes and that NPC1 had bound to the liposomes. One original goal in the project had been to use the Nanosight to measure whether or not fusion between the liposome and VLP had occurred. Due to the immense variation in size and shape of Ebola VLPs, it was impossible to utilize the Nanosight for this purpose. The Nanosight output showed a large number of peaks at varying sizes (data not shown). A potential variation of this experiment could be to use an rVSV-GP instead of the Ebola VLP (Miller et al., 2012a). This method could result in improved Nanosight results since there

would be much less variation in the size of the VSV than was encountered with the VLPs.

When looking back at past research on the Ebola virus, a common theme is that the infection process is a two stage process involving the GP attaching to the endosomal receptor, NPC1-C, followed by the second stage, fusion (Beniac and Booth, 2017; White and Schornberg, 2012). In this study, I have explored the factors required to observe attachment of the GP to NPC1-C. This study is confirmation that a sort of "double cleavage" event takes place during priming of the GP that allows GP to successfully interact with NPC1-C. What remains to be discovered is the exact trigger for fusion. While low pH is required, it is unclear if this requirement is simply for activity of endosomal cathepsins and low pH is not required for fusion (Markosyan et al., 2016) or if after the GP spike has been proteolytically cleaved, low pH is required further. This research suggests that further acidification of the environment is required since fusion did not occur when using thermolysin in lieu of cathepsins. If low pH was only required for cathepsin activity, fusion should have occurred in this experiment. Something else, perhaps low pH, is required to trigger fusion.

5. Conclusion and Future Works

5.1 Experimental Conclusions Summary

The focus of this project was to develop a cell-free model system to study virus-receptor interactions, and ultimately the fusion process of viral entry. The former was accomplished. This experiment has successfully developed a liposome-VLP model system for the future study of interactions between the fusion proteins of enveloped viruses and their receptors. I have obtained evidence that His-tagged NPC1-C will only bind to liposomes via an interaction between the His-tag and the Ni^{2+} on the liposome surface. His-tagged NPC1-C does not bind a liposome lacking Ni^{2+}, and proteins lacking a His-tag will not bind liposomes containing Ni^{2+}. I have shown that NPC1-C will only interact with thermolysin cleaved VP40 GPΔmuc VLPs, and it will attach, but not fuse under the conditions of this experiment. There was no binding of NPC1-C with the VP40 GPFull VLP, regardless of whether or not that VLP had been cleaved with thermolysin; and it would not interact with VP40 GPΔmuc VLPs that had not been cleaved with thermolysin.

5.2 Future Works

A logical future experiment regarding Ebola virus entry, would be to continue to explore the conditions required to achieve fusion. A new construct lacking both the MLD and the glycan cap could be designed to determine if thermolysin digestion is still required after gene modification. This experiment could also be done with a different composition of phospholipids making up the liposomes to see if a more accurate representation of endosomes resulted in fusion of the two membranes. Or, this exact experiment could be carried one step further by acidifying the environment in an attempt

to cause fusion to determine if low pH is indeed a trigger for fusion. Sphingomyelin in the phospholipid mixture and ASMase could also be added to see if it plays a role in causing fusion to occur.

One technique that could be employed to monitor the fusion dynamics between the VLPs and the NPC1-C liposomes is a lipid mixing assay. In this assay, VLPS can be dye-labelled with octadecyl rhodamine (R18). Upon hemifusion or fusion, lipid mixing will result in dilution of the fluorescent dye and the signal detected from a fluoremeter would increase due to the self-quenching of the R18 fluorescent dye (Wessels et al., 2007). This method does not differentiate between hemifusion and fusion, but it would be able to differentiate hemifusion or fusion from attachment. Another technique to detect fusion also involving lipid mixing is the nitrobenzoxadiazole (NBD)-Rhodamine Energy Transfer assay. In this assay, liposome membranes labeled with a combination of fluorescence energy transfer donors and acceptors are mixed with unlabeled membranes, such as VLPs. Fluorescence resonance energy transfer (FRET) decreases when the spatial separation of the probes is increased upon membrane fusion and lipid mixing (Thermo Fisher Scientific, 2018).

Many more experiments could be spawned from of this experiment. This method of studying interaction and fusion can be used to investigate the function of other proteins that are involved in fusion, including many other enveloped viruses. The development of this model system means that the study of virus-receptor interactions can be realized in virtually any biosafety level 2 laboratory.

6. References

Addgene. (2017). Lentiviral Guide url: https://www.addgene.org/viral-vectors/lentivirus/lenti-guide/#second-generation.*2018*

Adrian, M., Dubochet, J., Lepault, J., and McDowall, A.W. (1984). Cryo-electron microscopy of viruses. Nature *308,* 32-36.

Akbarzadeh, A., Rezaei-Sadabady, R., Davaran, S., Joo, S.W., Zarghami, N., Hanifehpour, Y., Samiei, M., Kouhi, M., and Nejati-Koshki, K. (2013). Liposome: classification, preparation, and applications. Nanoscale Res. Lett. *8,* 102-276X-8-102.

Avanti Polar Lipids. (2017). Liposome Preparation. url: https://avantilipids.com/tech-support/liposome-preparation/.*2017*

Baker, T.S., Olson, N.H., and Fuller, S.D. (1999). Adding the third dimension to virus life cycles: three-dimensional reconstruction of icosahedral viruses from cryo-electron micrographs. Microbiol. Mol. Biol. Rev. *63,* 862-922, table of contents.

Bale, S., Liu, T., Li, S., Wang, Y., Abelson, D., Fusco, M., Woods, V.L.,Jr, and Saphire, E.O. (2011). Ebola virus glycoprotein needs an additional trigger, beyond proteolytic priming for membrane fusion. PLoS Negl Trop. Dis. *5,* e1395.

Bangham, A.D., and Horne, R.W. (1964). Negative Staining of Phospholipids and their Structural Modification by Surface-Active Agents as Observed in the Electron Microscope. J. Mol. Biol. *8,* 660-668.

Bangham, A.D., Standish, M.M., and Weissmann, G. (1965). The action of steroids and streptolysin S on the permeability of phospholipid structures to cations. J. Mol. Biol. *13,* 253-259.

Bartesaghi, A., Sprechmann, P., Liu, J., Randall, G., Sapiro, G., and Subramaniam, S. (2008). Classification and 3D averaging with missing wedge correction in biological electron tomography. J. Struct. Biol. *162,* 436-450.

Beniac, D.R., and Booth, T.F. (2017). Structure of the Ebola virus glycoprotein spike within the virion envelope at 11 A resolution. Sci. Rep. *7,* 46374.

Beniac, D.R., Melito, P.L., Devarennes, S.L., Hiebert, S.L., Rabb, M.J., Lamboo, L.L., Jones, S.M., and Booth, T.F. (2012). The organisation of Ebola virus reveals a capacity for extensive, modular polyploidy. PLoS One *7,* e29608.

Bozzuto, G., and Molinari, A. (2015). Liposomes as nanomedical devices. Int. J. Nanomedicine *10,* 975-999.

Brecher, M., Schornberg, K.L., Delos, S.E., Fusco, M.L., Saphire, E.O., and White, J.M. (2012). Cathepsin cleavage potentiates the Ebola virus glycoprotein to undergo a subsequent fusion-relevant conformational change. J. Virol. *86,* 364-372.

Bubeck, D., Filman, D.J., and Hogle, J.M. (2005). Cryo-electron microscopy reconstruction of a poliovirus-receptor-membrane complex. Nat. Struct. Mol. Biol. *12,* 615-618.

Burgess, S.W., Moore, J.D., and Shaw, W.A. (1996). Handbook of Nonmedical Applications of Liposome: From Design to Microreactors, Vol. 3 (Ann Harbor, U.S.A.: CRC Press).

Carette, J.E., Raaben, M., Wong, A.C., Herbert, A.S., Obernosterer, G., Mulherkar, N., Kuehne, A.I., Kranzusch, P.J., Griffin, A.M., Ruthel, G.*, et al.* (2011). Ebola virus entry requires the cholesterol transporter Niemann-Pick C1. Nature *477,* 340-343.

Carson, M., Johnson, D.H., McDonald, H., Brouillette, C., and Delucas, L.J. (2007). His-tag impact on structure. Acta Crystallogr. D Biol. Crystallogr. *63,* 295-301.

Chikh, G.G., Li, W.M., Schutze-Redelmeier, M.P., Meunier, J.C., and Bally, M.B. (2002). Attaching histidine-tagged peptides and proteins to lipid-based carriers through use of metal-ion-chelating lipids. Biochim. Biophys. Acta *1567,* 204-212.

Citovsky, V., and Loyter, A. (1985). Fusion of Sendai virions or reconstituted Sendai virus envelopes with liposomes or erythrocyte membranes lacking virus receptors. J. Biol. Chem. *260,* 12072-12077.

Clarke, E.C., Collar, A.L., Ye, C., Cai, Y., Anaya, E., Rinaldi, D., Martinez, B., Yarborough, S., Merle, C., Theisen, M.*, et al.* (2017). Production and Purification of Filovirus Glycoproteins in Insect and Mammalian Cell Lines. Sci. Rep. *7,* 15091-017-15416-3.

Cote, M., Misasi, J., Ren, T., Bruchez, A., Lee, K., Filone, C.M., Hensley, L., Li, Q., Ory, D., Chandran, K., and Cunningham, J. (2011). Small molecule inhibitors reveal Niemann-Pick C1 is essential for Ebola virus infection. Nature *477,* 344-348.

Curry, A., Appleton, H., and Dowsett, B. (2006). Application of transmission electron microscopy to the clinical study of viral and bacterial infections: present and future. Micron *37,* 91-106.

Davidson, E., Bryan, C., Fong, R.H., Barnes, T., Pfaff, J.M., Mabila, M., Rucker, J.B., and Doranz, B.J. (2015). Mechanism of Binding to Ebola Virus Glycoprotein by the ZMapp, ZMAb, and MB-003 Cocktail Antibodies. J. Virol. *89,* 10982-10992.

Davies, J.P., and Ioannou, Y.A. (2000). Topological analysis of Niemann-Pick C1 protein reveals that the membrane orientation of the putative sterol-sensing domain is identical to those of 3-hydroxy-3-methylglutaryl-CoA reductase and sterol regulatory element binding protein cleavage-activating protein. J. Biol. Chem. *275,* 24367-24374.

de La Vega, M.A., Wong, G., Kobinger, G.P., and Qiu, X. (2015). The multiple roles of sGP in Ebola pathogenesis. Viral Immunol. *28,* 3-9.

Deffieu, M.S., and Pfeffer, S.R. (2011). Niemann-Pick type C 1 function requires lumenal domain residues that mediate cholesterol-dependent NPC2 binding. Proc. Natl. Acad. Sci. U. S. A. *108,* 18932-18936.

Dubochet, J., Adrian, M., Chang, J.J., Homo, J.C., Lepault, J., McDowall, A.W., and Schultz, P. (1988). Cryo-electron microscopy of vitrified specimens. Q. Rev. Biophys. *21,* 129-228.

Duong-Ly, K.C., and Gabelli, S.B. (2014). Using ion exchange chromatography to purify a recombinantly expressed protein. Methods Enzymol. *541,* 95-103.

Dykstra, M.J., and Reuss, L.E. (2003).
Biological Electron Microscopy Theory, Techniques, and Troubleshooting
(New York, New York, U.S.A.: Plenum Press).

Fields, W., and Kielian, M. (2015). Interactions involved in pH protection of the alphavirus fusion protein. Virology *486,* 173-179.

GE Healthcare Life Sciences. (2014). HiTrap Desalting columns with Sephadex G-25 resin. url: https://www.gelifesciences.com/shop/chromatography/prepacked-columns/desalting-and-buffer-exchange/hitrap-desalting-columns-with-sephadex-g-25-resin-p-05853?current=11000329.*2018*

GE Healthcare Life Sciences. (2012). HISTrap excel.
url: https://www.gelifesciences.com/shop/chromatography/prepacked-columns/affinity-tagged-protein/histrap-excel-p-00310?current=29048586.*2018*

GE Healthcare Life Sciences. (2011). Ficoll-Paque Plus density gradient media.
url: https://www.gelifesciences.com/shop/cell-therapy/media/ficoll-paque-plus-density-gradient-media-p-05824.*2018*

Goldsmith, C.S., and Miller, S.E. (2009). Modern uses of electron microscopy for detection of viruses. Clin. Microbiol. Rev. *22,* 552-563.

Heidcamp, W.H. (2015). *Dr. William H. Heidcamp, Biology Department, Gustavus Adolphus College,St. Peter, MN 56082 -- cellab@gac.edu.2017*

Henderson, R. (1995). The potential and limitations of neutrons, electrons and X-rays for atomic resolution microscopy of unstained biological molecules. Q. Rev. Biophys. *28,* 171-193.

Hogle, J.M. (2002). Poliovirus cell entry: common structural themes in viral cell entry pathways. Annu. Rev. Microbiol. *56,* 677-702.

Hood, C.L., Abraham, J., Boyington, J.C., Leung, K., Kwong, P.D., and Nabel, G.J. (2010). Biochemical and structural characterization of cathepsin L-processed Ebola virus glycoprotein: implications for viral entry and immunogenicity. J. Virol. *84,* 2972-2982.

Huang, Y., Xu, L., Sun, Y., and Nabel, G.J. (2002). The assembly of Ebola virus nucleocapsid requires virion-associated proteins 35 and 24 and posttranslational modification of nucleoprotein. Mol. Cell *10,* 307-316.

Jasenosky, L.D., Neumann, G., Lukashevich, I., and Kawaoka, Y. (2001). Ebola virus VP40-induced particle formation and association with the lipid bilayer. J. Virol. *75,* 5205-5214.

Johnson, R.F., Bell, P., and Harty, R.N. (2006). Effect of Ebola virus proteins GP, NP and VP35 on VP40 VLP morphology. Virol. J. *3,* 31.

Kaletsky, R.L., Simmons, G., and Bates, P. (2007). Proteolysis of the Ebola virus glycoproteins enhances virus binding and infectivity. J. Virol. *81,* 13378-13384.

Kobasa, D., Rodgers, M.E., Wells, K., and Kawaoka, Y. (1997). Neuraminidase hemadsorption activity, conserved in avian influenza A viruses, does not influence viral replication in ducks. J. Virol. *71,* 6706-6713.

Kolodziej, S.J., Penczek, P.A., and Stoops, J.K. (1997). Utility of Butvar support film and methylamine tungstate stain in three-dimensional electron microscopy: agreement between stain and frozen-hydrated reconstructions. J. Struct. Biol. *120,* 158-167.

Kuhn, J.H., Radoshitzky, S.R., Guth, A.C., Warfield, K.L., Li, W., Vincent, M.J., Towner, J.S., Nichol, S.T., Bavari, S., Choe, H., Aman, M.J., and Farzan, M. (2006). Conserved receptor-binding domains of Lake Victoria marburgvirus and Zaire ebolavirus bind a common receptor. J. Biol. Chem. *281,* 15951-15958.

Kuo., J. (2007). Electron Microscopy: Methods and Protocols (Totowa, New Jersey, U.S.A.: Humana Press Inc.).

Lee, J.E., Fusco, M.L., Hessell, A.J., Oswald, W.B., Burton, D.R., and Saphire, E.O. (2008). Structure of the Ebola virus glycoprotein bound to an antibody from a human survivor. Nature *454,* 177-182.

Licata, J.M., Johnson, R.F., Han, Z., and Harty, R.N. (2004). Contribution of ebola virus glycoprotein, nucleoprotein, and VP24 to budding of VP40 virus-like particles. J. Virol. *78,* 7344-7351.

Ludtke, S.J., Baldwin, P.R., and Chiu, W. (1999). EMAN: semiautomated software for high-resolution single-particle reconstructions. J. Struct. Biol. *128,* 82-97.

Malloy, A. (2011). Count, size and visualize nanoparticles. Materials Today *14,* 170-173.

Markosyan, R.M., Miao, C., Zheng, Y.M., Melikyan, G.B., Liu, S.L., and Cohen, F.S. (2016). Induction of Cell-Cell Fusion by Ebola Virus Glycoprotein: Low pH Is Not a Trigger. PLoS Pathog. *12,* e1005373.

McClain, D.L., Woods, H.L., and Oakley, M.G. (2001). Design and characterization of a heterodimeric coiled coil that forms exclusively with an antiparallel relative helix orientation. J. Am. Chem. Soc. *123,* 3151-3152.

McLellan, J.S., Yang, Y., Graham, B.S., and Kwong, P.D. (2011). Structure of respiratory syncytial virus fusion glycoprotein in the postfusion conformation reveals preservation of neutralizing epitopes. J. Virol. *85,* 7788-7796.

Melito, P.L., Qiu, X., Fernando, L.M., deVarennes, S.L., Beniac, D.R., Booth, T.F., and Jones, S.M. (2008). The creation of stable cell lines expressing Ebola virus glycoproteins and the

matrix protein VP40 and generating Ebola virus-like particles utilizing an ecdysone inducible mammalian expression system. J. Virol. Methods *148,* 237-243.

Miller, E.H., Obernosterer, G., Raaben, M., Herbert, A.S., Deffieu, M.S., Krishnan, A., Ndungo, E., Sandesara, R.G., Carette, J.E., Kuehne, A.I., *et al.* (2012a). Ebola virus entry requires the host-programmed recognition of an intracellular receptor. Embo J. *31,* 1947-1960.

Miller, M.E., Adhikary, S., Kolokoltsov, A.A., and Davey, R.A. (2012b). Ebolavirus requires acid sphingomyelinase activity and plasma membrane sphingomyelin for infection. J. Virol. *86,* 7473-7483.

Møller, H.J., and Poulsen, J.H. (2009). Chapter 52: Staining of Glycoproteins/Proteoglycans on SDS-Gels. In Protein Protocols Handbook. Springer Protocols Handbook. Walker, J. M. ed., (Totowa, U.S.A.: Humana Press) pp. 569.

Mulherkar, N., Raaben, M., de la Torre, J.C., Whelan, S.P., and Chandran, K. (2011). The Ebola virus glycoprotein mediates entry via a non-classical dynamin-dependent macropinocytic pathway. Virology *419,* 72-83.

Nanbo, A., Imai, M., Watanabe, S., Noda, T., Takahashi, K., Neumann, G., Halfmann, P., and Kawaoka, Y. (2010). Ebolavirus is internalized into host cells via macropinocytosis in a viral glycoprotein-dependent manner. PLoS Pathog. *6,* e1001121.

National Institute of Health. (2006). Biosafety Considerations for Research with Lentiviral Vectors. url: https://osp.od.nih.gov/wp-content/uploads/2014/01/Lenti_Containment_Guidance_0.pdf.*2018*

Nelson, D.L., and Cox, M.M. (2008a). Lehninger's Principles of Biochemistry, 5th edition, Chapter 10: Lipids (New York: W. H. Freeman and Company).

Nelson, D.L., and Cox, M.M. (2008b). Lehninger's Principles of Biochemistry, 5th edition, Chapter 27: Protein Metabolism (New York: W. H. Freeman and Company).

Nelson, D.L., and Cox, M.M. (2008c). Lehninger's Principles of Biochemistry, 5th edition, Chapter 3: Amino Acids, Peptides, and Proteins (New York: W. H. Freeman Company).

Nelson, D.L., and Cox, M.M. (2008d). Lehninger's Priniciples of Biochemistry, 5th edition, Chapter 7:Carbohydrates and Glycobiology (New York: W. H. Freeman and Company).

Niwa, H., Yamamura, K., and Miyazaki, J. (1991). Efficient selection for high-expression transfectants with a novel eukaryotic vector. Gene *108,* 193-199.

Noda, T., Sagara, H., Suzuki, E., Takada, A., Kida, H., and Kawaoka, Y. (2002). Ebola virus VP40 drives the formation of virus-like filamentous particles along with GP. J. Virol. *76,* 4855-4865.

Nussbaum, O., Rott, R., and Loyter, A. (1992). Fusion of influenza virus particles with liposomes: requirement for cholesterol and virus receptors to allow fusion with and lysis of neutral but not of negatively charged liposomes. J. Gen. Virol. *73 (Pt 11),* 2831-2837.

Philippot, J.R., and Schuber, F. (1995). Liposomes as Tools in Basic Research and Industry (Boca Raton: CRC Press Inc.).

Qiu, X., Alimonti, J.B., Melito, P.L., Fernando, L., Stroher, U., and Jones, S.M. (2011). Characterization of Zaire ebolavirus glycoprotein-specific monoclonal antibodies. Clin. Immunol. *141,* 218-227.

Qiu, X., Audet, J., Wong, G., Pillet, S., Bello, A., Cabral, T., Strong, J.E., Plummer, F., Corbett, C.R., Alimonti, J.B., and Kobinger, G.P. (2012). Successful treatment of ebola virus-infected cynomolgus macaques with monoclonal antibodies. Sci. Transl. Med. *4,* 138ra81.

Regules, J.A., Beigel, J.H., Paolino, K.M., Voell, J., Castellano, A.R., Hu, Z., Munoz, P., Moon, J.E., Ruck, R.C., Bennett, J.W.*, et al.* (2017). A Recombinant Vesicular Stomatitis Virus Ebola Vaccine. N. Engl. J. Med. *376,* 330-341.

Reiser, J., Harmison, G., Kluepfel-Stahl, S., Brady, R.O., Karlsson, S., and Schubert, M. (1996). Transduction of nondividing cells using pseudotyped defective high-titer HIV type 1 particles. Proc. Natl. Acad. Sci. U. S. A. *93,* 15266-15271.

Ruska, E. (December 8, 1986) Paper presented at The Development Of The Electron Microscope And Of Electron Microscopy (Berlin, Germany)

Saeed, M.F., Kolokoltsov, A.A., Albrecht, T., and Davey, R.A. (2010). Cellular entry of ebola virus involves uptake by a macropinocytosis-like mechanism and subsequent trafficking through early and late endosomes. PLoS Pathog. *6,* e1001110.

Schornberg, K., Matsuyama, S., Kabsch, K., Delos, S., Bouton, A., and White, J. (2006). Role of endosomal cathepsins in entry mediated by the Ebola virus glycoprotein. J. Virol. *80,* 4174-4178.

Sigma Aldrich. (2018). OptiPrep Density Gradient Medium.
url: https://www.sigmaaldrich.com/catalog/product/sigma/d1556?lang=en&region=CA.*2018*

Subramaniam, S., Bartesaghi, A., Liu, J., Bennett, A.E., and Sougrat, R. (2007). Electron tomography of viruses. Curr. Opin. Struct. Biol. *17,* 596-602.

Tao, Y., and Zhang, W. (2000). Recent developments in cryo-electron microscopy reconstruction of single particles. Curr. Opin. Struct. Biol. *10,* 616-622.

Thermo Fisher Scientific. (2018). Lipid-Mixing Assays of Membrane Fusion.
url: https://www.thermofisher.com/ca/en/home/references/molecular-probes-the-handbook/technical-notes-and-product-highlights/lipid-mixing-assays-of-membrane-fusion.html.*2018*

Thermo Fisher Scientific. (2012). HisPur Cobalt Resin.
url: https://www.thermofisher.com/order/catalog/product/89964.*2017*

Towner, J.S., Sealy, T.K., Khristova, M.L., Albarino, C.G., Conlan, S., Reeder, S.A., Quan, P.L., Lipkin, W.I., Downing, R., Tappero, J.W*., et al.* (2008). Newly discovered ebola virus associated with hemorrhagic fever outbreak in Uganda. PLoS Pathog. *4,* e1000212.

Tuthill, T.J., Bubeck, D., Rowlands, D.J., and Hogle, J.M. (2006). Characterization of early steps in the poliovirus infection process: receptor-decorated liposomes induce conversion of the virus to membrane-anchored entry-intermediate particles. J. Virol. *80,* 172-180.

Urade, R., Hayashi, Y., and Kito, M. (1988). Endosomes differ from plasma membranes in the phospholipid molecular species composition. Biochim. Biophys. Acta *946,* 151-163.

Walker, J.M. (2009). Chapter 21: SDS Polyacrylamide Gel Electrophoresis of Proteins. In Protein Protocols Handbook. Springer Protocols Handbook. Walker, J. M. ed., (Totowa, U.S.A.: Humana Press) pp. 177.

Wang, H., Shi, Y., Song, J., Qi, J., Lu, G., Yan, J., and Gao, G.F. (2016). Ebola Viral Glycoprotein Bound to Its Endosomal Receptor Niemann-Pick C1. Cell *164,* 258-268.

Weaver, A.K., Olsen, M.L., McFerrin, M.B., and Sontheimer, H. (2007). BK channels are linked to inositol 1,4,5-triphosphate receptors via lipid rafts: a novel mechanism for coupling [Ca(2+)](i) to ion channel activation. J. Biol. Chem. *282,* 31558-31568.

Wessels, L., Elting, M.W., Scimeca, D., and Weninger, K. (2007). Rapid membrane fusion of individual virus particles with supported lipid bilayers. Biophys. J. *93,* 526-538.

White, J.M., Delos, S.E., Brecher, M., and Schornberg, K. (2008). Structures and mechanisms of viral membrane fusion proteins: multiple variations on a common theme. Crit. Rev. Biochem. Mol. Biol. *43,* 189-219.

White, J.M., and Schornberg, K.L. (2012). A new player in the puzzle of filovirus entry. Nat. Rev. Microbiol. *10,* 317-322.

WHO. (2018). Ebola virus disease Fact Sheet.*2018,* 1.

Wilson, J.A., Bosio, C.M., and Hart, M.K. (2001). Ebola virus: the search for vaccines and treatments. Cell Mol. Life Sci. *58,* 1826-1841.

Yu, D.S., Weng, T.H., Wu, X.X., Wang, F.X.C., Lu, X.Y., Wu, H.B., Wu, N.P., Li, L.J., and Yao, H.P. (2017). The lifecycle of the Ebola virus in host cells. Oncotarget *8,* 55750-55759.

7. Supplementary Material

7.1 Supplementary Figures

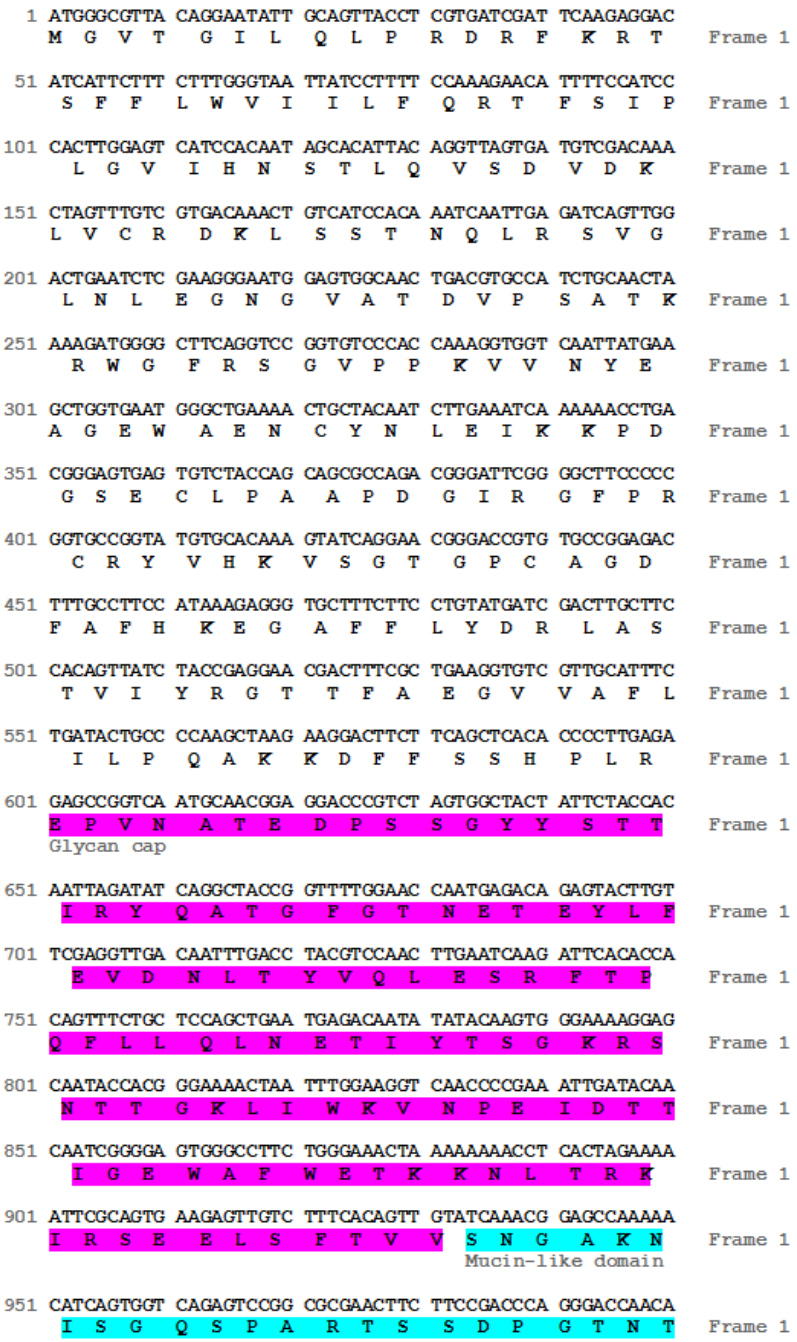

Supplementary Figure 1. Clone details for Ebola GP.

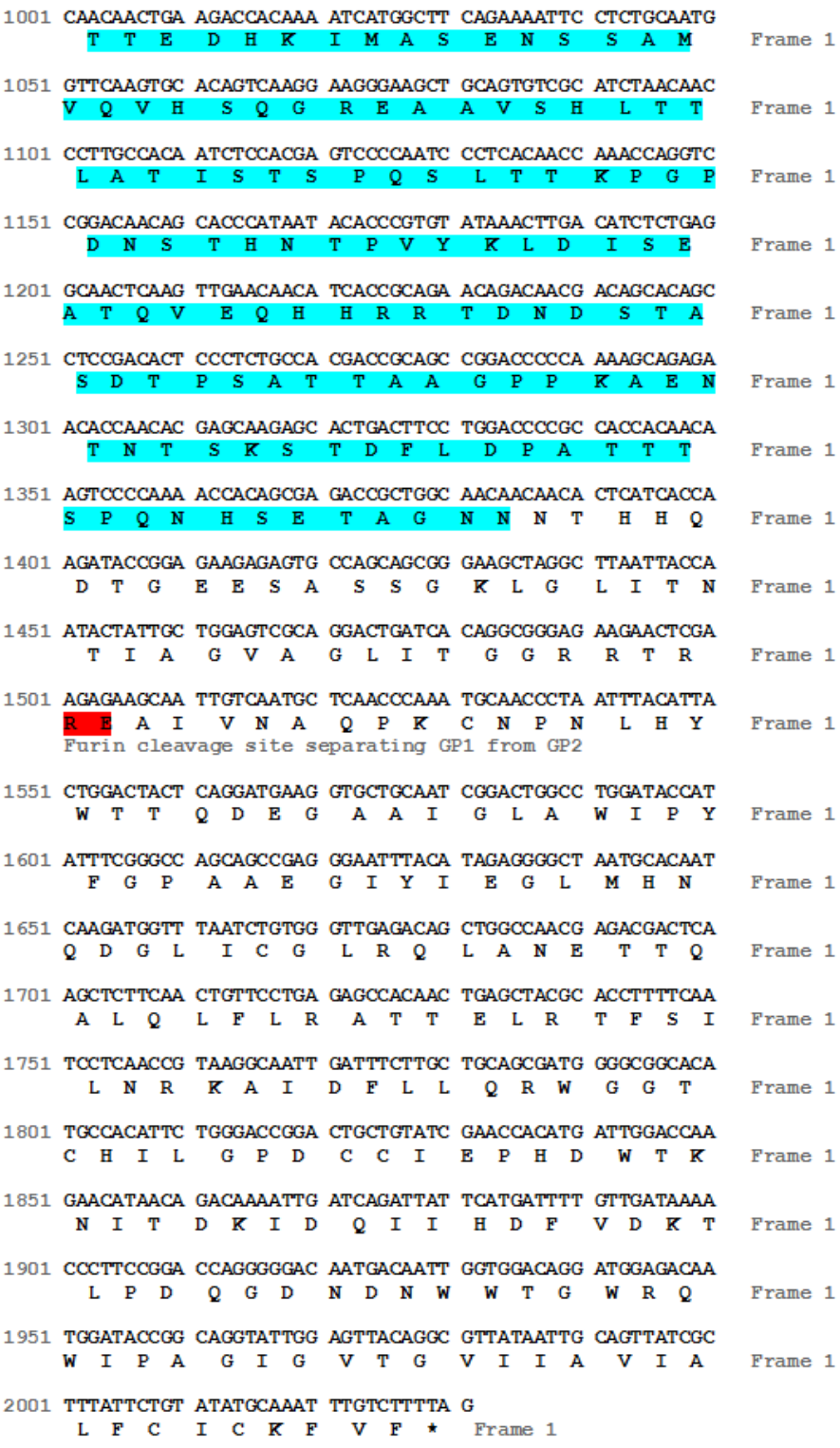

Supplementary Figure 1. continued

Supplementary Figure 2. Clone details for NPC1.

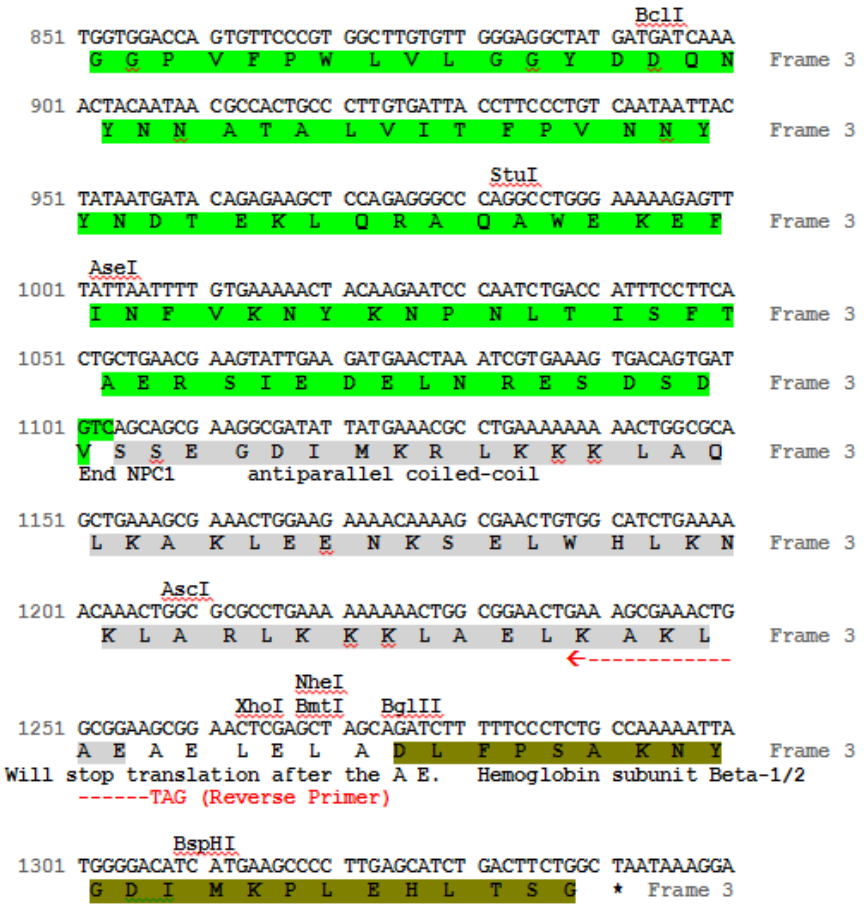

Supplementary Figure 2 continued.

7.2 Solutions

7.2.1 TNE Buffer

10 mM Tris-Cl (pH 7.5)
150 mM NaCl
10 mM EDTA

7.2.2 ThermoBuffer

50 mM Tris 8
150 mM NaCl
0.5 mM $CaCl_2$

7.2.3 200 mM sodium phosphate buffer

0.2 M dibasic phosphate buffer: 28.39 g Na_2HPO_4 in 1 L ddH_2O
0.2 M monobasic phosphate buffer: 31.21 g $NaH_2PO_4 \bullet H_2O$ in 1 L ddH_2O
Mix together 180 mL dibasic + 70 mL monobasic phosphate buffers

7.2.4 Dynabeads 2X binding/wash buffer

100 mM sodium phosphate, pH 8.0
600 mM NaCl
0.02% Tween-20
*dilute to 1X before use

7.2.5 Dynabeads His Elution buffer

300 mM imidazole
50 mM sodium phosphate, pH 8.0
300 mM NaCl
0.01% Tween-20

7.3 Copyright Approval

Figure 1 and Figure 2 were reproduced from White and Schornberg (2012). Please see copyright approval on page 162.

Figure 3 was reproduced with modifications from Davies and Ioannou (2000) published in the Journal of Biological Chemistry by the American Society for Biochemistry and Molecular Biology. This publisher allows reuse in theses or dissertations at no charge. A letter of permission is shown on page 163.

Figure 4 was reproduced from Deffieu and Pfeffer (2011) published by PNAS. This journal enables the use of original figures for noncommercial and educational use without requesting permission. As such, copyright approval was not required.

Figure 5 was reproduced from Avanti Polar Lipids Inc. Approval for written and online reuse was obtained from the company via e-mail. The e-mail thread is shown on page 164.

Figure 40 was reproduced from Sigma Aldrich Inc. Copyright approval is shown on page 165.

Figures 1 and 2 Copyright approval:

This Agreement between Ms. Lindsey Lamboo ("You") and Springer Nature ("Springer Nature") consists of your license details and the terms and conditions provided by Springer Nature and Copyright Clearance Center.

Your confirmation email will contain your order number for future reference.

License Number	4297661021726
License date	Feb 28, 2018
Licensed Content Publisher	Springer Nature
Licensed Content Publication	Nature Reviews Microbiology
Licensed Content Title	A new player in the puzzle of filovirus entry
Licensed Content Author	Judith M. White, Kathryn L. Schornberg
Licensed Content Date	Apr 11, 2012
Licensed Content Volume	10
Licensed Content Issue	5
Type of Use	Thesis/Dissertation
Requestor type	academic/university or research institute
Format	print and electronic
Portion	figures/tables/illustrations
Number of figures/tables/illustrations	2
High-res required	no
Will you be translating?	no
Circulation/distribution	<501
Author of this Springer Nature content	no
Title	Studies on the Roles of Viral Envelope Surface Proteins in Cell Attachment and Entry
Instructor name	Dr. Tim Booth
Institution name	University of Manitoba
Expected presentation date	Mar 2018
Portions	Figure 1. Life cycle of EBOV and Box 1 figure of the pathway of viral membrane fusion

Figure 3 Copyright approval:

11200 Rockville Pike
Suite 302
Rockville, Maryland 20852

August 19, 2011

American Society for Biochemistry and Molecular Biology

To whom it may concern,

It is the policy of the American Society for Biochemistry and Molecular Biology to allow reuse of any material published in its journals (the Journal of Biological Chemistry, Molecular & Cellular Proteomics and the Journal of Lipid Research) in a thesis or dissertation at no cost and with no explicit permission needed. Please see our copyright permissions page on the journal site for more information.

Best wishes,

Sarah Crespi

American Society for Biochemistry and Molecular Biology
11200 Rockville Pike, Rockville, MD
Suite 302

JBC | MCP | JLR

Figure 5 Copyright approval:

From: Lindsey Lamboo
Sent: Thursday, March 01, 2018 9:12 AM
To: Avanti Polar Lipids Info
Subject: image copyright

Hello,

I'm writing up my Masters thesis and I'd like to use an image I've found on your website. This is the link to the product: https://avantilipids.com/product/790404/

I used this lipid in my experiments and I'd like to put the image of the chemical structure of the lipid in my thesis.

Do I need some form of copyright approval to use this image? If so, how do I get that?

Thanks,
Lindsey Lamboo

Kendall Roberson (Kendall.Roberson@avantilipids.com)

Hi Lindsey,
Avanti would be happy to allow you to use the image in your thesis. We request that you reference Avanti as the source of the image and that it was printed with the permission of Avanti. You may want to confirm with the university that an e-mail is sufficient for their purposes. If an authorization letter is required that will take a little longer.

Cordially,

Kendall Roberson, JD, CPA
General Counsel

Hi Kendall,

Thank you very much! I've confirmed with the University of Manitoba that this e-mail is sufficient. However, the university noted that I should inform you that the thesis will be made available online as well as printed. Do I have permission to use it in the online version as well?

Thanks again,
Lindsey Lamboo

Lindsey,
Yes, you have Avanti's permission to include the referenced image below in the online publication of your Master's thesis.

If you need any additional information please let me know.

Cordially,

Kendall Roberson, JD, CPA
General Counsel

Figure 40 Copyright approval:

SIGMA-ALDRICH

sigma-aldrich.com

3050 Spruce Street, St. Louis, MO 63103 USA
Tel: (800) 521-8956 (314) 771-5765 Fax: (800) 325-5052 (314) 771-5757

Request to Use Sigma-Aldrich Copyrighted Material

Part I – to be filled in by Requester:

Request Date 2018-03-07 Requester Signature _____

Requester Information:

Name	Lindsey Lamboo	Building	Basic Medical Sciences Building
Title	Student	Street	Room 543 - 745 Bannatyne Avenue
Department	Medical Microbiology & Infectious Diseases	City	Winnipeg
Organization	University of Manitoba	State	Manitoba
Phone		Zip Code	R3E 0J9
Email		Country	Canada

Material Requested to be Used:

Form (check one) ☐ Printed ☑ Electronic

Source Publ. Name or URL [redacted]

Source Publ. Edition _____ Source Publ. Issue _____

Source Publ. Year _____ Source Publ. Pages _____

Source Publ. Volume _____

Description of Material and the intended use (Submit a photocopy or screen image of the context in which the copyrighted material will be used)

I'd like to reproduce the two images of Cathepsin L and thermolysin preferential cleavage sites in my Masters thesis to indicate the differences in cleavage between the two enzymes.

Attached is a screenshot of how the figure would be used in my thesis.

Type of Use (check one) ☐ For Profit ☑ Not for Profit

If Material will be reproduced, how many copies will be made? <10

Part II – to be filled in by Sigma-Aldrich Authorizer

Sigma-Aldrich Co. LLC hereby grants permission for one-time use of the material described above for the purpose stated,

- provided a suitable acknowledgment is given, *e.g.*, "Reproduced with permission from Sigma-Aldrich Co. LLC" or "Reproduced with permission of Sigma-Aldrich Co. LLC from publication name, year, volume, issue and pages"
- and subject to the following restrictions: _____

Authorized Signatu Date 8-Mar-2018

Please submit completed form and any attachments to legal@sial.com